Group one impurities in single crystalline Zinc Oxide

Klaus Magnus Håland Johansen

Thesis submitted in partial fulfillment
of the requirements for the degree of
Philosophiae Doctor

Department of Physics
University of Oslo

January 2011

Series of dissertations submitted to the
Faculty of Mathematics and Natural Sciences, University of Oslo
No. 1063

ISSN 1501-7710

Cover: Inger Sandved Anfinsen.
Printed in Norway: AIT Oslo AS.

Produced in co-operation with Unipub.
The thesis is produced by Unipub merely in connection with the
thesis defence. Kindly direct all inquiries regarding the thesis to the copyright
holder or the unit which grants the doctorate.

Jeg skal bygge lego,
jeg skal vise dem!

- Ung astrofestivaldeltager

Summary

Zinc Oxide (ZnO) has been used as a material in many different technologies from pharmaceuticals to electronics. This exciting material can also be utilized as a wide band gap semiconductor for application in optoelectronic devices. The availability of Zn, the possibility to grow single crystal bulk material and the exitonic binding energy of 60 meV makes this material especially interesting. Even though the material has been studied already since the late 1920s there are still some fundamental properties of ZnO as a semiconductor which are not yet fully understood e.g. the inherent n-type activity and the challenge of achieving stable p-type doping.

The present work is a study of dopants and impurities in ZnO, with a focus on H and Li and their interplay in hydrothermally grown (HT) ZnO. Doping with H typically increases the electron concentration in the material, either by direct donor activity or by passivation of acceptors. Doping by Li on the other hand typically results in material with high resistivity, which is explained by Li contributing both as acceptor and donor on the substitutional Zn-site and interstitial site, respectively. Both elements may therefore significantly contribute to the electrical properties of ZnO.

Both H and Li are light elements with small ionic radius, and thus the diffusivity along the interstitial route is expected to be high. In this work H diffusion has been studied by secondary ion mass spectrometry (SIMS). From this the H diffusion in hydrothermally grown material was found to be trap limited with an activation energy of 0.8-0.9 eV and with a dissociation energy from the diffusion trap of approximately 1.5 eV. Since H and Li are known to form a complex together and the concentration of Li is close to the observed trap concentration Li was suggested to be the diffusion trap for H, however contribution from other defects or impurities could not be ruled out.

To approach this question from a different angle, Fourier transformed infrared absorption spectroscopy (FTIR) was employed to study the 3577 cm^{-1} local vibrational mode, previously identified as a OH-Li-complex. The 3577 cm^{-1} line had been found to survive heat treatments of several hours at $1200°C$, which is inconsistent with the estimated dissociation energy of the H diffusion trap. However, in this thesis it is shown that the reason for the high thermal stability is efficient re-trapping of H (and possibly Li) when the sample is let to cool down slowly to

room temperature. In this way the complex responsible for the 3577 cm^{-1} vibrational mode is reformed and the peak can therefore be observed even after heat treatment at temperatures far above the thermal stability of the complex. Furthermore, by comparing results from both SIMS and FTIR, no correlation between the as-grown 3577 cm^{-1} peak intensity and the Li-concentration was found, indicating that most of the Li atoms in the as-grown state are not passivated by H. SIMS-measurements also revealed an in-homogeneous distribution of Li repeated in the lateral directions in some of the studied wafers. It is speculated that these in-homogeneities are related to the presence of c-axis inversion domains as observed by transmission electron microscopy (TEM) and it is speculated that they might contribute to the high apparent thermal stability of the 3577 cm^{-1} vibrational mode.

The third angle of approach employed in this thesis is the combination of SIMS and positron annihilation spectroscopy (PAS) together with theoretical estimates. The PAS-technique is very well suited to study open volume defects. One of the main results in this work is the identification of the positron annihilation signature of Li occupying the Zn-site, which showed that most of the Li atoms in as-grown n-type HT-ZnO is in the acceptor-state (substitutional Zn-site). It also showed that in melt grown ZnO doped with 1.5×10^{19} Li/cm^3 more than 2-3$\times10^{18}$ cm^{-3} of the Li atoms resides on the Zn-site, showing the possibility of obtaining large concentrations of Li on the Zn-site in the acceptor state.

The identification of the annihilation signature of Li_{Zn} also opened the possibility to study the effect of hydrogenation of HT-ZnO by PAS, where H is shown to efficiently passivate the Li-acceptors leaving Zn-vacancies as the dominant positron trap. However, in material where Li had been removed prior to hydrogenation H is found to be trapped by Zn-vacancies.

This work shows that there is a strong interplay between H and Li in ZnO. There are strong arguments that Li is the main trapping site for H-diffusion based on the combination of results from techniques like SIMS, FTIR and PAS, however other sites may not be completely excluded and there is also evidence of relatively complicated dynamics related to the behavior of H and Li in ZnO, involving several different sites for H. This work has also confirmed that several properties of hydrothermally grown ZnO may vary from wafer to wafer and using good reference samples are necessary to be able to draw correct conclusions.

Acknowledgments

The work on this thesis started about 5 years ago and over the years there have been a lot of people who have been helping me out and deserves a big thank you. First of all I would like to thank my main supervisor Bengt G. Svensson. I will be proud to be among the group of more than 30 candidates you have successfully guided towards the fulfillment of a Ph.D.-degree. It should not be underestimated how much it means to have backing from someone with such great amount of scientific experience and insight. Thanks for all the help and guidance. Secondly, I would like to thank Edouard V. Monakhov for his day-to-day supervision, the direct feedback and no bullshit attitude. It has been a privilege to share the office with you. Thanks goes also to Andrej Yu. Kuznetsov for acting as a co-supervisor and I'm especially grateful that you gave me the opportunity to go to Finland to do positron annihilation spectroscopy, which have ended up as a major part of this thesis. Thanks also to Truls Norby for acting as a co-supervisor. Unfortunately, no common papers have resulted from the intentions of collaborations with your group yet, but my guess it that it is just a matter of time now. Better late than never!

This work rely heavily on the help from our technical staff. First and foremost Viktor Bobal for implanting a seizable number of samples and in general keeping the lab running, at first together with Thomas Martinsen and then Mikael Sjödin. In addition to the in-house technical staff thanks also goes to Ole Bjørn Karlsen of the structural physics group for helping out whenever it was needed. No one makes smaller gas-filled quartz ampules than you, Ole Bjørn!

I would also like to thank Jens S. Christensen and Lasse Vines for helping me with measurements and teaching me how to use the SIMS. Over the years there have been a lot of members of the physical electronics group that have contributed in one way or another. In the last couple of years the flow of scientific information in-between the internal ZnO-community has in my opinion improved a lot. Several of the ideas followed up in this thesis have originated from excellent discussions, especially with Lasse Vines, Knut Erik Knutsen, Pekka Tapio Neuvonen, Esben Lund, Ramon Schifano and/or Hallvard Haug. Special thanks goes also to Hallvard for teaching me and helping me out with the FTIR-measurements and for the mutual agreement of exploitation. Thanks to Lasse Vines, Knut Erik Knutsen, Hallvard Haug and Ingvild Thue Jensen for proofreading parts of this thesis.

Scientific discussions also outside the group have been highly valued. Thanks to Øystein Prytz and Annett Thøgersen at the structural physics group, to Christian Kjølseth, Skjalg Erdal and Tor Bjørheim at the group for solid-state electrochemistry and to our friends in Finland; Filip Tuomisto, Asier Zubiaga Monsalve and Ilja Makkonen at the Aalto University for teaching me about and helping me out with the PAS-measurements and related modeling.

I would also like to thank all the people that have been present in the group during all these years for contributing to the good working environment. To mention a few; Mads Mikkelsen, Jan Bleka, Mareike Trunk, Vishnu Venkatachalapathy, Agnieszka Gorzkowska-Sobas, Lars Løvlie and all the rest of the guys that have previously been and those who still are making MiNa-lab to more than a relatively clean building in the mud.

It is no secret that reaching this point has not been an easy task. A high amount of sick leave is no killer combination with the demands of completing a Ph.D.-degree. The main turning point came as a consequence of guidance from Karianne Gulliksen together with the training and support from her co-workers at Norsk idretts medisinsk institutt (NIMI). Clearing my mind and helping me regain the focus.

However, defocusing might be as important as focusing. So thanks to Espen Isaksen, Petter Andersen, Levi Jensen and the rest of the Mjøndalen gang for forcing me to defocus and dragging me out from time to time. It is highly appreciated. Thanks also to Victoria for doing the same on a daily basis. Nothing clears the mind as throwing a ball for a couple of hours.

Studying at the Department of Physics at UiO has given me a lot. Not only good friends, like Øystein Prytz, Annett Thøgersen, Margit Dyrland, Sanja Hadzialic, Joakim Bergli, Olav Mundal, Mateusz Røstad, Kanutte Huse, Tor Helge Huse and many others, but the best friend of them all; Ingvild Julie Thue Jensen, the mother of my beautiful daughter Katja. Your support, both scientifically and morally is highly valued and cherished. It would have been hard to finish this work without the help of the others, but I know it would have been impossible without the help and support from you!

Klaus Magnus Håland Johansen
January 2011

Preface

Work on this thesis started in the autumn of 2005, and has been funded by the University of Oslo through the FUNMAT@UiO, the Norwegian Research Council (NANOMAT and FRINAT programs), NORDFORSK and the Academy of Finland. The major part of the research was carried out at the Department of Physics, under the supervision of Bengt Gunnar Svensson, Edouard V. Monakhov and Andrej Yu. Kuznetsov. The main focus of the work has been on studies of hydrogen and lithium impurities in ZnO by employing secondary ion mass spectrometry and infrared absorption spectroscopy. Transmission electron microscopy (TEM) studies have been preformed by Øystein Prytz in the Structural physics group at the Department of Physics, University of Oslo.

During the fall of 2009 two weeks were spent in Finland conducting positron annihilation spectroscopy (PAS) in close collaboration with Asier Mosalve Zubiaga and Filip Tuomisto on ZnO doped with Li and H.

In addition there have been some collaboration with Christian Kjølseth, Skjalg Erdal and Tor Bjørheim under the supervision of Truls Norby in the Group for Solid-State Electrochemistry at the Department of Chemistry, University of Oslo.

Below is a list of papers published during the time of this work which are not included in the thesis.

- K. M. Johansen, R. Schifano, E.V. Monakhov and B. G. Svensson. Investigation of contact material for cross section scanning spreading resistance microscopy on zinc oxide. *Physica Status Solidi* **5**, 3361-3363 (2008)
- B. G. Svensson, T. Moe Børseth, K. M. Johansen, T. Maqsood, R. Schifano, U. Grossner, J. S. Christensen, L. Vines, P. Klason, Q. X. Zhao, M. Willander, F. Tuomisto, W. Skorupa, E. V. Monakhov and A. Yu. Kuznetsov. Hydrothermally grown single-crystalline zinc oxide; characterization and modification *Mater. Res. Soc. Symp. Proc.* **1035** L04-01 (2008)

Table of Contents

Chapter 1

Motivation and general background

Currently there is an ongoing revolution related to the world's artificial illumination, which started with the introduction of white light emitting diodes (wLED) a few years back [1]. This transition towards wLED is mainly driven by the very successful development of the GaN-material system, materialized for instance in wLED based flashlights found in any nearby sports shop. Among the key advances as compared to other sources of illumination is the long lifetime and high efficiency (low production of waste heat) of the LEDs. Since the first wLED was sold a few years back, the efficiency has increased dramatically. In Ref.[2] the efficiency development as compared to other sources of white light can be found. However, to utilize the full potential of the wLED-technology the price must be reduced and, at the same time, environmental considerations should be taken into account. One of the potential competitors to GaN is ZnO. Both materials have a wide band gap of about 3.4 eV [3]. However, as opposed to GaN, ZnO is less poisonous and potentially much cheaper. Another important aspect is that high quality ZnO bulk material is available, which is not the case for GaN. Even if bulk growth of GaN is found to be viable the price expectancy exceeds that of high quality bulk growth of ZnO by a factor of more than 10.[4]

Interestingly, this ongoing revolution in artificial illumination opens up new possibilities for how we design both our interior and exterior environment, since the small LEDs may be incorporated into any wall, floor or furniture without the same fear of overheating and potential risk of fire as with other sources of light. However, more importantly it may also be part of an efficient, long lived and self-sustainable illumination system in combination with solar cells. In countries where

electricity is not readily available and the typical light source comes from burning wood or petrol indoors, there is a huge potential for increased life quality by employing such a system. Ways that this can be achieved are exemplified by initiatives like "Light up the world foundation"[5] and the "Barefoot engineers program"[6] that are based on investments in solar-systems and training of locals, both men and women, to run and maintain the installed systems. This is shown to lead to enormous changes in the way of life for the inhabitants, with side effects like promoting equal gender rights and potentially improving the local environment by allowing vegetation to grow back, since less vegetation is harvested for burning. It is, however, important to acknowledge that development of new technology is not enough to obtain such changes, but it opens up new possibilities and this surely motivates further investigations into relevant material systems.

Another relevant aspect is that several countries have banned the use of incandescent light bulbs, replacing them with more efficient compact fluorescent lamps (CFL). A problem, however, is that CFLs typically contain mercury, which complicates their disposal and raises questions about environmental aspects. ZnO, on the other hand, is regarded as a safe material from an environmental perspective, commonly used in baby powder, pigments, toothpaste, sunscreen etc.[7, 8]

Even though wLED is one of the main targets for the use of semiconducting ZnO, there are several other interesting properties to be exploited. One of them is the possibility to produce transparent conductive oxides (TCO). At present time, there are three commonly used inorganic material systems with this capability, Sn doped InO (ITO), F doped SnO_2 (FTO) and Al- or Ga- doped ZnO.[9] CdO, which was the first material discovered to act as a TCO is no longer commonly used due to the toxicity of the material. ITO, on the other hand, is already widely used in flat panel displays and other consumer electronics and also as a contact material for more efficient collection of charge carriers in photovoltaic solar cells. However, doped ZnO has again the potential to be a low cost and more environmentally friendly alternative. Another interesting feature of ZnO is as a dilute magnetic semiconductor for use in spintronic applications.[10] However, there are several issues with ZnO that one needs to address before all of these applications can be achieved.

The one major issue with ZnO is the lack of stable and low resistive p-type material.[11, 12] There is a general trend that wide bandgap semiconductors results in being either n- or p-type in the as-grown state; where achieving the opposite type (p- or n-type, respectively) is very challenging. This is referred to as an intrinsic doping asymmetry.[13] Despite this, there have been reports claiming p-type activity in ZnO, but typically reproducing the results have been found

difficult.[11, 12] Samples measured in one laboratory as p-type have ended up as n-type when being measured in another laboratory. Thus the production and understanding of the stability of p-type doping is a major issue. In more graphical terms it is tempting to think of this as a struggle between the researchers and the material. Every time some researcher tries to force ZnO out of its equilibrium to produce p-type activity, the material responds by inducing new donor states, often of unknown sort. Thus studying and limiting the materials ability to induce compensating donors is essential.

Hence, basic knowledge of ZnO is important. In this thesis the role of two common and electrically active impurities, namely H and Li are addressed. In hydrothermally grown material, which we have studied, Li is present in a concentration between 1-5$\times 10^{17}\,\mathrm{cm}^{-3}$. Measurement of the as-grown H concentration is, however, in general difficult due to the lack of sufficiently sensitive methods, but it is a readily available element and expected to play a key part in the electrical properties of ZnO. Some of the key references on both H- and Li-impurities in ZnO were published already in the 1950s and 1960s, so questions about these impurities are not of new date.[14, 15, 16, 17] However, new experimental techniques have been developed since that time, like SIMS and PAS, which enable us to reveal more details of the effects observed in ZnO. As a curiosity, it could also be mentioned that a Norwegian paper on ZnO from 1935 is among the first papers which deals with this exciting material[18], so we may build on a long standing tradition when we dive into some of the mysteries of ZnO.

References

[1] Zorpette, G. Let there be light [gallium nitride LED]. *Spectrum, IEEE* **39**, 70–74 (2002).

[2] Narukawa, Y., Ichikawa, M., Sanga, D., Sano, M. & Mukai, T. White light emitting diodes with super-high luminous efficacy. *Journal of Physics D: Applied Physics* **43**, 354002 (2010).

[3] Jagadish, C. & Pearton, S. J. *Zinc oxide bulk, thin films and nanostructures: processing, properties and applications* (Elsevier, 2006).

[4] Fukuda, T. & Ehrentraut, D. Prospects for the ammonothermal growth of large GaN crystal. *Journal of Crystal Growth* **305**, 304–310 (2007).

[5] Light up the world foundation (2010). Http://www.lutw.org/.

[6] Http://nthambazale.com/2010/02/women-solar-engineers-in-malawi-villages/.

[7] (2010). Http://naturalpigments.com/detail.asp?PRODUCT_ID=475-31S.

[8] Takahashi, K., Yoshikawa, A. & Sandhu, A. *Wide bandgap semiconductors: fundamental properties and modern photonic and electronic devices* (Springer, 2007).

[9] Ellmer, K., Klein, A. & Rech, B. *Transparent conductive zinc oxide: basics and applications in thin film solar cells* (Springer, 2008).

[10] Prellier, W., Fouchet, A. & Mercey, B. Oxide-diluted magnetic semiconductors: a review of the experimental status. *Journal of Physics: Condensed Matter* **15**, R1583–R1601 (2003).

[11] Klingshirn, C. ZnO: from basics towards applications. *physica status solidi (b)* **244**, 3027–3073 (2007).

[12] Look, D. C. & Claflin, B. P-type doping and devices based on ZnO. *physica status solidi (b)* **241**, 624–630 (2004).

[13] Zhang, S. B., Wei, S. & Zunger, A. Intrinsic n-type versus p-type doping asymmetry and the defect physics of ZnO. *Physical Review B* **63**, 075205 (2001).

[14] Thomas, D. G. & Lander, J. J. Hydrogen as a donor in zinc oxide. *The Journal of Chemical Physics* **25**, 1136–1142 (1956).

[15] Lander, J. J. Reactions of lithium as a donor and an acceptor in ZnO. *Journal of Physics and Chemistry of Solids* **15**, 324–334 (1960).

[16] Hutson, A. R. Hall effect studies of doped zinc oxide single crystals. *Phys. Rev.* **108**, 222–230 (1957).

[17] Mollwo, E. Die wirkung von wasserstoff auf die leitfahigkeit und lumineszenz von zinkoxydkristallen. *Zeitschrift für Physik* **138**, 478–488 (1954).

[18] Brækken, H. & Jore, O. *Röntgenuntersuchungen über thermische Ausdehnung von Zinkoxyd und Berylliumoxyd*, vol. 1935, no. 8 of *Skrifter* (Universitetsforlaget, Trondheim, 1935).

Chapter 2

Single crystal ZnO

2.1 ZnO growth and basic properties

There are mainly three different ways of growing single crystal ZnO bulk material on an industrial scale; hydrothermal (HT), seeded chemical vapor transport (SCVT) and melt growth (MG).

ZnO has a melting point of $1975°$C. At these temperatures the O vapor pressure is high, which means that an over-pressure of oxygen is needed to favor growth. The extreme growth conditions due to presence of oxygen combined with temperatures as high as $2000°$C make melt growth a challenging task. Despite this, material of reasonably high quality is made by melt grown techniques with growth rates as high as 5 mm/h. However, large temperature gradients during growth result in material with residual strain. Low angle grain boundaries and high etch pit densities are typically found in MG ZnO.[1]

For the SCVT-growth ZnO powder is heated to $1150°$C in a sealed reactor tube, while a seed is kept in the other end of the tube at a slightly lower temperature of about $1100°$C. H_2 is added in the reactor tube as a carrier gas, where it helps to dissolve the ZnO powder since the O- and Zn- vapor pressure is relatively low at these temperatures. When H_2-reacts with the ZnO powder it forms water vapor and Zn-vapor and the lower temperature of the ZnO seed favor growth of single crystalline material. SCVT grown ZnO is of high quality and has low impurity concentrations, but it is not easily scalable, hard to control and combined with low growth rates makes SCVT ZnO an expensive alternative.

Hydrothermal growth is conducted in an autoclave fitted with an inner liner made of Ag or Pt, which is filled by ZnO pellets of high purity, an aqueous solution containing LiOH and KOH and

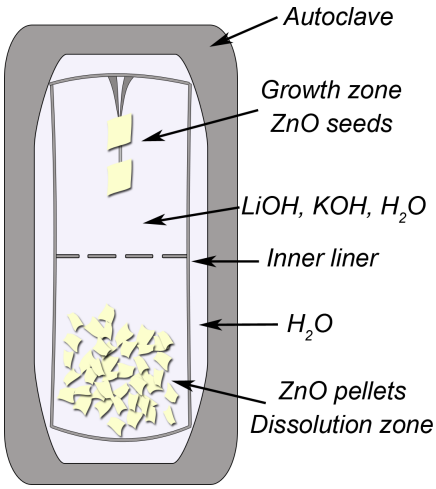

Figure 2.1: *Sketch the hydrothermal growth chamber. The inner liner is filled with a aqueous solution containing LiOH, KOH and/or NaOH. ZnO pellets are placed in the dissolution zone and ZnO seeds are suspended by Ti wires in the growth zone. The autoclave is heated and the growth zone is maintained at about* $20°C$ *below the dissolution zone to favor growth at the ZnO seeds. [1]*

ZnO seeds, see Fig. 2.1. The pellets are placed in the bottom (dissolution zone) of the liner and the seeds are suspended by Ti wires in the upper part (growth zone). The purpose of the liner is to avoid contamination from the autoclave and thus the liner is closed by welding before the growth starts. The autoclave is also closed and heated up to temperatures of $300°$C to $430°$C at pressures ranging between 70 MPa and 250 MPa. A temperature difference of $\leq 20°$C is maintained between the dissolution zone (hot) and the growth zone (cold), which leads to transport of ZnO by convection from the pellets towards the seeds. The lower temperature in the growth zone leads to supersaturation, which favor growth. The solution is kept under conditions that are above the critical point of water. At this point the solubility of ZnO is too low to facilitate proper growth, thus mineralizers as LiOH, NaOH and/or KOH are added to increase the solubility. A mix between LiOH and KOH has been found to give the best crystal quality. However, especially the presence of Li in the solution is found to contaminate the resulting material. E.g. in material obtained from SPC-Goodwill, the Li concentration is typically found in the 1-5$\times 10^{17}\,\mathrm{cm}^{-3}$-range (only in the $1\times 10^{15}\,\mathrm{cm}^{-3}$ range of K is observed).

Li is an amphoteric impurity in ZnO that may be in both a donor and acceptor state and typically leads to charge compensation.[2] Thus this electrically active defect is in general unwanted in

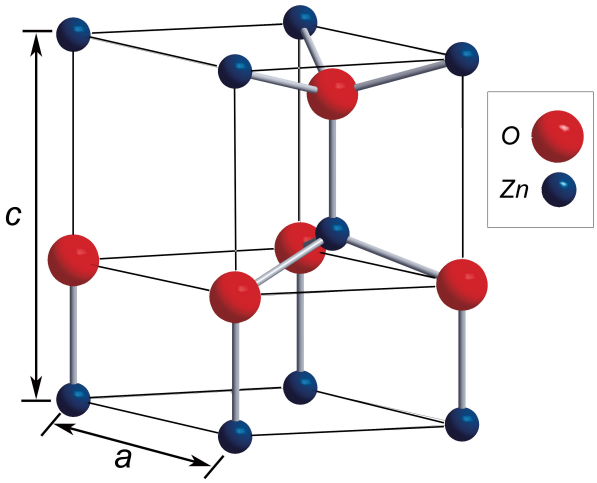

Figure 2.2: *Sketch of the wurtzite ZnO-structure*

the material and measures to remove it have to be investigated. The HT-ZnO material typically also contain other impurities like Al, Mg, Fe and Si ([3]). Nevertheless, hydrothermal growth leads to material of high quality and even though the growth rate is as low as $\leq$0.2 mm/day, the possibility to use several seeds in the same autoclave to scale up the growth process leads to relatively low costs as compared to the other techniques. In conclusion, hydrothermal growth is expected to be the most economically viable method to grow ZnO, as it has been for quartz and may prove to be for GaN growth[4]. However, more efforts are needed to reduce the amount of impurities in HT-ZnO. Extensive reviews of these growth techniques can be found both in Avrutin et al[1] and Özgür et al.[5].

ZnO normally grows in the wurtzite structure (see Fig. 2.2). However, under high over pressure (10-15 GPa) a phase transition of ZnO into the rocksalt structure can be obtained[6, 7], while the Zinc blende structure has only been observed when ZnO is grown on cubic substrates. [5]

In this work the focus is on hydrothermally grown material having the wurtzite structure. The experimentally observed lattice parameters are found to be a = 3.25 Å and c = 5.21 Å. [5, 8] The deviation in the ratio between c and a from an ideal hexagonal closed packed structure (c/a = $\sqrt{8/3} = 1.633$) combined with the partly ionic nature of the bonds and the lack of inversion symmetry along the c-axis yields a net dipole moment. As a result, ZnO shows a strong piezo-electric effect and the electrical potential of the $<0001>$-face and $<000\bar{1}>$-face differ from each

other. These two polar surfaces are usually referred to as the Zn-face and the O-face, respectively, named after the surface terminating species. When working with surface sensitive experiments on c-axis cut material the type of surface termination may influence on the observed effects.[5, 9]

As mentioned in the introduction, one of the main reasons to study ZnO is the wide band gap of 3.4 eV at room temperature in the wurtzite structure. Another interesting property usually pointed out, is the high exciton binding energy (60 meV) of ZnO as compared to GaN (25 meV). This means that excitons (quasi particles consisting of an electron bound to a hole) may exist at room temperature[5]. In general, recombination of electron and hole pairs can go through two different processes (i) direct where there is no difference between the momentum of the electron and hole and (ii) in-direct where the momentum of the two particles differ and to conserve the momentum the transition involves an additional coupling to phonons. In the first process the energy is emitted as light, while in the second process the energy may excite phonons, more commonly known as heating the material as opposed to emitting light.

The large band gap and the high exciton binding energy together should result in highly efficient direct optical transitions giving off photons with energy of the band gap, corresponding to ultra violet light. This may potentially then be realized as light emitting diodes (LEDs) or even as room temperature laser diodes (LDs).[10] The problem, however, is the lack of good, low resistive and stable, p-type material. Several groups have tried to circumvent this problem by using hetrojunctions, but to fully utilize the potential of the exitonic binding energy in ZnO the optical transition has to take place inside ZnO. More importantly, hetrojunctions will typically have high concentration of recombination centers and traps, strongly affecting the performance of such a device.

2.2 Semiconductor basics

To understand the difficulties of p-type doping in ZnO presented in the next section a short introduction to some semiconductor basics is needed. First lets start with the simplest case in quantum mechanics, namely the H-atom. When performing a quantum mechanical calculation of the energy states for a H-atom the energy is related to the vacuum level of the system. The ground state is found to be 13.6 eV below the vacuum level and in addition there exist a quantified number of energy states, which the electron can occupy by gaining additional energy from its environment. The fact that the electron energy may only increase in discrete steps in contrast to

an continuous increase is one of the fundamental properties that was first explained by quantum mechanics.

In solid-state materials electrons gain one additional degree of freedom as compared to those in atoms, in addition to the electron-energy they are also described by their momentum (or direction of movement). Thus the energy states describing electrons in isolated atoms are extended to include also the electron momentum. The energy state varies as a function of the electron momentum, commonly referred to as energy bands. In other words, the energy of the state an electron can occupy, depends on the direction it moves in the material.

In a slab of material, which does not experience any external electric or magnetic fields, the effective electron movement is zero. The result of applying an electric field over a piece of a solid-state material defines what type of material it is. The three main types of materials are metals, semiconductors and insulators. In metals the energy bands overlap and the electron-energy may vary continuously and thus the electrons are able to respond instantaneously to the applied field by setting up a net current in the metal. For insulators and semiconductors there exist a gap in the energy bands and all the electron states up to this gap are filled by electrons. Thus to be able to change the net electron movement in the material, electrons have to gain enough energy to overcome this gap (band gap) and thus the lack of available electron states effectively limits the possibility to drive a current through the material. The difference between isolators and semiconductors is merely the size of the band gap and in practical terms also the ability to obtain low and high charge carrier (electrons and holes) concentrations, respectively.

In general the energy band just below the band gap is referred to as the valence band, while the band situated above the gap is referred to as the conduction band. In semiconductors the materials ability to transport current depends mainly on the number of available charge carriers. Charge can be carried both by electrons in the conduction band (n-type doping) or by holes in the valence band (p-type doping). A hole is a quasiparticle, referring to the situation where one electron is missing in the valence band. Originally filled electron states close to the conduction band (shallow donors) work as efficient n-type dopants (results in excess of free electrons) while empty states close to the valence band (shallow acceptors) work as efficient p-type dopants by accepting electrons from the valence band by thermal excitation, leaving an empty state (a hole) in the valance band. The ability to introduce a large amount of charge carriers by doping is what in reality separates a semiconductor material from a electrically isolating material. Junctions of p- and n-doped materials are the basis of diodes and transistors and are thus essential for utilizing most of the semiconductor applications.

The Fermi level position is a measure of the electronic state of the semiconductor and is defined as the first empty electron state at T = 0 K. However, it is also commonly used for any temperature, where it may be viewed as the energy needed to move an electron from a reservoir into the material, i.e. the lowest available energy state of the system, or alternatively, the energy where half of the available states are filled. The Fermi level is typically given in reference to the valence band maximum (VBM) and/or the conduction band minimum (CBM).

There are several limitations to successful doping of semiconductors. One is the solubility of a given impurity in the crystal. Another is the energy of formation, where a high formation energy will efficiently reduce the probability of formation of that specific defect. For charged defects the formation energy depends on the Fermi level position and is also highly dependent on the chemical composition of the material. For instance in ZnO the formation energy of the Zn-vacancy (V_{Zn}) is higher in Zn-rich material than in O-rich material and the doubly negative acceptor state is more favorable in n-type material than in p-type material etc.

2.3 The p-type challenge

In several wide band gap semiconductors (ZnO, GaN, ZnTe etc) one typically experience difficulties in obtaining both efficient n- and p-type doping of the same material. Some materials favor n-type (ZnO, GaN) while other favor p-type doping (ZnTe). The observed doping limitations cannot be explained by the size of the band gap alone since materials with similar band gap size exhibit completely different doping behavior (e.g. ZnO and ZnTe).[11] However, the so-called amphoteric defect model (ADM), where doping induced amphoteric[1] defects are predicted to lead to compensation, provides a phenomenological rule that explains the experimentally observed trends over a range of semiconductor materials, including ZnO.[11, 12] As mentioned in the previous section the electrical properties of a semiconductor is usually described by the Fermi level position in reference to the band gap edges. However, within the ADM it is argued that to understand the doping limitations the relevant reference point is the vacuum level.

Prior to the amphoteric defect model it had been found that when doping with transition metals the position of the impurity energy level did not show any clear trend in reference to the band gap edges for different semiconductor materials. However, when the same levels were referred to the vacuum level instead, a remarkable material invariance of the levels in III-V and II-VI

[1] Can act both as a donor and an acceptor depending on the Fermi level position

semiconductors was found.[13] This is understandable since transition metal impurities typically lead to highly localized states in the band gap, where the atomic energy states (as referred to the vacuum level) are only slightly perturbed by the host lattice. This means that the position of the energy states of the transition metal impurities can inversely be used to align the semiconductor band edges to the vacuum level and thereby acting as a reference for comparing the band edges in between different semiconductor materials.

A similar reference point can be found in materials that have been heavily irradiated. The irradiation will induce intrinsic defects, which may be of amphoteric nature. After a sufficiently high irradiation dose the defects are observed to self compensate and lead to so called Fermi level pinning, where the Fermi level becomes insensitive to further damage caused by the irradiation.[11] The Fermi level pinning position is material specific and can be viewed as an intrinsic property of the material. Walukiewicz et al. refer to this Fermi level pinning energy as the stabilization energy E_{FS}, which is found to be about 4.9 eV below the vacuum level over a range of materials.[11] It is argued that for the formation of such compensating defects it is not the Fermi level deviation from the mid band gap that is important, but rather the deviation from E_{FS}. A similar process can also explain the doping limitations as found in wide band gap materials, where a large deviation from E_{FS} caused by deliberate doping leads to the lowering of the formation energy of undesired compensating defects. According to Walukiewicz [11] the effective equilibrium doping limits are given by E_{FS} $\pm 1.3\,\mathrm{eV}$. In Zang et al.[14] theoretically predicted and experimentally determined doping levels for a range of materials are presented. In ZnO the conduction band minimum is found to be only 0.2 eV above the E_{FS}, thus explaining why it is relatively easy to obtain high n-type conductivity while p-type conductivity is difficult, if not even impossible, since a deviation of about 3 eV from E_{FS} is necessary to obtain low resistive p-type material.[11, 14]

The amphoteric defect model does indeed explain the trends observed over a range of semiconducting materials with regards to doping limits and points out exactly how big of a challenge it is to obtain p-type doping in ZnO. It also clearly shows that to obtain p-type doping the way to go is out of equilibrium.[15] One line of investigation that has been proposed is to use neutral complexes consisting of an acceptor of choice together with a donor, which may be removed in a post processing step. In this way the idea is that the system is only forced out of equilibrium after the main processing steps are performed. The donor usually mentioned is H.[16, 17, 18, 19, 20] Thus the properties of H both as a compensating donor and as one of the candidates for the inherent n-type activity as found in all as-grown materials is important and is also the topic of the next section. However, it should also be mentioned that in spite of the big challenge there are several

claims of successful p-type doping and even some reports that claim operational light emitting diodes.[21, 22] So there is definitively light in the end of the tunnel.

2.4 Hydrogen and n-type conductivity

In the as-grown state ZnO is always n-type. The source of the n-type conductivity is still not fully understood, in spite of huge efforts to reveal the mechanisms behind it. Since the different growth techniques all produce n-type material, the first assumption that one can make is that there is only one defect present in all samples responsible for the n-type activity. Originally it was thought that a native defect such as zinc interstitial (Zn_i) or oxygen vacancy (V_O) was the source of n-type conductivity in ZnO. [23, 24, 25]

Later it has been found from first principle calculations that the formation energy for these defects is relatively high, so one should not expect any considerable amount of the mentioned point defects to be present in the material. The one with the lowest formation energy is V_O. However, this defect seems to induce a donor state which is too deep to account for the observed n-type activity. In addition, V_O is predicted to behave as a negative U-center, where the doubly negative charge state is more favorable than the singly negative charge state.[26] In 2000 Van de Walle et al.[27] suggested that hydrogen could be the source of the n-type conductivity. Based on first principle calculations they found that H only acts as a donor in ZnO (and may thus passivate acceptors only). This is in contrast to what is found in other semiconductors, like Si, where H typically passivate both acceptors and donors. H is also a readily available impurity, which easily could be present in material originating from all the different growth techniques. Donor activity from H was observed already by Thomas and Lander [28] in 1956 and Hutson et al. [29] in 1957. The donor activity of H has also more recently been confirmed by several authors [30, 31, 32, 33], responding to the proposal by Van de Walle. H is thus shown to have both the means and possibility to be responsible for the unintentional n-type conductivity in ZnO. A thorough review on the role of H in ZnO is given by Monakhov et al.[9].

However, based on infrared absorbtion spectroscopy measurements [33, 34, 35, 36], H effusion measurements [32, 37] and thermal treatment of implanted ^{2}H as measured by secondary ion mass spectrometry[38] the thermal stability of H in ZnO is typically found to be low, ranging from 150°C-750°C. At the same time high temperature heat treatment at 1500°C is shown to decrease, not increase, the resistivity by several orders of magnitude in HT-ZnO. This is evidence of a donor with high thermal stability and thus not consistent with the findings for H.[3, 39]

From temperature dependent Hall measurements on as-grown samples it is also found that H is a relevant, but not dominant donor.[40] These examples show that H contributes to donor activity, but it cannot be the only active n-type dopant responsible for the inherent n-type activity in all samples. It should also be noted that in most of the samples where donor related vibrational O-H modes have been studied, H have been deliberately introduced.[34, 41] In as-grown HT-ZnO the dominating OH-related vibrational mode is the one observed at 3577 cm^{-1}. This mode is, however, suggested to originate from a neutral complex consisting of OH-Li_{Zn}.[42, 43, 44] Thus being an example of acceptors passivation rather than donor activity. As mentioned in the previous section utilizing the ability of H to passivate acceptors is part of a suggested route to obtain p-type doping where H is removed at a later stage. Acceptor passivation will of course indirectly contribute to the n-type conductivity, however this can not explain the intrinsic n-type activity on its own and it is clear that H cannot be the only source of the unintentional n-type doping in ZnO grown by different methods.

2.5 Origin of the inherent n-type activity

As pointed out by Vines et al. [3] and McCluskey et al. [45] there are also other sources of n-type doping like Al, Ga, Si[46] etc. present in samples originating from several of the ZnO-growth techniques. The more likely scenario is thus that the n-type activity does not originate from only one type of defect, but rather vary depending on the growth technique and possibly also from wafer to wafer from the same growth process.

References

[1] Avrutin, V. *et al.* Bulk zno: Current status, challenges, and prospects. *Proceedings of the IEEE* **98**, 1339 –1350 (2010).

[2] Lander, J. J. Reactions of lithium as a donor and an acceptor in ZnO. *Journal of Physics and Chemistry of Solids* **15**, 324–334 (1960).

[3] Vines, L. *et al.* Lithium and electrical properties of ZnO. *Journal of Applied Physics* **107**, 103707 (2010).

[4] Fukuda, T. & Ehrentraut, D. Prospects for the ammonothermal growth of large GaN crystal. *Journal of Crystal Growth* **305**, 304–310 (2007).

[5] Özgür, Ü. *et al.* A comprehensive review of ZnO materials and devices. *Journal of Applied Physics* **98**, 041301 (2005).

[6] Bates, C. H., White, W. B. & Roy, R. New High-Pressure polymorph of zinc oxide. *Science* **137**, 993 (1962).

[7] Karzel, H. *et al.* Lattice dynamics and hyperfine interactions in ZnO and ZnSe at high external pressures. *Physical Review B* **53**, 11425 (1996).

[8] Norton, D. P. *et al.* ZnO: growth, doping & processing. *Materials Today* **7**, 34–40 (2004).

[9] Monakhov, E. V., Kuznetsov, A. Y. & Svensson, B. G. Zinc oxide: bulk growth, role of hydrogen and schottky diodes. *Journal of Physics D: Applied Physics* **42**, 153001 (2009).

[10] Huang, M. H. *et al.* Room-Temperature ultraviolet nanowire nanolasers. *Science* **292**, 1897–1899 (2001).

[11] Walukiewicz, W. Intrinsic limitations to the doping of wide-gap semiconductors. *Physica B: Condensed Matter* **302-303**, 123–134 (2001).

[12] Walukiewicz, W. Amphoteric native defects in semiconductors. *Applied Physics Letters* **54**, 2094–2096 (1989).

[13] Caldas, M. J., Fazzio, A. & Zunger, A. A universal trend in the binding energies of deep impurities in semiconductors. *Applied Physics Letters* **45**, 671 (1984).

[14] Zhang, S. B., Wei, S. & Zunger, A. A phenomenological model for systematization and prediction of doping limits in II–VI and I–III–VI[sub 2] compounds. *Journal of Applied Physics* **83**, 3192 (1998).

[15] Zhang, S. B. The microscopic origin of the doping limits in semiconductors and wide-gap materials and recent developments in overcoming these limits: a review. *Journal of Physics: Condensed Matter* **14**, R881–R903 (2002).

[16] Vechten, J. A. V., Zook, J. D., Horning, R. D. & Goldenberg, B. Defeating compensation in wide gap semiconductors by growing in h that is removed by low temperature De-Ionizing radiation. *Japanese Journal of Applied Physics* **31**, 3662–3663 (1992).

[17] Yan, Y., Li, J., Wei, S. & Al-Jassim, M. M. Possible approach to overcome the doping asymmetry in wideband gap semiconductors. *Physical Review Letters* **98**, 135506 (2007).

[18] Lee, E. & Chang, K. P-type doping with group-I elements and hydrogenation effect in ZnO. *Physica B: Condensed Matter* **376-377**, 707–710 (2006).

[19] Jokela, S. J. & McCluskey, M. D. Structure and stability of N–H complexes in single-crystal ZnO. *Journal of Applied Physics* **107**, 113536 (2010).

[20] Jokela, S. J. & McCluskey, M. D. Unambiguous identification of nitrogen-hydrogen complexes in ZnO. *Physical Review B* **76**, 193201 (2007).

[21] Look, D. C. & Claflin, B. P-type doping and devices based on ZnO. *physica status solidi (b)* **241**, 624–630 (2004).

[22] Tsukazaki, A. *et al.* Blue Light-Emitting diode based on ZnO. *Japanese Journal of Applied Physics* **44**, L643–L645 (2005).

[23] Look, D. C., Hemsky, J. W. & Sizelove, J. R. Residual native shallow donor in ZnO. *Physical Review Letters* **82**, 2552 (1999).

[24] Kasai, P. H. Electron spin resonance studies of donors and acceptors in ZnO. *Physical Review* **130**, 989 (1963).

[25] Kohan, A. F., Ceder, G., Morgan, D. & de Walle, C. G. V. First-principles study of native point defects in ZnO. *Physical Review B* **61**, 15019 (2000).

[26] de Walle, C. G. V. Defect analysis and engineering in ZnO. *Physica B: Condensed Matter* **308-310**, 899–903 (2001).

[27] de Walle, C. G. V. Hydrogen as a cause of doping in zinc oxide. *Physical Review Letters* **85**, 1012 (2000).

[28] Thomas, D. G. & Lander, J. J. Hydrogen as a donor in zinc oxide. *The Journal of Chemical Physics* **25**, 1136–1142 (1956).

[29] Hutson, A. R. Hall effect studies of doped zinc oxide single crystals. *Phys. Rev.* **108**, 222–230 (1957).

[30] Cox, S. F. J. *et al.* Experimental confirmation of the predicted shallow donor hydrogen state in zinc oxide. *Physical Review Letters* **86**, 2601 (2001).

[31] Hofmann, D. M. *et al.* Hydrogen: A relevant shallow donor in zinc oxide. *Physical Review Letters* **88**, 045504 (2002).

[32] Nickel, N. H. & Brendel, K. Hydrogen density-of-states distribution in zinc oxide. *Physical Review B* **68**, 193303 (2003).

[33] McCluskey, M. & Jokela, S. Hydrogen donors in zinc oxide. In *Zinc Oxide — A Material for Micro- and Optoelectronic Applications*, 125–132 (Springer, 2005).

[34] Lavrov, E. V., Weber, J., Börrnert, F., de Walle, C. G. V. & Helbig, R. Hydrogen-related defects in ZnO studied by infrared absorption spectroscopy. *Physical Review B* **66**, 165205 (2002).

[35] Li, Y. J., Zhang, B. & Lu, W. Infrared absorption spectroscopy on OH–Ni complex in hydrothermally grown ZnO. *Journal of Applied Physics* **105**, 093516–6 (2009).

[36] Herklotz, F., Lavrov, E. V., Kolkovsky, V., Weber, J. & Stavola, M. Charge states of a hydrogen defect with a local vibrational mode at 3326 cmˆ-1 in ZnO. *Physical Review B* **82**, 115206 (2010).

[37] Nickel, N. H. Hydrogen migration in single crystal and polycrystalline zinc oxide. *Physical Review B* **73** (2006).

[38] Ip, K. *et al.* Hydrogen incorporation and diffusivity in plasma-exposed bulk ZnO. *Applied Physics Letters* **82**, 385 (2003).

[39] Svensson, B. G. *et al.* Hydrothermally grown single-crystalline zinc oxide; characterization and modification. In *Mater. Res. Soc. Symp. Proc.*, vol. 1035, L04–01 (2008).

[40] Look, D. C., Coskun, C., Claflin, B. & Farlow, G. C. Electrical and optical properties of defects and impurities in ZnO. *Physica B: Condensed Matter* **340-342**, 32–38 (2003).

[41] Jokela, S. J., McCluskey, M. D. & Lynn, K. G. Infrared spectroscopy of hydrogen in annealed zinc oxide. *Physica B: Condensed Matter* **340-342**, 221–224 (2003).

[42] Lavrov, E. V., Börrnert, F. & Weber, J. Dominant hydrogen-oxygen complex in hydrothermally grown ZnO. *Physical Review B* **71**, 035205 (2005).

[43] Shi, G. A., Stavola, M. & Fowler, W. B. Identification of an OH-Li center in ZnO: infrared absorption spectroscopy and density functional theory. *Physical Review B (Condensed Matter and Materials Physics)* **73**, 081201–3 (2006).

[44] Halliburton, L. E. *et al.* Infrared absorption from OH[sup -] ions adjacent to lithium acceptors in hydrothermally grown ZnO. *Journal of Applied Physics* **96**, 7168–7172 (2004).

[45] McCluskey, M. & Jokela, S. Sources of n-type conductivity in ZnO. *Physica B: Condensed Matter* **401-402**, 355–357 (2007).

[46] Das, A. K., Misra, P. & Kukreja, L. M. Effect of si doping on electrical and optical properties of ZnO thin films grown by sequential pulsed laser deposition. *Journal of Physics D: Applied Physics* **42**, 165405 (2009).

Chapter 3

Methodology

The main characterization techniques employed in this thesis are: secondary ion mass spectrometry, Fourier transformed infrared spectroscopy and positron annihilation spectroscopy. A short review of these techniques will be given in the following sections.

3.1 Secondary Ion Mass Spectrometry (SIMS)

SIMS is a focused ion beam technique where primary ions are used to sputter a crater in the sample under investigation. A secondary ion beam is created by accelerating the charged atoms and molecules emerging from the sputtered crater. This secondary ion beam is then analyzed in a mass spectrometer and the ion intensity is measured as a function of magnetic field strength, time or position (or combinations of these). In this way the system has the ability to record mass spectra, impurity depth profiles and to study differences in the impurity concentrations along the lateral directions by ion-imaging. Fig. 3.1 shows an overview of a magnetic sector instrument, illustrating the primary ion beam, the secondary ion beam, the spectrometer and the three different measurement modes mentioned. By the use of standards it is also possible to quantify the concentration of a given species as a function of depth in the sample. The ability to produce quantified results with parts per billion sensitivity and dynamic range over 5 orders of magnitude makes SIMS very well suited to study impurities in semiconductors.

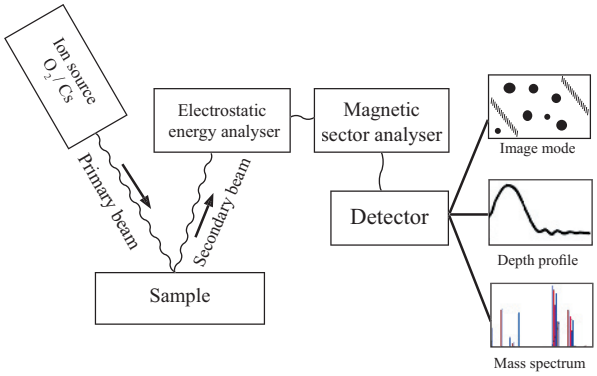

Figure 3.1: *Sketch of a dynamic SIMS with a magnetic sector spectrometer, showing the capability of recording both ion images, mass spectra and impurity depth profiles.*

3.1.1 Instrumentation

A SIMS-instrument is usually categorized by the type of mass spectrometer used. There are three types of spectrometers available (i) time of flight (TOF), (ii) quadrupole and (iii) sector magnet spectrometers.

In a TOF-spectrometer a pulsed primary ion beam is used to sputter the studied sample. For each primary ion pulse, the secondary ions having the same kinetic energy are selected and then allowed to travel down a long path before they reach the detector. Given the same kinetic energy, light elements have higher velocity than heavy elements and the light elements will therefore reach the detector first, thus the long path separates the ions in time depending on their mass. The strength of this technique is the ability to study the composition of a single monolayer in the sample under investigation, since the primary ion beam intensity is usually kept so low that only in the range of 1% of a monolayer of the sample is removed by each pulse (static mode). This technique is thus well suited to study surfaces or thin films, large molecules/organic material and material with high resistivity. In addition, both the mass spectrum and depth profiles can be recorded simultaneously. The quadrupole spectrometer is mainly used in the case of low energy primary beams while the sector magnet spectrometers are preferred due to their higher mass resolution and improved sensitivity. In the next section a more thorough treatment of the magnetic sector spectrometer will be given.

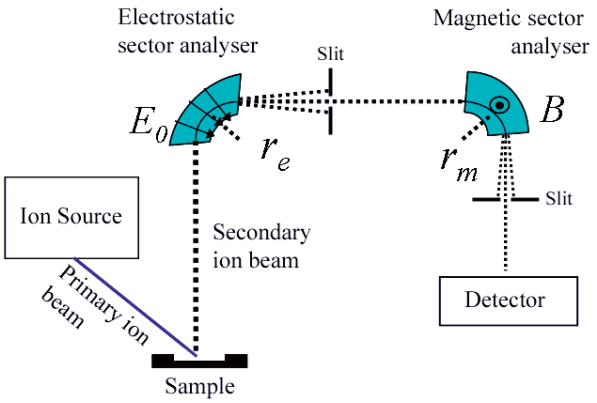

Figure 3.2: *The electrostatic energy analyser shown together with the rest of the magnetic sector spectroscope. r_e and r_m are the curving radius of a given ion traveling through the energy filter and magnetic sector spectrometer, respectively.*

3.1.2 Theory

In this thesis a Cameca IMS-7f system equipped with both a Duoplasmatron (normally operated with oxygen) and a cesium primary ion source and a magnetic sector spectrometer have been used. Fig.3.2 shows a sketch of the magnetic sector spectrometer. A continuous primary ion beam is rastered over an area in a typical range of $50\times50\,\mu m^2$ up to $500\times500\,\mu m^2$. A crater is sputtered in the sample and the ionized part of the sputtered particles emerging from the crater is accelerated towards an electrostatic energy analyser (ESA). The ESA is constructed of two curved metallic plates in parallel, which both repel the ions forcing them to follow the curvature. In a linear homogenous electric field the force applied to each ion $\vec{F}$ equals the electrostatic potential E_0 times the elementary charge q, which is countered by the centripetal force:

$$\vec{F} = -\frac{mv_e^2}{r_e}\frac{\vec{r_e}}{r_e}, \tag{3.1}$$

where m is the mass of an atomic ion or ionized molecule (for simplicity both will be referred to as ions in the following text), v_e is the velocity of the ion when traveling through the electrostatic analyzer and $\vec{r_e}$ is the radius of the metallic plate curvature. Thus only the ions having a kinetic energy matching the curvature radius r_e (which is controlled by the electric field E_0) will pass through the ESA-exit slit and continue into the magnetic sector analyser (MSA). In the MSA

there is a magnetic field ($\vec{B}$) perpendicular to the beam trajectory. This will again bend the secondary ion beam as described by the Lorentz force:

$$\vec{F} = q(\vec{v}_m \times \vec{B}), \tag{3.2}$$

where q is the charge of the ion/molecule and v_m is the ion velocity through the MSA. Thus from the ESA and the MSA we get, respectively:

$$qE_0 = \frac{mv_e^2}{r_e}, qvB = \frac{mv_m^2}{r_m}, \tag{3.3}$$

where r_e and r_m is the curving radius of the ions passing through the electrostatic (E_0) and magnetic field (B) respectively. Assuming that there is no loss in energy when passing through the analysers the velocity v_e of the ion in the electrostatic sector analyser equals the v_m in the magnetic sector analyzer. Therefore only the ions that satisfy the following equation will be let through the MSA-exit slit and hit the detector:

$$\frac{m}{q} = \frac{(r_m B)^2}{r_e E_0}, \tag{3.4}$$

where E_0, r_m and r_e are kept constant. Thus depending on the amplitude of the magnetic field any given ratio between the charge and mass of the ion can be selected by the combination of both the electrostatic and the magnetic fields. The secondary ion beam intensity is then recorded by an electron multiplier or Faraday cup as a function of time, magnetic field or primary ion beam position.

To obtain quantitative results the recorded intensity must be related to the concentration of each element. The proportionality between the recorded secondary ion intensity and the actual concentration depends on the species investigated and the material studied. The intensity (I_t) for a given ion t is:

$$\mathrm{I}_t = \mathrm{I_P Y} \gamma_t \mathrm{T C}_t \tag{3.5}$$

where I_P is the primary ion beam intensity, Y is the sputtering yield, γ_t is the ionization efficiency, T is the instrument transmission function and C_t is the actual concentration of species t. The I_P is set for each measurement and is usually in the range from 10 nA up to 1 μA. I_P equal to 100 nA is the most commonly used value in this work.

The sputtering yield Y depends on the primary ion mass, energy and angle of incidence and the matrix of the sputtered sample. For an extensive review of the sputtering process, please refer to

Sigmund[1]. The dependence of the matrix means that one needs to be especially careful when measuring layered structures/heterostructures or heavily doped material (typically 1% or above). As an example the sputtering yield may change by a factor of almost 3 when going from pure Si to pure Ge [2].

The ionization probability γ_t, also called the secondary ion formation and survival probability depends on the element under consideration, the matrix, and the type of primary ion used. The Cameca IMS-7f system has two primary ion sources, a Cs source and a Duoplasmatron. The Duoplasmatron source is usually operated with O_2-gas, however other gas sources like H_2 and Ar may also be used. The Cs- or Duoplasmatron sources are used depending on the ionization potential and electron affinity of the element studied. For elements having high ionization potential (which requires a large energy to remove one electron) the Cs-source is used, since it is one of the most electropositive elements of the periodic table and thus increases the probability of negative ionization instead. However, negative ionization depends on the electron affinity of the element under investigation. Nitrogen is an example of an element with high ionization energy and zero electron affinity, thus when measuring N a molecule, which include N is preferable. This of course, severely limits the sensitivity for N and the secondary ion intensity may also be limited by the other constituents of the molecule and not give reliable results. For elements with low ionization potential the Duoplasmatron is used to increase the probability of positive ionization, since O itself is strongly electronegative. In practical terms for this work this means that to measure H or D the Cs-source is used, while the Duoplasmatron (with O_2) is used to study Li, Na, K etc. in ZnO. Unfortunately, no quantitative theoretical models exist for predicting the ionization probability.

The instrument transmission function T is an instrument specific parameter. It also depends on the secondary apertures, which are set for each measurement. The Cameca IMS-7f have four contrast apertures (CA) and four field apertures (FA) to choose from on the secondary beam line. The sizes of the apertures are given in table 3.1. Both CA and FA can be used to limit the secondary ion current, in addition CA is used to control the image contrast while FA defines the size of the analyzed area together with the max area (defined in the measurement setup with a typically diameter of 150 μm):

$$\text{Analyzed area diameter} = \frac{\text{FA} \times \text{Max area diameter}}{1800(\mu m)}. \tag{3.6}$$

Thus FA1 is mainly used for beam alignment. While FA2 or FA3 are typically used for measurements. FA4 is used in special cases mainly to limit the secondary ion intensity even further. As

Table 3.1: *Overview of the available secondary beam line field- and contrast apertures (FA and CA, respectively) Diameter size in μm*

	FA	CA
1	1800	400
2	750	150
3	400	50
4	100	20

an example, when using FA3 the analyzed area is 33 μm^2. In addition to the aperture there is an electronic filter limiting the analyzed area (typically to 70%) of the raster size. By limiting the recorded ion-intensity to the center of the crater secondary ions emerging from the crater walls are excluded. This is especially important when measuring with a small raster size and recording abrupt depth distributions.

All the proportionality factors are commonly collected into one, which is called the sensitivity factor $S_f = I_P Y \gamma_t T$. Calculating the sensitivity factor for each element is not trivial, thus a common approach is to use samples implanted with a known dose of the element of interest to produce a reference sample. As mentioned the effect of the matrix may be large, therefore it is important to use a reference sample, which is as close as possible to the sample that will be studied. The sensitivity factor is then found as the ratio between the secondary ion beam intensity I_t (counts/second) and the known concentration (typically in 1/cm^3) of the specific impurity for a given set of measurement conditions.

The sensitivity for Li in ZnO is typically high, where concentrations as low as $1\times10^{13}\,\mathrm{cm}^{-3}$ can be measured. However, even though the instrument runs under ultra high vacuum conditions, H in the sample chamber is responsible for a noise signal, setting the detection limit, normally, to about $1\times10^{18}\,\mathrm{cm}^{-3}$ and only under good conditions one may reach $5\times10^{17}\,\mathrm{cm}^{-3}$. It is worth noting, that the ionization efficiency of H in ZnO is relatively low as compared to other materials like, e.g., Si. However, by using ^{2}H instead of H the detection limit may be lowered to below $10^{15}\,\mathrm{cm}^{-3}$.

3.1.3 Mass spectrum

As seen from Eq. 3.4, when recording the secondary ion intensity as a function of the magnetic-field in the MSA a mass spectrum of all the ions emerging from the sample can be obtained.

However, mainly due to the differences in ionization potential between the elements such a mass spectrum can only give qualitative information and may not be used to quantify differences between the impurity elements present in the sample without specific calibration of each element separately.

3.1.4 Depth profiling

The measurement mode mostly used in this thesis is the recording of depth profiles. The magnetic field is then cycled for one or more fixed values corresponding to the charge to mass ratio of interest and the secondary ion intensity is then recorded as a function of time for each element. The time can be converted to depth if the erosion rate is known. The erosion rate E_r is in general proportional to the primary ion beam intensity I_P and the inverse of the raster area (S):

$$E_r = \alpha \frac{I_P}{S}, \tag{3.7}$$

where the proportionality constant α depends on the material sputtered and the type and energy of the primary ion beam. α can be found by assuming a constant erosion rate and by measuring the depth of the resulting crater by e.g. a Dektak Stylus profilometer.

The erosion rate is constant as long as the primary ion beam intensity is constant and the measured sample is homogeneous, i.e. all impurity variations in the matrix are below $\sim$1%. When measuring heterostructures the erosion rate for each material needs to be examined first and taken into account when calibrating the depth scale.

3.1.5 Ion imaging

The third possibility is to record the secondary ion intensity as a function of primary ion beam position during rastering to produce an ion image. In this mode the primary ion current is typically low (1-10 nA) to obtain a small beam spot size. Further, it is possible to obtain a spatial resolution of less than 1μm and when the measurement is done in combination with cycling of the magnetic field ion images for several ions can be obtained from the same measurement.

3.1.6 Electron gun

Since SIMS relies on a focused primary ion beam, the sample needs to have a low enough resistivity to remove excess charge for proper secondary ion detection. The Cameca IMS-7f has a built-in electron gun directed towards the sample for charge compensation. However, such charge compensation has a limited capability making the present setup unsuitable for thick insulating layers.

3.2 Fourier transformed infrared absorption spectroscopy (FTIR)

Infrared absorption spectroscopy is a technique where infrared (IR) light is absorbed by matter. IR-light over a range of frequencies is either reflected from or transmitted through the sample of interest and the resulting spectrum is then compared to a reference spectrum (e.g. measured in vacuum or a relevant reference sample). In this way the samples ability to absorb light may be studied over a range of frequencies. The technique has traditionally been used to study vibrations of molecular bonds in the gas- or liquid phase and is commonly used in identification of different molecules and constituents. However, it may also be extended to study defects in solid state material, including semiconductors.

3.2.1 Theory

In general, a molecule consisting of N atoms have 3N degrees of freedom, 3 of which are rotational, 3 translational and the remaining 3N-6 are vibrational modes [3]. The vibrational modes of a diatomic molecule can in the simple cases be described using Newtonian mechanics, where the atoms can be viewed as two point masses connected by a massless spring. For small displacements (harmonic approximation) the force (F) is proportional to the displacement (x) as described by Hook's law; $F = -kx$, where k is the force constant (in units of N/m). The vibration (x(t)) can be described by solving Newtons second law:

$$-kx(t) = \mu \frac{d^2x(t)}{dt^2}, \tag{3.8}$$

$$x(t) = A\cos\omega t, \tag{3.9}$$

where A is the maximum displacement, $\omega = \sqrt{k/\mu}$ is the angular frequency and $\mu = \frac{m_1 m_2}{m_1+m_2}$ is the reduced mass. One of the key features of IR-spectroscopy is the possibility to observe shifts

in the frequency when replacing one of the elements (m_1) with another isotope (m_1^*) of the same element. Assuming that the chemical bond will be unchanged ($k = k^*$), the shift only depends on the change of mass. The vibrational frequency will then change according to:

$$\frac{\omega}{\omega^*} = \sqrt{\frac{k}{\mu}\frac{\mu^*}{k^*}} = \sqrt{\frac{(m_1+m_2)}{m_1 m_2}\frac{m_1^* m_2}{m_1^*+m_2}}. \tag{3.10}$$

Even though this simple model actually gives a quite accurate description of the molecular vibrations, it fails to describe the interaction with light and for this a quantum mechanical approach is needed. Solving the Schrödinger equation for a harmonic potential of $U(x) = \frac{1}{2}kx^2$ one can find that the vibrational energy of an harmonic oscillator is:

$$E_{vib} = \hbar\omega(n + \frac{1}{2}), \tag{3.11}$$

where $\hbar$ is the reduced Planck's constant (1.05457×10^{-34} Js) and n is the quantum number that take integer values of 0,1,2, etc, each one characterizing a different eigenstate of the harmonic oscillator. These energy states also describe the molecules ability to absorb light. Only transitions from one eigenstate to another are allowed, thus only light with an energy matching the transition may be absorbed. The energy of light is given as $E = \hbar\omega$. In the spectroscopic tradition, the wave number unit $\tilde{\nu}$ (cm^{-1}) is normally used, given by:

$$\tilde{\nu} = \frac{1}{\lambda} = \frac{\omega}{2\pi c}, \tag{3.12}$$

where λ is the wave length and c is the speed of light (2.9979×10^{10} cm/s). The wave number is proportional to the energy as $E = 1.24 \times 10^{-4}\,\tilde{\nu}$ eV cm. The energy difference of transitions from the ground state (n=0) to the first excited state (n=1) of most vibrational modes correspond to absorption in the mid-infrared range (400-4000 cm^{-1}), making IR spectroscopy a useful tool to study such vibrations[3]. However, the electromagnetic waves of light can only interact with the vibrational modes, which have a time-varying electric dipole moment. As a consequence of this, symmetrical stretch modes like that of the H_2-molecule cannot be observed by IR-spectroscopy. Such modes can, however, be studied by Raman spectroscopy, which is a complementary technique where a laser is used to excite modes by inelastic scattering in the material. The corresponding shift in frequency of the scattered light is then related to vibrational modes in the material. As an example, Lavrov et al.[4] have, based on the combined efforts of both Fourier transformed infrared spectroscopy and Raman spectroscopy, studied different states

of H in ZnO including H_2.

When extending this treatment to solid-state materials, first of all, translational and rotational modes will no longer be available for excitation. The second difference is that instead of exciting local modes as described above, the whole of the lattice will be affected and thus a set of vibrational waves propagating throughout the lattice will be formed, called phonons. These phonons are quasi particles, which carry lattice vibrations throughout the material and thus play an important role in the physical properties of solids, like electrical- and thermal conductivity. Phonons may be longitudinally- (where the atomic vibration is in the same direction as the propagating wave) or transversally polarized (where they vibrate normal to the direction of the propagating wave). In addition, when considering materials with two (or more) elements in the primitive cell, the two elements may vibrate in phase or out of phase, these modes are called acoustical or optical-modes, respectively. As the name indicates the optical modes can be excited by electromagnetic waves (e.g. IR-light), if the two elements have opposite charge.

ZnO belongs to the C_{v6} space group and there are four atoms in the primitive unit cell, which result in 12 different types of phonons, one longitudinal acoustic (LA), two transverse acoustic (TA), three longitudinal optical (LO) and six transverse optical (TO) modes. [5] The so-called A_1 and E_1 branches are related to vibration along the c-axis and to vibration within the plane normal to the c-axis, respectively, and are the only ones to be both IR- and Raman active. In addition there are two non-polar Raman active modes related to the E_2-symmetry, one for vibrations in the Zn-sub-lattice (called $E_{2,low}$) and one related to vibration in the O-sub-lattice (called $E_{2,high}$).[5, 6, 7] The main contribution to IR-absorption in ZnO is by multiple phonon band absorption in the range of 800-1100 cm^{-1}, see Refs. [7, 8] and references therein.

When point defects are introduced into the material, they will perturb the symmetry of the lattice and introduce new vibrational modes. Modes with wave number in between the ZnO vibrational bands are referred to as gap vibrational modes, while modes with wave numbers exceeding the maximum band wave number is referred to as localized vibrational modes (LVM).

The focus in this thesis is the study of local vibrational modes of the O-H stretch modes related to different defects as observed in ZnO. In the case of OH-defects in oxides, the interaction between the induced LVM's and the crystal lattice is small, thus the LVM in a material can be viewed as a perturbation of the vibration of a free molecule. The harmonic wave number estimated for a free hydroxyl ion is 3738 cm^{-1}, while the OH-bonds are typically found to absorb in the range from 3200 up to 3700 cm^{-1} in several oxides[9] and thus clearly separated from the mentioned band modes in ZnO. The shift to lower wave numbers is related to anharmonic changes in the

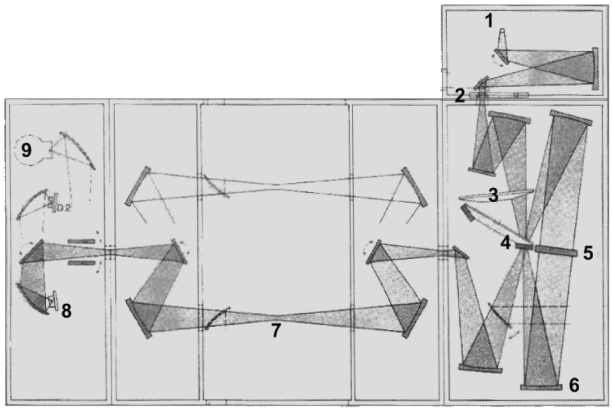

Figure 3.3: *Overview of the IR-beam path in the Bruker IFS 113v FTIR spectrometer, obtained from the instrument manual. 1) Globar source, 2) Aperture, 3) Filter exchanger (not used), 4) Beam splitter, 5) Double-sided movable mirror, 6) Stationary mirrors, 7) Sample position, 8) DTGS detector (not used), 9) InSb detector.*

potential experienced by the molecule and reflects the nature and local chemical environment of the OH-bond. As described in equation 3.10 a shift will also result from a change in between isotopes of a given element. As an example, the structural model of the defect responsible for the 3577 cm^{-1} absorption peak have been proposed based on isotope shifts between both ^{1}H and ^{2}H, and ^{6}Li and ^{7}Li proving the involvement of these elements [10, 11]. In addition, since the defect only absorbs in certain directions the detailed structure (direction of the OH-bond) of the defect may also be described (e.g. by the use of polarized light).[12]

3.2.2 Instrumentation

The setup used in this work is a Bruker IFS 113v Fourier transform transmission spectrometer with a SiC globar light source and a Genzel type interferometer. A cold finger cryostat is used to cool the sample down to 20 K in vacuum. In Fourier transform infrared absorption spectroscopy (FTIR) an interferogram containing all wave numbers is produced instead of using a monochromator to scan through each wave number. In this way the spectral response may be obtained in a shorter time and with less noise as compared to the traditional grating spectrometers.[3]

To produce an interferogram, light is emitted (in this case) from the globar light source emitting black body radiation in the range of 100 - 6000 cm^{-1}. Fig. 3.3 gives an overview of the beam

path through the spectrometer with each part labeled from 1 to 9. The emitted light (1) is first focused onto a beam splitter (4) made of Si on a CaF_2-substrate (spectral range of 1250 - 15000 cm^{-1}), where part of the beam is reflected and the rest is transmitted. Both the reflected and transmitted IR-beams are then directed towards each side of a moving mirror (5), which reflect the two beams back towards the beamsplitter. After returning to the beam splitter the two beams interfere constructively or destructively depending on the wavelength and difference in the path length. For each scan of the mirror the full frequency range can be covered, where the spectral resolution depends on the maximum mirror displacement (see apodization below). The interfered beam is transmitted through the sample or the sample reference (7) and is then recorded by a detector (8 or 9). The detector used in this setup is a photovoltaic InSb detector (9) cooled by liquid N_2 with a spectral range of 1850 - 10000 cm^{-1}.

Since the difference in path length is known at any given time (measured by a reference laser) the wavelength may be extracted from the resulting signal. In the case of a monochromatic IR-source, the resulting intensity would simply be a single cosine as a function of the mirror displacement, where the frequency is equal to the frequency of the monochromatic source. However, since the IR-source consists of a range of frequencies and the resulting beam intensity is a superposition of all the cosine-functions over the emitted frequency range, called an interferogram. The ideal interferogram can be described by a weighted integral of cosine-functions over all wave numbers, $\tilde{\nu}$:

$$I(\delta) = \int_{-\infty}^{\infty} S(\tilde{\nu}) \cos(2\pi\tilde{\nu}\delta) d\tilde{\nu}, \tag{3.13}$$

where δ is the mirror displacement and the weighting function $S(\tilde{\nu})$ is the spectral distribution from the black body source modified by absorption in the mirrors, beamsplitter and the sample. Equation 3.13 can be recognized as the cosine Fourier transform of $S(\tilde{\nu})$, thus the spectrum can be retrieved by taking the inverse Fourier transform:

$$S(\tilde{\nu}) = \int_{-\infty}^{\infty} I(\delta) \cos(2\pi\tilde{\nu}\delta) d\delta. \tag{3.14}$$

In a real interferometer the mirror can of course not move an infinite distance. Thus in the real integral, the intensity $I(\delta)$ is in addition multiplied by an apodization-function $A(\delta)$ to account for the limited mirror displacement:

$$S(\tilde{\nu}) = \int_{-\infty}^{\infty} I(\delta) A(\delta) \cos(2\pi\tilde{\nu}\delta) d\delta. \tag{3.15}$$

In the simplest case $A(\delta)$ is a boxcar-function, defined as 1 within the range of the mirror displacement and 0 otherwise. The choice of apodization-function will, however, affect the shape of the peaks in the absorption spectrum. In this work a Blackman-Harris 3-term function is used[3]:

$$A_{BH}(\delta) = \begin{cases} C_1 \cos(\pi \frac{\delta}{M}) + C_2 \cos(2\pi \frac{\delta}{M}) + C_3 \cos(3\pi \frac{\delta}{M}) & \text{for} - M \leq \delta \leq M \\ 0 & \text{for all other values of } \delta \end{cases} \tag{3.16}$$

where M is the maximum mirror displacement and the constants C_1, C_2 and C_3 are 0.42323, 0.49755 and 0.07922, respectively.[3] The resolution ($\Delta\tilde{\nu}$) scales approximately as the inverse of M:

$$\Delta\tilde{\nu} \approx \frac{1}{M}. \tag{3.17}$$

Increasing the the displacement of the mirror will thus increase the spectral resolution, however, at the same time the measurement noise will also increase. Thus the optimum choice of M will vary, depending on the instrument and the measured sample. In this work a spectral resolution of $\Delta\tilde{\nu} = 1\,\mathrm{cm}^{-1}$ have been used.

3.2.3 Data analysis

When the data have been collected and the inverse Fourier transform has been performed the absorption spectrum can be obtained. However, the spectrum still contains information about the source, the mirrors and the beam splitter in addition to the absorption that take place in the sample. To remove the instrument specific effects the spectrum measured through the sample (I) is normalized to a reference spectrum measured through a reference sample or (in the way it have been done in this work) through an empty sample holder in vacuum (I_0).

When including multiple internal reflections in the sample, the transmission through the sample is given by[3, 7]:

$$T(\tilde{\nu}) = \frac{I}{I_0} = \frac{(1-R)^2 e^{-\alpha(\tilde{\nu})d}}{1 - R^2 e^{-2\alpha(\tilde{\nu})d}}, \tag{3.18}$$

where d is the sample thickness, $\alpha(\tilde{\nu})$ is the linear absorption coefficient at $\tilde{\nu}$ and R is the sample reflectivity.

For ZnO, R is found to be $\sim$0.11 in the spectral region of interest[7]. Since $e^{-2\alpha d} \leq 1$ for all α then $R^2 e^{-\alpha 2d} \ll 1$. Thus equation 3.18 can be simplified to:

$$T(\tilde{\nu}) = (1-R)^2 e^{-\alpha d} = I_0 (1-R)^2 e^{-(\alpha_1(\tilde{\nu}) + \alpha_2(\tilde{\nu}))d} = C(\tilde{\nu}) e^{-\alpha_2(\tilde{\nu})d}, \tag{3.19}$$

where $\alpha = \alpha_1 + \alpha_2$ and α_1 is the absorption from free charge carriers and the host crystal, while α_2 is the absorption related the crystal defects. The separation of α in α_1 and α_2 is based on the assumption that α_1 and thus the factor $C(\tilde{\nu}) = (1-R)^2 e^{-\alpha_1 d}$ only varies slowly as a function of $\tilde{\nu}$ in the studied spectral range while the absorption from OH-related defects may be seen as sharp peaks at low temperature.

According to Beer-Lambert's law the absorbance (A) by a species (i) is proportional to the defect concentration (c_i) and the sample thickness (d), where the proportionality is referred to as the absorption strength ϵ. The absorbance is defined as:

$$A(\tilde{\nu}) = -\ln(T) = -\ln(C(\tilde{\nu})) + \alpha_2(\tilde{\nu})d, \tag{3.20}$$

thus the specific absorption coefficient can be found from:

$$\alpha_2(\tilde{\nu}) = -\frac{(\ln(T) - \ln(C(\tilde{\nu}))}{d}. \tag{3.21}$$

Since the absorption peaks for a given defect (i) have a finite width, the absorption strength ϵ is usually defined as:

$$\epsilon_i = \frac{\int_a^b \alpha_i(\tilde{\nu}) d\tilde{\nu}}{c_i}, \tag{3.22}$$

where the integral limits a and b cover the peak range and c_i is the concentration of the absorbing defect.

If ϵ_i is known the concentration can be estimated. If the defect responsible for the LVM includes one or several impurity elements, the lower limit for ϵ_{SIMS} can be found by measuring their concentration by SIMS. In the case of $\epsilon_{\mathrm{SIMS}} = \epsilon_i$ all of the impurity atoms, as measured by SIMS, contribute to the absorbing defect.

Finally, to be able to measure in the transmission mode, the sample needs to be sufficiently transparent. However, in low resistive samples the free carrier absorption may reduce the transmission below the noise level of the detector, thus making it impossible to extract any absorption peaks.

3.3 Positron Annihilation Spectroscopy

The existence of positrons was first predicted by Dirac in 1928, as the positive counterpart of the electron [13]. Without any knowledge about the earlier work by Dirac, this antiparticle was

experimentally observed some years later by Anderson in 1932 when it emerged in a Wilson cloud chamber [14]. A thorough review of the events that led to the discovery of this exotic particle is given in Ref. [15]. Later, in 1936 Andersen was awarded the Nobel Prize in physics for his discovery of this exotic particle, which when it meets an electron annihilate and emit two γ-photons with an energy of 511 keV each. This fundamental property is utilized in positron annihilation spectroscopy (PAS) to study negatively charged and/or neutral open volume defects. Since the positron is positive, positively charged defects will repel the positron and they can thus only be observed indirectly if one is able to induce a change in the charge state of the defect. Positron annihilation is adaptable to several material systems and in one of the most famous techniques positron emission tomography (PET-scan) it may be used to study functional processes in the human body[16]. The focus here, however, will be on solid-state materials or more precisely on single crystal ZnO.

As mentioned, the essence of PAS is the process when a positron meets an electron and annihilate and two gamma photons carrying approximately 511 keV of energy each (separated by 180 degrees in direction) emerge. Positron lifetime spectroscopy, Doppler broadening spectroscopy, coincidence Doppler broadening spectroscopy and angular correlation of annihilation radiation (ACAR) are some of the sub-techniques of PAS and the three first will be treated in some detail here. For a more comprehensive review of these techniques including ACAR, the readers are referred Refs. [17, 18].

3.3.1 Positron lifetime spectroscopy

The positron lifetime is defined as the time from creation until annihilation. The β^+-decay of ^{22}Na is the most commonly used source of positron creation in the PAS-techniques, which is described by:

$$^{22}_{11}\mathrm{Na} = \mathrm{e}^+ + \gamma(1.27MeV) + ^{22}_{10}\mathrm{Ne} + v_e, \tag{3.23}$$

where e^+ is the positron and v_e is a neutrino. The positron will, as mentioned, eventually interact with an electron and annihilate:

$$\mathrm{e}^+ + \mathrm{e}^- = 2\,\gamma\,(511\mathrm{keV}). \tag{3.24}$$

One of the reasons why the decay-process of ^{22}Na is used as a positron source is the simultaneous emission of one γ-photon during the decay process, as seen in equation 3.23. The time between

the creation of this first γ-photon and the two γ-photons emerging after the annihilation can thus be taken as a measure of the positron lifetime, τ. Solid state materials, can be viewed as consisting of positively charged ion-cores surrounded by valence electrons, where the ion cores repel the positively charged positron. However, in an open volume defects there are (of course) no positively charged ion cores and thus the positron may be trapped. One exception is when the open volume defect is positively charged, which would be the case for V_O^{2+} in ZnO.

In general, the positron lifetime is found to be proportional to the electron density in the area probed by the positron, as a consequence the lifetime is also related to the size of the open volume defect and can thus be used to study details of such neutral and negatively charged open volume defects. In material that does not contain any positron traps the positron will annihilate in a delocalized bulk state, this material specific parameter is defined as the bulk lifetime, τ_B.

To record the lifetime spectrum, a ^{22}Na-source is sandwiched in between two identical pieces of the studied sample to ensure that all the emitted positrons enter the sample. Typically 10^6 lifetime events are collected: First the γ-photon emerging from the β-decay and then the two γ-photons emerging from the annihilation. The recorded experimental lifetime spectrum represents the probability of positron annihilation at a given time, t. This spectrum may consist of several exponential decay components representing the different defects (i) present in the material:

$$-\frac{dn(t)}{dt} = \sum_i \frac{I_i}{\tau_i} e^{-t/\tau_i} \tag{3.25}$$

where n(t) is the probability of the positron to be alive at time t, τ_i represents the positron lifetime components and I_i is the fraction of each defect contributing to the spectrum. This may also be represented by the average positron lifetime τ_{ave}:

$$\tau_{ave} = \sum_i I_i \tau_i, \tag{3.26}$$

where the τ_i relates to the size of the open volume defect and from the intensity I_i the concentration of each defect can be obtained. In the case of measurements at room temperature of samples containing only e.g. V_{Zn}, $\tau_1^{-1} = \tau_B^{-1} + \kappa_V$, where κ_V is the positron trapping rate of the V_{Zn} and $\tau_2 = \tau_V$.[17] Thus the second component is directly related to the lifetime of the defect present, while the first component always will have a value lower than τ_B.

However, before the data can be analyzed properly, random background radiation and annihilation events taking place in the source have to be corrected for. Due to this and because of the

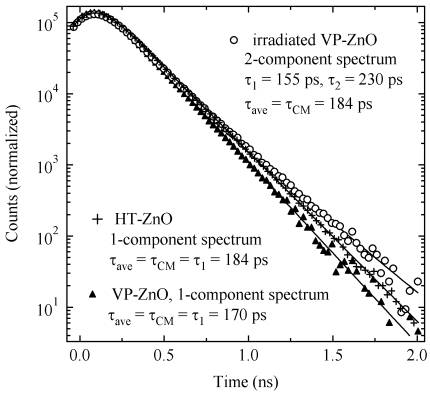

Figure 3.4: *A lifetime spectrum from Paper V, which shows the difference between a low concentration of V_{Zn}, saturation trapping in the Li_{Zn} and delocalized bulk annihilation.*

limited resolution only 1-3 lifetime components may be extracted from the lifetime spectrum, depending on the distribution in lifetime and concentration. To separate two components in the lifetime spectrum the ratio τ_2/τ_1 needs to be $\geq 1.3 - 1.5$.

In this technique the positrons are not moderated before they enter the sample and a lifetime measurement is therefore often referred to as a fast positron technique. The positrons resulting from the decay of $^{22}_{11}$Na exhibits a broad energy distribution of up to 540 keV in energy, thus probing deep into the bulk of the material ($\sim$170 μm in ZnO see Eq. 3.27). This means that the technique is best suited to measure thick samples since otherwise most of the positrons would penetrate through and annihilate in the substrate instead of in e.g. a thin film. In addition, to simplify the data analysis the samples should preferably be homogenous.

Figure 3.4 shows the lifetime spectrum obtained in a piece of (i) ZnO grown by the vapour phase technique (VP-ZnO), (ii) irradiated VP-ZnO and (iii) hydrothermally grown ZnO (HT-ZnO), respectively. The data from the as-grown VP-ZnO show a one component spectrum with an τ_{ave} of 170 ps while the irradiated VP-ZnO have a τ_{ave} of 184 ps. From this spectrum it is possible to extract two separate lifetime components τ_1 equal to 155 ps and τ_2 equal to 230 ps. The second component is typical of annihilation in a V_{Zn}, while the first component corresponds to τ_{B} = 170 ps and represents annihilation in the delocalized bulk state.[19]

3.3.2 Doppler Broadening Spectroscopy

Doppler broadening spectroscopy (DBS) is categorized as a slow positron beam technique. The positrons are first slowed down (moderated) and then accelerated to a given energy, typically between 0.5 to 40 keV, depending on the setup. By controlling the energy it is then possible to implant the positrons to the required depth where the positron peak position can be estimated empirically by:

$$R_p = AE^n\,(keV), \tag{3.27}$$

where A = $4/\rho$ (μg/cm^2), n$\simeq$ 1.6 and ρ= 5.606 g/cm^3 for ZnO.

Depth profiles of the studied sample can be obtained by scanning the positron implantation energy. It is, however, important to note that when the energy is increased the width of the implanted positron distribution also increases, i.e. in the deep end of the profile substantial averaging of the recorded signal will occur.

The amount of loss of positrons during the moderation step is dependent on the moderator material. In the case of a single crystalline tungsten foil a moderation efficiency of typically 10^{-4} is commonly achieved[18], the rest of the positrons annihilate with electrons in the moderator or come out as fast positrons. To compensate for this loss of positrons the source needs to be much stronger as compared to the fast positron techniques to reach a similar count rate. But then, due to the high intensity of the source, it is no longer possible to correlate the emission of the start and stop γ-photons and the positron lifetime can no longer be obtained.

From the conservation of momentum in the annihilation process between the positron and electron one can obtain information about the initial momentum of the annihilated electrons by measuring the momentum distribution of the emitted γ-photons, since the kinetic energy of the positron is much lower than the kinetic energy of the average electron which it annihilates. Both positrons and electrons are fermions, but since the positron density of states is much larger than the positron density the positrons will easily thermalize to an unoccupied low energy state, i.e. the main contribution to the change in momentum of the emitted γ-photons comes from the annihilated electrons. The thermalization typically takes from 1-3 ps, which is a short time compared to the mentioned τ_b=170 ps.[17]

There are two ways to measure the momentum deviation in the emitted γ-photons, one is to study the deviation from the 180° angle in between the two γ-photons emitted from the annihilation process (the ACAR-technique) and the other is to study the energy distribution of the γ-photons

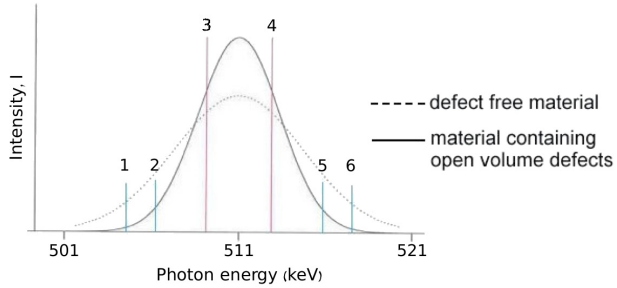

Figure 3.5: *Sketch of the energy distribution of the γ-photons. The spectrum is parameterized by the S- and W-parameters, where S is defined as the integrated signal of the central region and W is the integrated signal of the wing-regions.*

(DBS-technique). ACAR is a rather time consuming technique, since it is necessary to use a low positron beam intensity to be able to correlate the two emitted γ-photons for each annihilation process. For DBS it is, in general, not necessary to correlate the two γ-photons, however, by doing so the signal to noise ratio can be improved by several orders of magnitude. The technique is then called coincidence Doppler broadening spectroscopy, which will be treated in the next section.

In solid materials, electrons may be categorized as core-electrons or valence electrons. In a simplified description the core electrons orbit the core with a small radius and a high kinetic energy, while the valence electrons, which contribute to the crystal bonds, have a small kinetic energy. In open volume defects the core electron-density is lower, thus the probability of annihilating with an electron with high momentum is decreased. This difference can be observed when measuring the energy distribution of the emitted γ-photons. Fig 3.5 shows a sketch of the energy distribution measured in a defect free material and in material containing open volume defects, respectively. The energy distribution measured for the defect free material is, as mentioned, broader than that of the material containing open volume defects. The open volume defects increase the probability of annihilating with low momentum valence electrons and thus the deviation in kinetic energy from the 511 keV is less, resulting in a sharper energy distribution. These distributions are commonly parameterized by the S- (shape) and W (wing)-parameters. S is also often referred to as the valence annihilation parameter and W as the core annihilation parameter, since they are mostly sensitive to changes in the valence electron and core electron density, respectively. The S and W are defined as the integral of the central low-momentum part and the high momentum

part of the spectrum, respectively:

$$S = \frac{\int_{3}^{4} I(E)dE}{\int_{-\infty}^{+\infty} I(E)dE}, W = \frac{\int_{1}^{2} I(E)dE + \int_{5}^{6} I(E)dE}{\int_{-\infty}^{+\infty} I(E)dE}, \tag{3.28}$$

where the integral limits are defined in Fig 3.5, and I(E) is the intensity at a given energy E. It is important that the integral limits are defined such that the W parameter is not influenced by the S parameter and vice versa. In this work the energy range has been set to, $|E - 511\,\text{keV}| \leq 0.8\,\text{keV}$ for S (corresponding to electron an momentum of 0.4 a.u.), and $2.9\,\text{keV} \leq |E - 511\,\text{keV}| \leq 7.4\,\text{keV}$ for W (1.6 - 4.0 a.u.). It should also be mentioned that the S- and W-parameters depend on the energy resolution of the spectrometer. In this work two Ge detectors with an energy resolution of 1.24 keV at 511 keV were used. To be able to compare results from different setups the S- and W-parameters should be normalized to the bulk annihilation values obtained under the same measurement conditions.

The S and W parameters are typically plotted as a function of positron implantation energy/positron implantation depth (S(E) and W(E)) or in a W(S)-plot. The first plot shows how defects are distributed as a function of depth, however, it is not a straight forward to interpret if the material contains several types of defects. As a first approximation an increase in the S-parameter can be viewed as an increase in the concentration of the open volume defect where the annihilation takes place. However, it may also reflect an increase in size of the open volume of the defect. To resolve this, both the W- and S-parameters have to be taken into account; one way of doing this is to plot the W- as a function of the S-parameter. Fig. 3.6 shows a sketch of a W(S)-plot for ZnO. The plot is normalized to annihilation values of the delocalized bulk state, labeled "ZnO lattice". Each open volume defect will have a unique set of W- and S-parameters, corresponding to a point in the W(S)-plot. The V_{Zn} is found to be W =0.7888(4) and S = 1.0487(5) [19, 20, 21]. When the material contains a gradient of V_{Zn} and this is the only defect trapping positrons all values of the W(S) fall on a line connecting the V_{Zn}-point to the "ZnO lattice". The V_{Zn}-concentration can then be calculated from:

$$[V_{Zn}] = \frac{N_a}{\mu_V \tau_B} \frac{(W - W_B)}{(W_V - W)}, \tag{3.29}$$

where N_a is the atomic density ($8.3\times10^{22}\,\text{cm}^{-3}$ for ZnO), μ_V is the positron trapping rate of the V_{Zn} ($3\times10^{15}\,\text{s}^{-1}$), τ_B is the bulk lifetime of ZnO (170 ps) and W_B and W_V are the annihilation parameter of the bulk annihilation state and the V_{Zn} annihilation state, respectively. When only

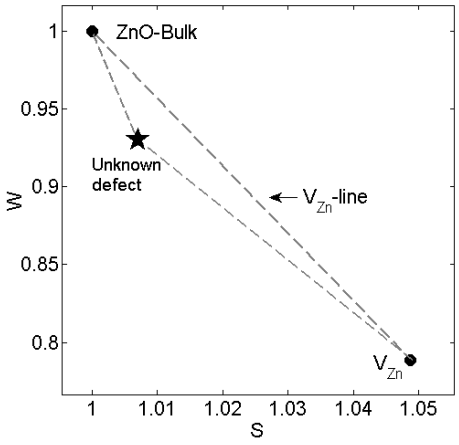

Figure 3.6: *Sketch of the WS-plot showing the different annihilation states present i ZnO. The surface, bulk, V_{Zn} and an example of an unknown defect. The lines indicate the area where the values of the W- and S-parameters will occupy depending on how much each defect contribute to the averaged signal.*

one defect (in this case the V_{Zn}) contribute to the positron trapping:

$$\frac{S - S_B}{S_V - S} = \frac{W - W_B}{W_V - W}, \tag{3.30}$$

thus both the S- and W-parameters may be used to calculate the defect concentration independently and from DBS it may be presented as a function of positron implantation depth. When the two curves overlap it means that the assumption that only one defect (in addition to bulk annihilation) contributes to the annihilation parameters is correct. Fig. 3.7 shows an example of such a curve from Paper VI. The curve reveals if there are contribution from other defects than the V_{Zn} (in a similar manner as in the WS-plot), however, in addition the defect concentration as a function of depth can be read directly out of the figure. In the example in Fig. 3.7 one can see that around the projected range of the H- implantation additional defects (vacancy clusters) contribute, but as one goes deeper into the sample away from the projected range the V_{Zn} is the dominating positron trap and a decrease in the V_{Zn}-concentration is observed towards the bulk.

When more than one defect is present the measured W- and S-parameters will be a linear combination of three or more points where their contribution depends on the concentration and trap-

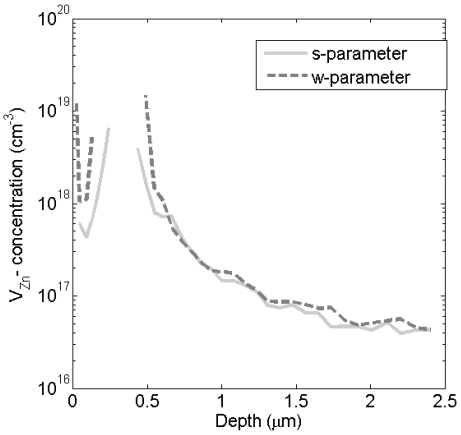

Figure 3.7: *The V_{Zn}-concentration as a function of depth. When the two curves calculated from the W- and S-parameter respectively overlap, only the V_{Zn}-contributes as a positron trap. Full details of the experimental procedure can be found in Paper VI*

ping rate of each defect. Unless one of the defects dominate as a positron trap it is in general not possible to extract detailed information about the defects in such a system from the W(S)-plot. However, deviation from this line indicates the presence of another defect trapping positrons. In Paper V an example of identification of such a defect is given by the combination of lifetime measurements, DBS, coincidence DBS and theoretical predictions.

3.3.3 Coincidence Doppler Broadening Spectroscopy

Background γ-radiation originating from annihilation in the source or along the beam line limits the dynamic range of the energy distribution. This can, however, be improved by only counting the γ-photons that originate from the same annihilation process, where the two γ-photons are collected by two detectors placed on each side of the sample separated by $\sim 180^{\circ}$. This effectively reduces the background level in the high and low energy range by up to three orders of magnitude, revealing a much more detailed picture, see Fig 3.8. This part of the energy spectrum is mostly sensitive to core electron annihilation, thus the coincidence Doppler broadening spectroscopy technique may reveal more details about the chemical and geometrical identity of

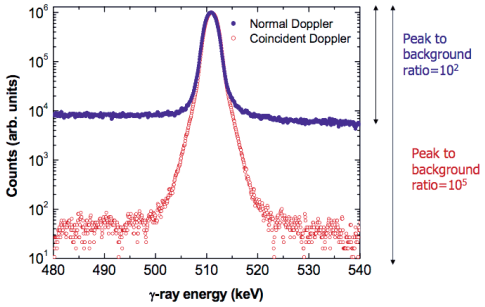

Figure 3.8: *Two γ-photon energy spectra measured in by Doppler broadening spectroscopy and coincidence Doppler broadening spectroscopy, respectively. The sensitivity of the CDBS-technique is increased by three orders of magnitude as compared to the CDB-technique. Obtained from ref. [22].*

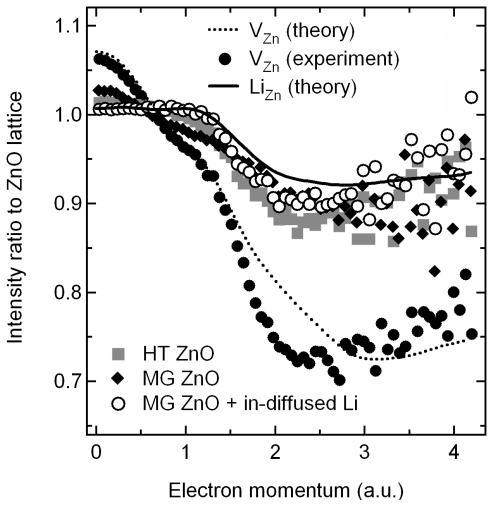

Figure 3.9: *The figure is an example from Paper V of ratio curves measured in samples containing either V_{Zn} or Li_{Zn} together with theoretical predictions for the same defects.*

the defects involved. In the ratio curve the momentum distribution is normalized to the momentum distribution of the bulk annihilation state. However, to interpret the ratio curves theory and modeling are needed. Details about such modeling are described in Ref. [23]. Figure 3.9 is obtained from Paper V and shows the ratio curves for different samples containing either V_{Zn} or Li_{Zn} together with theoretical estimates.

References

[1] Sigmund, P. Theory of sputtering. i. sputtering yield of amorphous and polycrystalline targets. *Phys. Rev.* **184**, 383–416 (1969).

[2] Christensen, J. S., Radamson, H. H., Kuznetsov, A. Y. & Svensson, B. G. Diffusion of phosphorus in relaxed $Si_{1-x}Ge_x$ films and strained $Si/Si_{1-x}Ge_x$ heterostructures. *Journal of Applied Physics* **94**, 6533–6540 (2003).

[3] Griffiths, P. R. & de Haseth, J. A. *Fourier transform infrared spectrometry* (John Wiley and Sons, 2007), second edition edn.

[4] Lavrov, E. Hydrogen in ZnO. *Physica B: Condensed Matter* **404**, 5075–5079 (2009).

[5] Özgür, Ü. *et al.* A comprehensive review of ZnO materials and devices. *Journal of Applied Physics* **98**, 041301 (2005).

[6] Jagadish, C. & Pearton, S. J. *Zinc oxide bulk, thin films and nanostructures: processing, properties and applications* (Elsevier, 2006).

[7] Emelie, P. Y., Phillips, J. D., Buller, B. & Venkateswaran, U. D. Free carrier absorption and lattice vibrational modes in bulk ZnO. *Journal of Electronic Materials* **35**, 525–529 (2006).

[8] Morozova, N. K., Plotnichenko, V. G., Gavrishchuk, E. M. & Blinov, V. V. Absorption spectrum of ZnO precipitates in ZnSe. *Inorganic Materials* **39**, 783–787 (2003).

[9] Wöhlecke, M. & Kovács, L. OH- ions in oxide crystals. *Critical Reviews in Solid State and Materials Sciences* **26**, 1 (2001).

[10] Lavrov, E. V. Infrared absorption spectroscopy of hydrogen-related defects in ZnO. *Physica B: Condensed Matter* **340-342**, 195–200 (2003).

[11] Shi, G. A., Stavola, M. & Fowler, W. B. Identification of an OH-Li center in ZnO: infrared absorption spectroscopy and density functional theory. *Physical Review B (Condensed Matter and Materials Physics)* **73**, 081201–3 (2006).

[12] Lavrov, E. V., Börrnert, F. & Weber, J. Dominant hydrogen-oxygen complex in hydrothermally grown ZnO. *Physical Review B* **71**, 035205 (2005).

[13] Dirac, P. A. M. The quantum theory of the electron. *Proceedings of the Royal Society of London. Series A, Containing Papers of a Mathematical and Physical Character* **117**, pp. 610–624 (1928).

[14] Anderson, C. D. The positive electron. *Phys. Rev.* **43**, 491–494 (1933).

[15] Hanson, N. R. Discovering the positron (i). *The British Journal for the Philosophy of Science* **12**, pp. 194–214 (1961).

[16] Phelps, M. E., Hoffman, E. J., Mullani, N. A. & Ter-Pogossian, M. M. Application of Annihilation Coincidence Detection to Transaxial Reconstruction Tomography. *J Nucl Med* **16**, 210–224 (1975).

[17] Tuomisto, F. Defect characterization in semiconductors with positron annihilation spectroscopy. In Dhanaraj, G., Byrappa, K., Prasad, V. & Dudley, M. (eds.) *Springer Handbook of Crystal Growth*, 1551–1579 (Springer Berlin Heidelberg, 2010).

[18] Krause-Rehberg, R. & Leipner, H. S. *Positron annihilation in semiconductors: defect studies* (Springer, 1999).

[19] Tuomisto, F., Ranki, V., Saarinen, K. & Look, D. Evidence of the zn vacancy acting as the dominant acceptor in n-Type ZnO. *Physical Review Letters* **91**, 205502 (2003).

[20] Tuomisto, F., Saarinen, K., Look, D. C. & Farlow, G. C. Introduction and recovery of point defects in electron-irradiated ZnO. *Physical Review B* **72**, 085206 (2005).

[21] Zubiaga, A. *et al.* Mechanisms of electrical isolation in O^+-irradiated ZnO. *Physical Review B* **78**, 035125 (2008).

[22] Amarendra, D. G. Positron annihilation net (2010). Http://www.positronannihilation.net.

[23] Makkonen, I., Hakala, M. & Puska, M. J. Modeling the momentum distributions of annihilating electron-positron pairs in solids. *Physical Review B* **73**, 035103 (2006).

Chapter 4

Results

The scientific results of this Ph.D. work are presented in the six papers appended to the introductory chapters 1-4 of the thesis. A brief summary of each article is given below followed by a general discussion of the results, a presentation of a few preliminary and unpublished results and suggestions for further work.

4.1 Overview and discussion of the appended papers

One of the first things we wanted to learn more about was the diffusivity of H in ZnO. Intimate knowledge of how this important electrically active impurity migrates in the material is of great importance, both in the quest for p-type activity, but also if one wants to utilize n-type doping by H directly. In both Paper I and II we utilize SIMS to study the diffusion mechanisms of ^{2}H by heat treatment of single crystalline ZnO implanted with ^{2}H to a dose of $1\times10^{15}\,\mathrm{cm}^{-2}$ and $1\times10^{16}\,\mathrm{cm}^{-2}$, respectively. In this way we wanted to address the on-going discussion about the diffusivity of H. Results obtained in the 1950s by Thomas and Lander[1] claimed that the activation energy for H-diffusion is close to 0.9 eV, but several authors challenged this and claimed that the activation energy is equal to or even below 0.5 eV. However, we were able to show that the activation energy is indeed 0.8-0.9 eV. In addition, these two papers also show how H exhibits so-called trap limited diffusion process, which may explain some of the discrepancy in the reported values for the activation energy. The trap in question was tentatively assigned to Li and the dissociation energy of this complex was found to be roughly 1.5 eV.

There seems to be a slight dose dependency between the experimental data and the estimated trap concentration presented in Paper I and II, $4.5\times10^{16}\,\mathrm{cm}^{-3}$ versus $7\times10^{16}\,\mathrm{cm}^{-3}$, respectively.

Such a dose dependency is not likely to be explained by trapping by Li as the only trap since the Li-concentration is comparable in the two samples (cut from the same wafer). Thus further experiments would be necessary to reveal if this is a real effect and, if so, to understand the mechanisms behind it. Results obtained in Paper VI show that V_{Zn} might be an additional candidate for H trapping. However, to explain the dose dependency in the trap concentration by V_{Zn}, the V_{Zn} diffusivity must be comparable to the H-diffusivity. There is, however, no evidence of V_{Zn} diffusion from the implanted peak at $300°C$ as seen in Paper VI.

Motivated by the diffusion studies, the next aspect addressed was the interaction between H and Li. As mentioned, the hydrothermally grown ZnO contains Li due to the presence of LiOH in the growth solution. Furthermore the Li concentration is observed to vary in between different as-grow wafers. In Paper III the aim was to correlate this variation in the Li-concentration as measured by SIMS with the intensity of the infrared absorption peak at $3577\,cm^{-1}$ in several different wafers. Such a correlation would be expected since the absorption peak has previously been attributed to the vibrational stretch mode of OH adjacent to Li_{Zn} and has been claimed to include 99% of the Li-atoms present in the material.[2, 3, 4] However, no correlation between the as-grown Li-concentration and the absorption strength of the $3577\,cm^{-1}$-peak was found, indicating that only a small fraction of the Li atoms present in the as-grown samples contributes to the complex. In addition, an interesting feature was found in the results of the SIMS-measurements as presented in Paper III: In three of the studied wafers an unexpected variation in the Li-concentration as a function of depth, which is repeated in the lateral directions, can be seen. This indicates the presence of an underlying defect structure, which follows the basal planes normal to the c-axis of the material. These defects were in Paper III tentatively ascribed to c-axis inversion domains.

The complex responsible for the $3577\,cm^{-1}$ absorption peak[2, 3, 4] could be a good candidate for the H-trap-complex observed in Paper I and II. However, this complex has been reported to be stable up to $1200°C$ for several hours, which is not consistent with the dissociation rate found for the H-trap in Paper I and II. Such a high thermal stability for a low-order defect complex is, however, very surprising. Moreover, an unexpected dependency on the detailed history of heating and cooling indicated that the details of this complex are not fully understood[3]. Thus in Paper IV we address the thermal stability of the $3577\,cm^{-1}$-peak. The results obtained in Paper I and II, suggest that Li may act as a efficient trap for H, motivated by this, the samples were quenched after heat treatment to possibly limit any re-trapping of H. In this way it was found, indeed, that the thermal stability of this complex is much lower than previously reported. However, even when quenching the samples by dropping them into water at room temperature,

the trapping could not be suppressed completely. Thus an upper limit for the dissociation energy was estimated to be 2.5 eV and when taking the trapping into account this may, after all, be consistent with the dissociations energy found in Paper I and II of roughly 1.5 eV.

For the next angle of approach PAS and SIMS together with theory and modeling were utilized to study the effect of Li in both hydrothermally grown (HT) and melt grown samples (MG). In Paper V the PAS-signature of the Li_{Zn}-defect is identified. In addition, it is shown that the discrepancy in the reported bulk positron lifetime for ZnO grown by different methods is explained by the presence of Li. Moreover, the OH-Li_{Zn}-defect[5] and a defect complex (Li_{Zn}-H-Li_{Zn}) proposed by Sann et al.[6] are found to have similar theoretical annihilation signatures as Li_{Zn}, while the Li_{Zn}-Li_i proposed by Wardle et al.[5] is not found to trap positrons at all. Based on these results it is also found that in as-grown HT-ZnO most of the Li atoms are present in the acceptor state on the Zn-site, which is consistent with the results of Paper III. It was also found that a relatively high concentration, at least (2-3)$\times 10^{18}\,\mathrm{cm}^{-3}$ of Li in the Li-doped MG-ZnO (corresponding to about 20% of the Li-present), is situated on the Zn-site and thus showing the ability to obtain large acceptor concentrations on the Zn-site. Further, in Paper V it is speculated that the V_{Zn}-concentration of $5\times 10^{16}\,\mathrm{cm}^{-3}$ as found in the Li-lean HT-ZnO sample is present also in as-grown state of HT-ZnO.

In Paper VI the PAS-signature of Li_{Zn}, as found in paper V, is utilized to study the effect of deliberate introduction of H in both Li-rich and Li-lean ZnO. Interestingly, after the introduction of H the signal related to Li_{Zn} in the Li-rich sample disappears even though there is no change in the Li-concentration in the sample. This is consistent with the formation of the neutral OH-Li_{Zn}-complex. It should be noted that even though the PAS-signature was found to be similar for both Li_{Zn} and OH-Li_{Zn} in Paper V the trapping rate depends on the charge state. Since the OH-Li_{Zn}-complex is believed to be neutral, it is thus not expected to trap positrons as efficiently as Li^{-}_{Zn}. The rate can be as much as one order of magnitude lower in the neutral state.[7], enabling V_{Zn} to become the dominant trap in the Li-rich sample after hydrogenation despite a concentration of "only"$5\times 10^{16}\,\mathrm{cm}^{-3}$. Furthermore, this V_{Zn} concentration overlaps perfectly with that found after removal of Li by high temperature heat treatment and thus strengthens the assumption from Paper V that V_{Zn} is present with a concentration in the range of $5\times 10^{16}\,\mathrm{cm}^{-3}$ in as-grown HT-ZnO. On the other hand, hydrogenation of the Li-lean HT-ZnO leads to a reduction in the apparent V_{Zn} concentration from $5\times 10^{16}\,\mathrm{cm}^{-3}$ to $1\times 10^{16}\,\mathrm{cm}^{-3}$, which can be explained by the formation of the neutral V_{Zn}-H_2-complex. In comparison, for the Li-rich material no reduction in the V_{Zn} is detected, which indicates that Li_{Zn} is a more efficient trap for H as compared to V_{Zn}.

The results obtained in all the presented papers show that in hydrothermally grown material, Li is indeed a good candidate for the diffusion trap observed in H-diffusion experiments. However, trapping by V_{Zn} may also play an important role. This is further substantiated by the results obtained by Ohashi et al. [8]. They have studied H/^{2}H-plasma doping of HT-grown, chemical vapor transport grown (CVT) and flux-grown ZnO and show that the diffusion profiles differ quite dramatically in between the samples originating from different growth methods. The ^{2}H-profile obtained in the HT-ZnO resembles that of trap limited diffusion as observed in Paper I and II with a trap concentration just below $1\times10^{18}\,\mathrm{cm}^{-3}$, consistent with the Li-concentration in their sample. In the flux-grown sample the diffusion profile also resembles trap-limited diffusion, however, the trap seems to be different from the one in the HT-sample. For the CVT-sample the ^{2}H-concentration is about one order of magnitude lower (except close to the surface) as compared to the HT sample. The flux-grown sample has an Al-concentration of about 10^{18} cm^{-3}, while the CVT-sample does not contain any considerable amount of Li and have only $1\times10^{15}\,\mathrm{cm}^{-3}$ of Al. The low amount of in-diffused H in the CVT-sample is also consistent with a relatively low solubility of H in ZnO.[1] According to Ohashi et al. the Al contamination in the flux grown sample originate from the Al_2O_3 furnace tube which may introduce V_{Zn} as described by the following equation[8]:

$$Al_2O_3 = 2Al^{+}_{Zn} + V^{-2}_{Zn} + 3O_O \tag{4.1}$$

Thus the trap in the flux grown sample may be the V_{Zn}. Both observations are in accordance with the conclusions of the work presented in this thesis.

In summary, all the results presented are in accordance with the notion that both Li_{Zn} and V_{Zn} act as traps during H diffusion with Li_{Zn} being more efficient than V_{Zn}. As mentioned in Paper VI, H can most probably quite easily escape from a V_{Zn}-H complex thus the probability to capture two H at the same V_{Zn} is low. On the contrary, Li_{Zn} is found to be relatively stable[9] and is in this work also found to be a very efficient trap for H. It should also be emphasized that as seen in Paper III the properties of hydrothermally grown ZnO can vary from wafer to wafer and also within the same wafer. These differences call for extra caution when comparing results from different wafers.

4.2 Preliminary and unpublished results

During the work on this thesis, there are several experiments that have shown promising results, however, they have for different reasons not yet been published. A short review of some of the

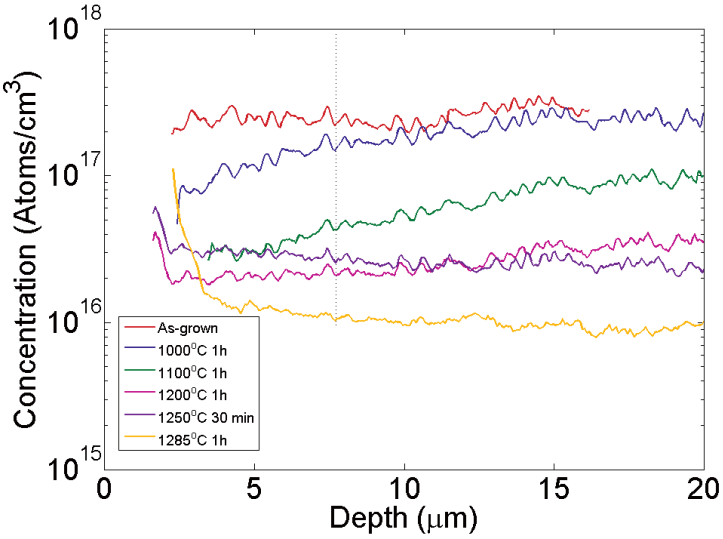

Figure 4.1: *Shows preliminary data of in-homogeneously distributed Li after different annealing treatments. The reproducible "noise features"in the profiles remain even after 1 h annealing at* $1285°C$.

preliminary results is given in the following sections.

4.2.1 Thermal stability of the in-homogeneously distributed Li

In Paper III, we speculated that the in-homogeneously distributed Li could be related to inversion boundary domains and that these might contribute to the apparent high thermal stability of the $3577\,\mathrm{cm}^{-1}$ peak. Fig. 4.1 shows preliminary data of in-homogeneously distributed Li as a function of annealing temperature. In this experiment the sample was removed from the furnace and let to cool down slowly after each heat treatment. For additional experimental details, see Paper II and IV. It is evident that the underlying defect structure remains up to $1250°\mathrm{C}$ and can also be seen vaguely even after heat treatment at $1285°\mathrm{C}$ for 1 h, even though the total Li-concentration is reduced from $2\times10^{17}\,\mathrm{cm}^{-3}$ to $\sim1\times10^{16}\,\mathrm{cm}^{-3}$. In Fig. 4.2 the IR-absorption results of the $3577\,\mathrm{cm}^{-1}$ peak is shown. Interestingly, it is found that the peak intensity varies slightly as a function of heat treatment temperature. Surprisingly, it is also seen that the peak intensity is reduced in the first measurement after heat treatment at $1250°\mathrm{C}$, while the intensity is restored and

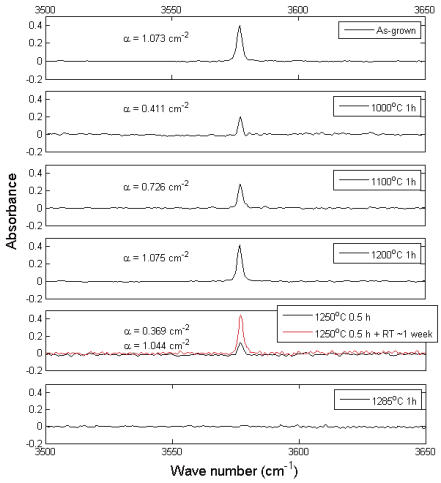

Figure 4.2: *IR-absorption spectra showing the 3577 cm^{-1} peak obtained from the same sample as in Fig. 4.1 heat treated subsequently up to 1285°C. The spectra are offset vertically for clarity. Unpolarized light was used with the wave vector, $\vec{k}$, directed perpendicular to the c-axis of the sample, $\vec{k} \perp \vec{c}$.*

comparable to the as-grown measurement after storing the sample at RT in air for approximately one week. However, after 1 h at 1285°C no trace of the 3577 cm^{-1} absorption peak is found. It should be kept in mind that these results are of a preliminary character and need to be confirmed. However, they are consistent with the results presented in paper IV and the previously reported stability of the 3577 cm^{-1} peak after slow cooling.[3] Even though the details of the processes involved in restoring the absorption peak during 1 week at RT are unclear, re-trapping of mobile H by Li is a likely explanation.

Moreover, by correlating the Li-concentration ($\sim 3\times10^{16}$ cm^{-3}) with the integrated absorption (1.044 cm^{-2}) as observed by FTIR after heat treatment at 1250°C an upper limit for the absorption strength (ϵ_{3577}) is estimated to be $\sim 3.5\times10^{-17}$ cm. This value corresponds rather well to the value found for another OH-related absorption mode in ZnO of ϵ_{3611} 2.46×10^{-17} cm.[10] Thus, it appears that the 3577 cm^{-1} signal observed in the as-grown HT-ZnO only corresponds to a limited fraction (10-20% or 3-4$\times10^{16}$ cm^{-3}) of the Li present in the samples, in accordance with the findings in Paper III and VI and the notion that Li is predominantly in the acceptor state in as-grown HT-ZnO[9, 11]. It is also interesting to note that the thermal stability of the in-homogeneously distributed Li as seen in Fig. 4.1 seems to be comparable to the apparent

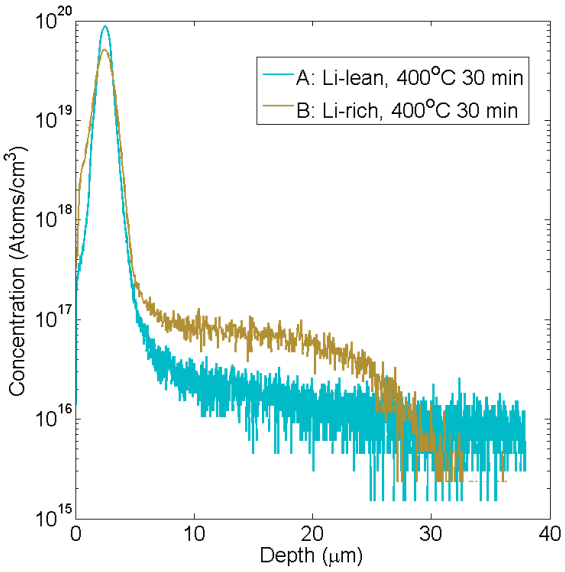

Figure 4.3: *^{2}H-concentration as a function of depth in a Li-rich (as-grown HT-ZnO) and a Li-lean ($1500°C$ treated HT-ZnO) sample, respectively. In the Li-lean sample no diffusion and/or trapping is clearly observed. The signal at $\sim 1\times10^{16}\,\mathrm{cm}^{-3}$ corresponds to the detection limit for the specific measurement. In the Li-rich sample, however, a trap limited diffusion profile is observed, consistent with the profiles found in Papers I and II.*

stability of the $3577\,\mathrm{cm}^{-1}$ peak in Fig. 4.2 when cooled down slowly. However, it may not be concluded from these results that they are related and further studies are needed.

4.2.2 H diffusion in Li-lean HT-ZnO

To get more insight into the trap observed for H-diffusion in Paper I and II, two samples were prepared; one similar to the samples used in Paper II (Li-rich) and another Li-lean sample. In the Li-lean sample the Li-concentration was reduced to the $1\times10^{15}\,\mathrm{cm}^{-3}$ range by heat treatment at $1500°C$ for 1 h followed by surface polishing. Both samples were then implanted with ^{2}H to a dose of $1\times10^{16}\,\mathrm{cm}^{-2}$ followed by a heat treatment at $400°C$ for 30 min to let ^{2}H diffuse. The results of this experiment are shown in Fig. 4.3 where the ^{2}H concentration is plotted as a function of depth as measured by SIMS. In the Li-rich sample a trap limited diffusion profile consistent

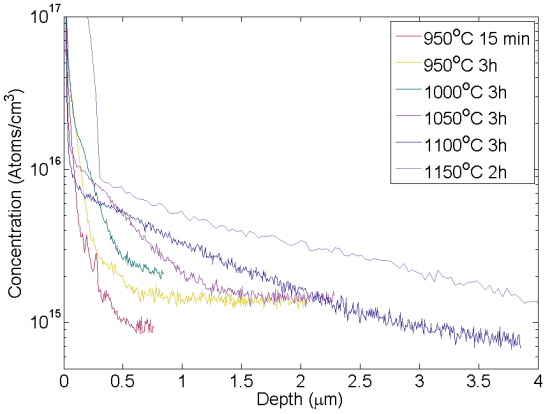

Figure 4.4: *The Na-concentration as a function of depth as measured by SIMS in 6 pieces of the same wafer heat treated in the range of* $950°C$ *to* $1150°C$ *in air.*

with the ones found in Paper I and II is observed, while in the Li-lean sample no diffusion and/or trapping can be clearly observed[1]. This is consistent with the notion that Li is the main trap for H-diffusion, however, the heat treatment at $1500°$C might also affect other defects in the sample, like V_{Zn} and V_O. The results obtained in Papers V and VI indicate that there is no change in the V_{Zn} concentration as a result of the $1500°$C heat treatment. Another candidate would be V_O, which has been shown to be able to trap H.[12] However, high temperature heat treatment in air is expected to increase, not decrease, the V_O-concentration due to preferential loss of O[3] and V_O is thus not consistent with the observed reduction in trap concentration as seen in Fig. 4.3. Another possibility is that the trap is occupied by other impurities introduced during the heat treatment. Na is found to increase from the 10^{13}-10^{14} cm^{-3}-range up to 1×10^{16} cm^{-3} as a result of the heat treatment, see the next section. However, 1×10^{16} cm^{-3} is almost one order of magnitude lower than the original trap concentration and can thus not explain a reduction in the H-trap. Except for Li and Na, there is no observed change in the concentration of any other known impurities as a result of the heat treatment at $1500°$C[11]. Hence, the most likely candidate for the H-diffusion trap is still Li_{Zn}.

[1]The signal intensity observed deeper than 30 μm in the measurement of the Li-lean sample is limited by the dynamic range of the SIMS-instrument of 5 orders of magnitude.

4.2.3 Na contamination during high temperature heat treatments

As mentioned in Chapter 1, the ability to remove Li is of crucial importance. This holds both from a technological point of view, since the presence of Li typically leads to self-compensation and highly resistive material, but also from a scientific point of view to be able to learn more about the different defect mechanisms taking place in ZnO. In this thesis the method for removal of Li has been high temperature heat treatment in air. However, as mentioned in the previous section it leads to contamination by Na from the sample boat and/or furnace tube in the $1\times10^{16}\,\mathrm{cm}^{-3}$ range. To learn more about the process behind this Na-contamination one hydrothermally grown wafer was cut into six pieces and heat treated in air in the range from 950°C up to 1150°C. Fig. 4.4 shows the Na-concentration as a function of depth in all the 6 sample pieces. For the sample piece treated at 1150°C for 2 h an accumulation of Na at depths shallower than 0.5 μm is observed. For the samples heat treated at temperatures $\geq 1050^{\circ}$C there is a clear change in the diffusion process relative to that $\leq$1000°C, as observed in the measured data when the Na-concentration falls below $1\times10^{16}\,\mathrm{cm}^{-3}$. The data obtained deeper than 0.5 μm are consistent with a trap limited diffusion process. These results are of a preliminary nature and further studies will be needed to reveal the identity of such a trap. The most obvious site for Na is the substitutional Zn-site. However, as indicated in the results of Papers V and VI the V_{Zn}-concentration is expected to be $5\times10^{16}\,\mathrm{cm}^{-3}$, which is higher than the trap level. It should be noted that the $5\times10^{16}\,\mathrm{cm}^{-3}$ of V_{Zn} is observed even in samples that are already contaminated by Na. Na might also form complexes with other impurities present in the sample or maybe even reside on the substitutional O-site. Further studies are needed to reveal the trap-site for the Na-contamination.

4.3 Suggestions for further work

In addition to pursuing some of the preliminary work, which have already been presented, there are several other interesting issues to study further.

- First of all, H and ^{2}H in combination with SIMS, FTIR and PAS have been shown to make a great tool to study different properties of ZnO. The true solubility of H in high quality ZnO material is relatively low, thus the presence of H typically reflects the presence of other impurities and the formation of different defect complexes. In this way H can act as a marker for other defects and might also be used to indirectly study other impurities

and defects like V_{Zn} and V_O. E.g. by performing hydrogen in-diffusion from gas phase on ZnO samples prepared in different ways.

- As mentioned, the observed dose dependency of the estimated trap concentration for H-diffusion as observed in Paper I and II needs to be checked for validity. It would be interesting to conduct further studies of samples prepared in such a way that different H traps, like the intrinsic vacancies and impurities other than Li are the dominating ones, in line with the first suggestion. In this way, the diffusion properties of H could be rigorously established and dissociation energies for the different H-traps could be estimated.

- Systematic SIMS and TEM studies are needed to reveal the origin and implications of the c-axis inversion boundary domains and to potentially correlate them to the observed inhomogeneity in the Li-distribution as found in Paper III. Their effect on electron mobility and measures to remove them should also be investigated.

- A detailed study of the infrared absorption peak observed at $3577\,\mathrm{cm}^{-1}$ with the aim to further quantify the absorption strength of this local vibrational mode by combining SIMS and FTIR is needed, e.g. in Li and H co-doped samples.

- Further studies of hydrogen in the implanted peak region by PAS, SIMS and scanning spreading resistance microscopy techniques could be pursued to reveal the details of the implantation induced defects. E.g. to further understand the nature of the observed Li-accumulation and also to understand the detailed nature of the H induced donor activity in the implanted peak.

- Extending the quenching experiments to study the thermal stability of the $3577\,\mathrm{cm}^{-1}$ absorption peak as presented in paper IV is needed to make better estimates for the dissociation energy of the OH-Li_{Zn}-complex. Further, modeling of both dissociation and re-trapping should be employed to describe the observed effects in more detail. In addition, it will be important to focus on the role of other competing traps for H and their impact on the apparent stability of the complex. Following the detailed interplay between H and other impurities by combining both FTIR, Raman spectroscopy and SIMS as a function of heat treatments, could reveal more of the complex dynamics, which are found to take place.

- In general, further work is also needed to identify and quantify different H-related infrared absorption peaks by combining SIMS and FTIR, especially since some of the reported absorption peaks have questionable identification.

References

[1] Thomas, D. G. & Lander, J. J. Hydrogen as a donor in zinc oxide. *The Journal of Chemical Physics* **25**, 1136–1142 (1956).

[2] Shi, G. A., Stavola, M. & Fowler, W. B. Identification of an OH-Li center in ZnO: infrared absorption spectroscopy and density functional theory. *Physical Review B (Condensed Matter and Materials Physics)* **73**, 081201–3 (2006).

[3] Lavrov, E. V., Börrnert, F. & Weber, J. Dominant hydrogen-oxygen complex in hydrothermally grown ZnO. *Physical Review B* **71**, 035205 (2005).

[4] Halliburton, L. E. *et al.* Infrared absorption from OH[sup -] ions adjacent to lithium acceptors in hydrothermally grown ZnO. *Journal of Applied Physics* **96**, 7168–7172 (2004).

[5] Wardle, M. G., Goss, J. P. & Briddon, P. R. Theory of li in ZnO: a limitation for li-based p -type doping. *Physical Review B* **71**, 155205 (2005).

[6] Sann, J., Hofstaetter, A., Pfisterer, D., Stehr, J. & Meyer, B. K. Acceptor doping in ZnO with group-I elements. *physica status solidi (c)* **3**, 952–955 (2006).

[7] Puska, M. J., Corbel, C. & Nieminen, R. M. Positron trapping in semiconductors. *Physical Review B* **41**, 9980 (1990).

[8] Ohashi, N. *et al.* Passivation of active recombination centers in ZnO by hydrogen doping. *Journal of Applied Physics* **93**, 6386–6392 (2003).

[9] Svensson, B. G. *et al.* Hydrothermally grown single-crystalline zinc oxide; characterization and modification. In *Mater. Res. Soc. Symp. Proc.*, vol. 1035, L04–01 (2008).

[10] Lavrov, E. Hydrogen in ZnO. *Physica B: Condensed Matter* **404**, 5075–5079 (2009).

[11] Vines, L. *et al.* Lithium and electrical properties of ZnO. *Journal of Applied Physics* **107**, 103707 (2010).

[12] Janotti, A. & de Walle, C. G. V. Hydrogen multicentre bonds. *Nat Mater* **6**, 44–47 (2007).

Paper I

Hydrogen Migration in Single Crystalline ZnO

K. M. Johansen, J. S. Christensen, E. V. Monakhov, A. Yu. Kuznetsov and B. G. Svensson,

Materials Research Society Symposium Proceedings **1035**, L03-10 (2008)

Mater. Res. Soc. Symp. Proc. Vol. 1035 © 2008 Materials Research Society 1035-L03-10

Hydrogen Migration in Single Crystalline ZnO

Klaus Magnus Håland Johansen[1,2], Jens Sherman Christensen[2], Edouard V. Monakhov[2], Andrej Yu. Kuznetsov[2], and Bengt Gunnar Svensson[2]
[1]Centre for Materials Science and Nanotechnology, University of Oslo, PB 1126 Blindern, Oslo, 0318, Norway
[2]Department of Physics, University of Oslo, PB 1048 Blindern, Oslo, 0316, Norway

ABSTRACT

Hydrogen has been proposed as one of the contributors to the native n-type doping in as-grown Zinc Oxide and can also be used as an active (intentional) n-type dopant. In this work we have employed Secondary Ion Mass Spectrometry (SIMS) to study deuterium diffusion profiles in single crystalline ZnO. The samples used are hydrothermally grown, high-resistive (10 kΩ cm) monocrystalline ZnO implanted with deuterium to a dose of 1×10^{15} cm^{-2} yielding a peak concentration of approximately 5×10^{18} cm^{-3} at a depth of 2.2 µm. Diffusion profiles have been studied after 30 minutes isochronal heat treatments from 100 ºC up to 400 ºC in steps of 50 ºC. The observed redistribution can be explained by employing a diffusion model which includes trapping of ^2H by Li-impurities and an activation energy of 0.85 eV is extracted for the diffusion of ^2H.

INTRODUCTION

Hydrogen is one of the most common impurities in ZnO[1, 2]. Its diffusion properties were studied already in the 1950's and are now revisited due to the increased interest in ZnO as a semiconductor material for optoeletronic devices. One of the first studies on the diffusion of H in ZnO was performed by Thomas and Lander[3]. They studied hexagonal ZnO needles with diameters of 50 - 150µm grown by the Schwarowsky's technique and heating the samples in H atmosphere led to an increase in the electrical conductivity. This increase was attributed to in-diffusion and electrical activation of H as a shallow donor. When the H was subsequently removed by out-diffusion the conductivity returned to the original value. Under the assumptions that all H atoms are activated as donors and that the electron mobility is independent of concentration the diffusivity was extracted for different temperatures. This resulted in an activation energy (Ea) for H diffusion perpendicular to the wurtzite c-axis in ZnO of 0.91 eV with a prefactor $D_0 = 3 \times10^{-2}$ cm^2s^{-1}.

More recently, Ip et al. [4] and Nickel [5] studied the diffusion of ^2H in bulk wurtzite (0001) single crystal ZnO by SIMS in plasma-exposed samples. In Ref. 4, the samples were exposed to ^2H-plasma at temperatures of 100 ºC -300 ºC allowing ^2H to diffuse into the samples for 30 min. Assuming a semi-infinite source model, Ip et al. deduced a ^2H diffusivity with an activation energy of 0.17 ± 0.12 eV and a prefactor $D_0 = 2.5 \times 10^{-8}$ cm^2s^{-1}. In Ref. 5, two diffusion regions have been reported: (i) a region with slow diffusion ranging from the surface down to 1 µm and (ii) a fast diffusion bulk region from 1 µm to 3 µm deep. Assuming the semi-infinite source model, the data in the fast diffusing region have been fitted by the complementary error function. From this fit an apparent activation energy of Ea = 0.23 eV with a prefactor D_0 close to 3×10^{-8} cm^2s^{-1} have been obtained. In addition effusion measurements were performed in Ref. 5 and the apparent activation energy was estimated to a slightly higher value of 0.37 eV

with a prefactor of 2×10^{-4} $cm^2 s^{-1}$. In another study by Theys et al.[6] metalorganic chemical vapor deposited (MOCVD) films grown on sapphire were exposed to a ^2H-plasma at 220 ºC for 5 h and 30 min. The authors have fitted the recorded SIMS-profiles with the complementary error function and extracted a diffusivity of 1.6×10^{-13} cm^2 s^{-1}, a value three orders of magnitude lower than what would be expected from the results in Refs. 4 and 5.

M. G. Wardle et al.[7] have performed a first principle theoretical study of the diffusion of H in ZnO. They concluded that the migration barrier for H in ZnO is approximately 0.5 eV. They also argue that with such a low barrier, isolated H will be mobile at room temperature (RT) and will easily be trapped by other defects or impurities, which suggests that isolated H is not the most probable state of H in ZnO at RT.

Hence, the existing data for hydrogen diffusion in ZnO do not provide a consistent picture and further studies are required. In this work, we have performed SIMS studies on the diffusion of ion-implanted ^2H in hydrothermal bulk single crystalline ZnO. It is shown that interaction with traps has a considerable impact on the redistribution of ^2H. To extract the diffusvity of ^2H a trap limited diffusion model is employed. From this model, the dissociation parameters for the dominant ^2H-trap complex are deduced, where the trap is believed to be residual Li impurities.

EXPERIMENT

The samples used in this study were cut from a hydrothermally grown mono-crystalline ZnO wafer (high-resistive (~ 10 kΩcm)). They were implanted with ^2H at an energy of 1.4 MeV to a dose of 1×10^{15} cm^{-2} through a 15 µm thick Al-film, resulting in a peak concentration of approximately 5×10^{18} cm^{-3} at a depth of 2.2 µm. The implantations were performed at an incident angle of 7° off the < 000-1 > crystal axis in order to minimize channeling. The samples were then heated isochronally for 30 min in air from 100 °C up to 400 °C in steps of 50 °C. It should be emphasized that the heat treatments and the SIMS measurements were performed consecutively on the same sample, in order to reduce possible variation of impurity content and structural properties. Between each heat treatment the concentration versus depth profiles were

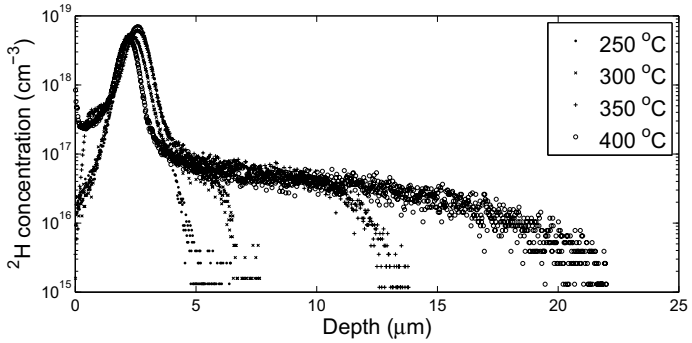

Figure. 1: ^2H concentration versus depth profiles after each heat treatment. All profiles below 250ºC are identical to the one at 250ºC and are therefore not shown.

measured in a Cameca IMS7f Secondary Ion Mass Spectrometer (SIMS). A primary beam of 15 keV Cs^+ ions was rastered over a surface area of 100×100 μm^2 and secondary $^2H^-$ ions were collected from the central part of the sputtered crater for determination of the ^2H concentration. Crater depths were subsequently measured with a Dektak 8 stylus profilometer, and a constant erosion rate was assumed for depth calibration. The ^2H concentration calibration was performed using an as-implanted (1×10^{15} cm^{-2}) sample as reference. Mass spectrum of impurities in the samples was also measured and Li was found to be the main impurity with a concentration of approximately 4.5×10^{16} cm^{-3}.

RESULTS AND DISCUSSION

Fig. 1 shows the concentration of ^2H versus depth after implantation and subsequent annealing at different temperatures. No diffusion is observed for temperatures < 250 ºC. After 300 ºC a diffusion length of 2 μm occurs. One can notice, however, that the diffusion takes place only for a concentration below 10^{17} cm^{-3} and no significant broadening of the peak is detected towards the surface. After annealing at 350 ºC, ^2H diffuses deeper into the bulk to a depth of 13 μm at the detection limit of 10^{15}cm^{-3}. Again the transport occurs below 10^{17} cm^{-3}. After the 400 ºC annealing step ^2H was detected at a depth of 22 μm into the bulk and in addition some redistribution of ^2H is observed towards the surface of the sample at a concentration of 3×10^{17} cm^{-3} for the two highest temperatures used. The details of the ^2H redistribution in close proximity to the implanted peak are, however, beyond the scope of this study and we will focus on the diffusion into the bulk. In the papers by Ip et al.[4] and Nickel et al. [5], two different methods for extraction of the diffusivities from SIMS-depth profiles and thus the activation energy have been used. Both papers assume a semi-infinite source model [8] with the analytical solution given by:

$$C(x,t) = C_s\, erfc\left(\frac{x}{2\sqrt{Dt}}\right), t > 0 \qquad (1)$$

where erfc is the complementary error-function, C_s is the source or solubility concentration, x the depth, D the diffusivity and t the time. The characteristic diffusion length L is given by $2\sqrt{Dt}$. Ip et al. [4] put the characteristic diffusion length equal to the depth where the concentration had fallen to 5×10^{15} cm^{-3} and estimated the diffusivity, while Nickel [5] fitted the experimental curve with the complementary error-function to obtain the diffusivity. Fig. 2 (a) shows a fit to the redistributed ^2H depth profile after the 400 ºC annealing step with the complementary error-function calculated for a source concentration of 7×10^{16} cm^{-3} and a diffusion length of 100 μm, corresponding to a diffusivity of 1.4×10^{-8} cm^2 s^{-1}. The fit is reasonably good to a depth of 15 μm but then the experimental curve starts to drop and deviate from the semi-infinite source model. In an attempt to more accurately describe the observed diffusion into the bulk, we have firstly employed an approach based on numerical solution of Fick's law of diffusion [8] (Eq.2) including a simplified solid solubility model (Eq.3) [9]:

$$\frac{\partial[H]}{\partial t} = D_H \frac{\partial^2}{\partial x^2}[H_{SS}] \qquad (2)$$

$$[H_{SS}] = \frac{[H]\,SS}{[H] + SS} \qquad (3)$$

where [H] denotes the total concentration of ^{2}H in ZnO and D_H the diffusivity of ^{2}H. The amount of ^{2}H which is free to migrate is assumed to be limited by the solid solubility (SS) and thus given by [H_{SS}]. Fig. 2 (b) shows a fit of the model described by Eqs 2 - 3 to the measured ^{2}H profile after the annealing at 400 ºC. This fit was obtained by using $D_H = 1\times10^{-10}$ cm^{2}s^{-1} and SS = 1×10^{17} cm^{-3}. The ^{2}H concentration depth profile after heat treatment at 350 ºC was taken as the initial condition after noise reduction via a median filter. As boundary conditions the amount of ^{2}H was set to zero in the bulk limit and constant in time at the surface. Although the model describes the absence of broadening of the implanted peak at high concentrations, the fit of the diffusion tail at concentrations <10^{17} cm^{-3} is not satisfactory. It can be speculated that a more complicated solubility model can provide a better agreement with the experimental data.
However, one of the main arguments against both this model and the semi-infinite source model is that they both require a solubility limit close to 10^{17} cm^{-3}, which would be in strong contradiction to the reported value of 4×10^{15} cm^{-3} at 400 ºC,[3].

It has been shown previously that H in ZnO can be trapped by implantation induced defects [10, 11] and dopants/impurities [12, 13], including Li [14, 15]. Since Li is the main impurity in the studied samples, one can suggest that trapping by Li affects the migration of H. Moreover, the ^{2}H redistribution is observed just below the concentration level of 1×10^{17} cm^{-3} (Fig. 1), which is close to the concentration of Li in the samples (4.5×10^{16} cm^{-3}). Thus, a model is proposed that invokes trapping and de-trapping of ^{2}H by Li. Together with Eqs. 2 - 3, this model [16] can be described by the following equations:

$$\frac{\partial[HLi]}{\partial t} = \kappa[H][Li] - \nu[HLi] \quad (4)$$

$$[Li] = Li_{Tot} - [HLi] \quad (5)$$

$$\kappa = 4\pi R D_H \quad (6)$$

Where [HLi] denotes the concentration of trapped deuterium, κ the trapping rate, [Li] the concentration of empty traps, ν the dissociation rate, Li_{tot} the total concentration of traps in the material and R the reaction radius between ^{2}H and Li.

Fig. 3 shows a fit of the experimental data obtained after heat treating at 300ºC, 350ºC and 400ºC by the model described by Eqs. (2 - 6) putting R = 5 Å and SS = 4×10^{15}cm^{-3}, as obtained by Thomas and Lander [3] at 400ºC with a hydrogen partial pressure of 1 atm and Li_{tot} = 4.5×10^{16} cm^{-3}. These values were kept constant for all heat treatment steps, thus the temperature dependency was obtained by varying only the diffusion coefficient,

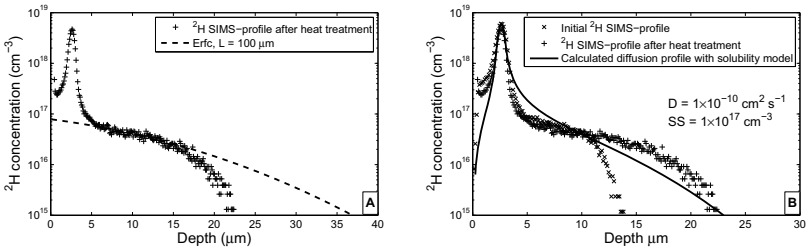

Figure 2: The diffusion profile after 400ºC fitted with (A) the analytical solution of the infinite source model. The zero value of the error function is set to the peak position, the source concentration is 7×10^{16} cm^{-3} and the diffusion length 100µm. (B) illustrates a numerical solution of the diffusion problem, using the solid solubility model. A diffusivity of 1×10^{-10} cm^{2}s^{-1} and a solubility of 1×10^{17} cm^{-3} are applied in the calculation.

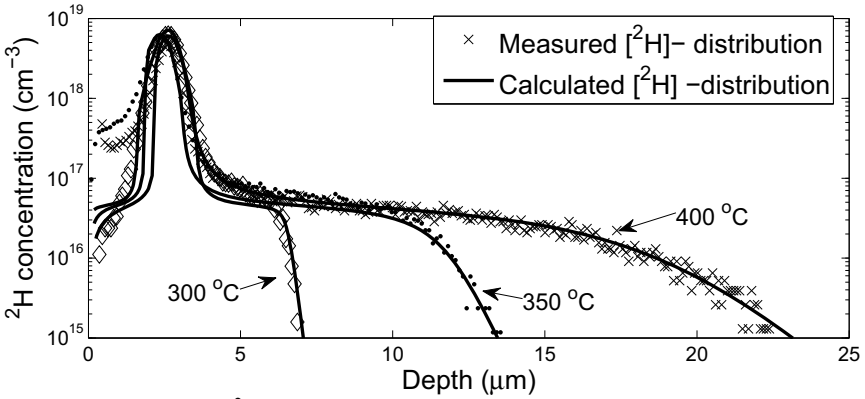

Figure 3: The measured ^{2}H depth profiles after 300ºC, 350ºC and 400ºC heat treatment fitted with the trap-limited diffusion model. The parameters used to fit the curves is given in table I.

Table I: Parameters used to fit the experimental curves in figure 3.

T (ºC)	D_{2_H} (cm^{2}s^{-1})	ν (s^{-1})
300	2.3×10^{-10}	0.01
350	1.5×10^{-9}	0.3
400	2.9×10^{-9}	1.5

D_{2_H} and the dissociation rate, ν (see table I). An activation energy of 0.85±0.35 eV with a prefactor of 8.2×10^{-3}cm^{2}s^{-1} is deduced for D_{2_H} and the dissociation rate of the impurity-H complex (presumably Li-H), is found to occur with an activation energy of 1.7±0.5 eV with a prefactor of 7×10^{12}s^{-1}. The diffusivity of ^{1}H and ^{2}H is expected to differ by 40% in the prefactor, with the activation energies being the same. The diffusivity prefactor is in the range of the theoretical predictions given by Nickel[5] and the activation energy agrees with that of Thomas and Lander[3]. Further, as expected the prefactor of the dissociation process is found to be close to the Debye frequency. Neglecting the influence of trapping impurities may thus explain the discrepancies in the activation energies reported recently.[4,6] Thomas and Lander[3] used ZnO grown by a vapor phase technique which is expected to exibit lower concentration of impurities as compared to other techniques[17]. Hence, it can be speculated that the discrepancies in the diffusivities obtained by different authors are caused by the presence of trapping impurities at different concentrations in the samples used.

CONCLUSIONS

The diffusion of H into hydrothermally grown ZnO bulk samples is shown to be well described by a trap-limited process. The concentration of trapping sites corresponds to that of Li in the samples. A rough estimate of the activation energy suggest a value of 0.85±0.35 eV with a prefactor of 8×10^{-3} cm^{2}s^{-1}. Dissociation of the Li-^{2}H complex is described by an activation energy of 1.7±0.5 eV with an attempt frequency of 7×10^{12}s^{-1} under the assumption of a reaction radius of 5 Å.

ACKNOWLEDGMENTS

The authors would like to acknowledge partial financial support from the University of Oslo through the FUNMAT@UiO program.

REFERENCES

1. N. H. Nickel and K. Brendel, Phys. Rev. B 68, 193303 (2003).
2. D. M. Hofmann, A. Hofstaetter, F. Leiter, H. Zhou, F. Henecker, B. K. Meyer, S. B. Orlinskii, J. Schmidt, and P. G. Baranov, Phys. Rev. Lett. 88, 045504 (2002).
3. D. G. Thomas and J. J. Lander, The Journal of Chemical Physics 25, 1136 (1956).
4. K. Ip, M. E. Overberg, Y. W. Heo, D. P. Norton, S. J. Pearton, C. E. Stutz, B. Luo, F. Ren, D. C. Look, and J. M. Zavada, Applied Physics Letters 82, 385 (2003).
5. N. H. Nickel, Physical Review B (Condensed Matter and Materials Physics) 73, 195204 (pages 9) (2006).
6. B. Theys, V. Sallet, F. Jomard, A. Lusson, J.-F. Rommeluere, and Z. Teukam, Journal of Applied Physics 91, 3922 (2002).
7. M. G. Wardle, J. P. Goss, and P. R. Briddon, Physical Review Letters 96, 205504 (2006).
8. S. A. Campbell, The science and enginering of microelectronic fabrication (Oxford University Press, 2001), page 45.
9. E. V. Monakhov, B. G. Svensson, M. K. Linnarsson, A. L. Magna, C. Spinella, C. Bongiorno, V. Privitera, G. Fortunato, and L. Mariucci, Applied Physics Letters 86, 151902 (pages 3) (2005).
10. E. V. Monakhov, J. S. Christensen, K. Maknys, B. G. Svensson, and A. Y. Kuznetsov, Applied Physics Letters 87, 191910 (pages 3) (2005)
11. K. Ip, M. E. Overberg, Y. W. Heo, D. P. Norton, S. J. Pearton, S. O. Kucheyev, C. Jagadish, J. S. Williams, R. G. Wilson, and J. M. Zavada, Applied Physics Letters 81, 3996 (2002).
12. F. Borrnert, E. V. Lavrov, and J.Weber, Physical Review B (Condensed Matter and Materials Physics) 75, 205202 (pages 5) (2007).
13. X. Li, B. Keyes, S. Asher, S. B. Zhang, S.-H.Wei, T. J. Coutts, S. Limpijumnong, and C. G. V. de Walle, Applied Physics Letters 86, 122107 (pages 3) (2005).
14. M. G. Wardle, J. P. Goss, and P. R. Briddon, Physical Review B (Condensed Matter and Materials Physics) 71, 155205 (pages 10) (2005).
15. G. A. Shi, M. Stavola, and W. B. Fowler, Physical Review B (Condensed Matter and Materials Physics) 73, 081201 (pages 3) (2006).
16. M. S. Janson, A. Hallén, M. K. Linnarsson, and B. G. Svensson, Phys. Rev. B 64, 195202 (2001).
17. D. C. Look, D. C. Reynolds, J. R. Sizelove, R. L. Jones, C. W. Litton, G. Cantwell, and W. C. Harsch, Solid State Communications 105, 399 (1998).

Paper II

Deuterium diffusion and trapping in hydrothermally grown single crystalline ZnO

K. M. Johansen, J. S. Christensen, E. V. Monakhov, A. Yu. Kuznetsov and B. G. Svensson

Applied Physics Letters **93**, 152109 (2008)

Deuterium diffusion and trapping in hydrothermally grown single crystalline ZnO

K. M. Johansen,[a] J. S. Christensen, E. V. Monakhov, A. Yu. Kuznetsov, and B. G. Svensson
Centre for Materials Science and Nanotechnology, University of Oslo, P.O. Box 1126 Blindern, N-0318 Oslo, Norway

(Received 4 September 2008; accepted 26 September 2008; published online 17 October 2008)

Secondary ion mass spectrometry is employed to investigate diffusion of ^{2}H implanted in hydrothermally grown single crystal ZnO. Diffusion profiles have been studied after 30 min isochronal heat treatments from 100 to 400 °C and evaluated using three different models: the infinite source model, a solid solubility limited model, and a trap limited model. Only the latter one reproduces closely the measured values. From this model an activation energy E_a=0.85 eV is extracted, and it is speculated that trapping may be a source of the discrepancies between the reported values of E_a in the literature. © *2008 American Institute of Physics*.
[DOI: 10.1063/1.3001605]

Hydrogen is one of the most common impurities in ZnO.[1,2] Its diffusion properties were studied already in the 1950s and are now revisited due to the increased interest in ZnO as a semiconductor material for optoelectronic devices. One of the first studies on diffusion of H in ZnO was performed by Thomas and Lander.[3] They studied hexagonal ZnO needles and found that heating in H atmosphere led to an increase in the electrical conductivity. This increase was attributed to in-diffusion and electrical activation of H as a shallow donor. They estimated an activation energy for the H diffusion of E_a=0.91 eV with a prefactor $D_0=3\times10^{-2}$ cm^2 s^{-1}.

More recently, Ip *et al.*[4] and Nickel[5] studied the diffusion of ^{2}H along the (0001) direction in bulk wurtzite single crystal ZnO by secondary ion mass spectrometry (SIMS) in plasma-exposed samples. ^{2}H is expected to diffuse in a similar manner as H,[6] but the SIMS sensitivity is about three orders of magnitude better for ^{2}H than that for H. In Ref. 4, the samples were exposed to ^{2}H-plasma at temperatures of 100, 200, and 300 °C, and, assuming a semi-infinite source model, a ^{2}H diffusivity with $E_a=0.17\pm0.12$ eV and $D_0=2.5\times10^{-8}$ cm^2 s^{-1} as deduced. In Ref. 5, two diffusion regions were discussed: (i) a region with slow diffusion ranging from the surface to a depth of 1 μm and (ii) a fast diffusion bulk region from 1 to 3 μm depth. Assuming the semi-infinite source model, the data in the fast diffusing region were fitted by a complementary error function. From this fit an apparent E_a=0.23 eV with D_0 close to 3×10^{-8} cm^2 s^{-1} as obtained. In addition, effusion measurements have been performed in Ref. 5 and the apparent activation energy is estimated to a slightly higher value of 0.37 eV with a prefactor of 2×10^{-4} cm^2 s^{-1}. From estimation of the ^{2}H chemical potential it is argued in Ref. 5 that the true activation energy is most likely above 0.8 eV and a possible reason for the discrepancy may be trapping of H.

Recently, Wardle *et al.*[7] performed a first principles theoretical study of the diffusion of H in ZnO. They concluded that the migration barrier for H in ZnO is approximately 0.5 eV. They also argued that with such a low barrier, isolated H will be mobile at room temperature (RT) and will be trapped easily at other defects or impurities, which suggests that isolated H is not the most probable state of H in ZnO at RT.

In this work, we have performed SIMS studies on diffusion of ion-implanted ^{2}H in hydrothermally grown bulk single crystalline ZnO. To explain the diffusion profiles three different models have been evaluated, the infinite source model, a solid solubility (SS) limited model, and a trap limited model. Only the latter one reproduces closely the experimental results showing that interaction with impurities and structural defects have a considerable impact on the redistribution of ^{2}H. From these results the diffusivity for ^{2}H and the dissociation parameters for the dominant trapping complex have been deduced.

The samples used in this study were cut from a hydrothermally grown and subsequently annealed (1100 °C for 1 h) monocrystalline ZnO wafer (resistivity ~10 kΩ cm). They were then implanted at RT with 1.0×10^{16} ^{2}H/cm^2 through a 15 μm thick Al foil at an energy of 1.4 MeV to an average depth of 2.2 μm, performed at an angle of 7° off the $\langle000\bar{1}\rangle$ crystal axis in order to minimize channeling. The samples were subjected to 30 min of isochronal heat treatment in air from 100 up to 400 °C in steps of 50 °C. Between each heat treatment the chemical concentration versus depth profiles were measured in a Cameca IMS7f microanalyzer. It should also be emphasized that the heat treatments and the SIMS measurements were performed consecutively on the same samples, in order to reduce possible influence by variations in impurity content and structural properties of the material. A primary beam of 15 keV Cs^+ ions was rastered over a surface area of 100×100 μm^2 and secondary $^2H^-$ ions were collected from the central part of the sputtered crater for determination of the ^{2}H concentration. Crater depths were subsequently measured with a Dektak 8 stylus profilometer, and a constant erosion rate was assumed for depth calibration. The ^{2}H concentration calibration was performed using an as-implanted sample as reference.

Figure 1 shows the concentration of ^{2}H versus depth profiles after implantation and subsequent annealing at different temperatures. No diffusion is observed for temperatures ≤250 °C. For temperatures ≥300 °C redistribution of ^{2}H into the samples is observed but only below a concentration level of 10^{17} cm^{-3}. After heat treatment at 300, 350, and

[a]Electronic mail: klausmj@fys.uio.no.

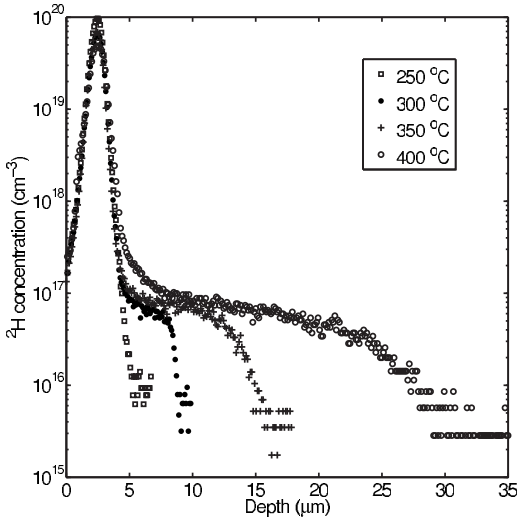

FIG. 1. ^{2}H concentration vs depth profile as measured by SIMS. All profiles below 250 °C including the as-implanted are identical to that at 250 °C and are not shown.

400 °C, ^{2}H was detected at depths extending to 4, 16, and 29 μm, respectively. The diffusion front falls off with a slope that decreases as the temperature increases.

In accordance with Refs. 4 and 5 we first assume a semi-infinite source model[8] with the analytical solution given by

$$C(x,t) = C_s \ \mathrm{erfc}\left(\frac{x}{2\sqrt{Dt}}\right), \tag{1}$$

where erfc is the complementary error function, C_s is the source or solubility concentration, x is the depth, D is the diffusivity, and t is the diffusion time. The characteristic diffusion length L equals $\sqrt{2Dt}$. Figure 2 shows a fit to the ^{2}H depth profile after 400 °C treatment with the complementary error function calculated for $L=20$ μm and $L=6.8$ μm with corresponding source concentration/SS of 1.2×10^{17} and 4.9×10^{19} cm^{-3}, respectively. The 20 μm fit approximates adequately the experimental data only between 7 and 25 μm while in the vicinity of the surface as well as deeper in the bulk the fitting is not satisfactory. Decreasing the diffusion length to 6.8 μm, allows a better agreement deeper in the sample, but the fitting of the rest of the profile is not satisfactory. Hence, it is concluded that the semi-infinite source model is not appropriate and the assumption that all the ^{2}H atoms are mobile is not valid.

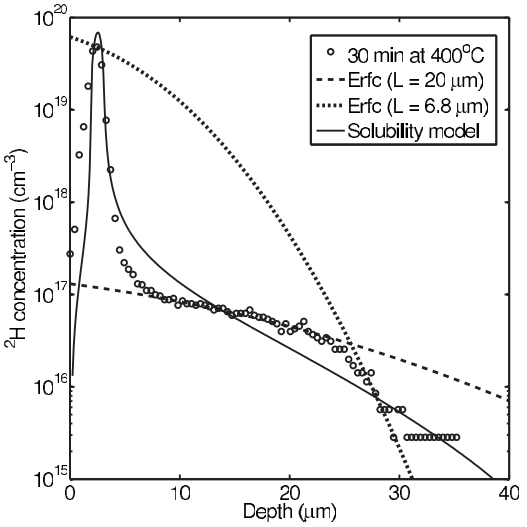

FIG. 2. ^{2}H distribution after heat treatment at 400 °C fitted with two examples of the analytical solution of the infinite source model (dashed and dotted lines) and one numerical solution using the SS model (solid line).

A significant improvement can be made to the interpretation of the profiles in Fig. 1 by including a SS model[9] when solving Fick's diffusion equations,[8]

$$\frac{\partial[\mathrm{H}]}{\partial t} = D_\mathrm{H}\frac{\partial^2}{\partial x^2}[\mathrm{H_{SS}}], \tag{2}$$

$$[\mathrm{H_{SS}}] = \frac{[\mathrm{H}]\mathrm{SS}}{[\mathrm{H}]+\mathrm{SS}}, \tag{3}$$

where [H] denotes the total concentration of ^{2}H, and D_H is the ^{2}H diffusivity. The amount of ^{2}H, which is free to migrate is assumed to be limited by the SS and labeled [H_{SS}] in Eqs. (2) and (3). As boundary conditions, the amount of deuterium is set to zero in the bulk limit and constant in time at the surface. Indeed the profile obtained from Eqs. (2) and (3) using $D_\mathrm{H}=3\times10^{-10}$ cm^2 s^{-1} and $\mathrm{SS}=2\times10^{17}$ cm^{-3} improves significantly the agreement with the experimental data (solid line in Fig. 2). In the calculations, the ^{2}H concentration versus depth profile after the previous heat treatment step (at 350 °C) was taken as the initial condition after noise reduction via a median filter.

However, and in spite of that, the SS model describes the absence of broadening of the implanted peak at high concentrations, the fit of the diffusion tail at concentrations $\leq10^{17}$ cm^{-3} is not satisfactory. It can be argued that a more refined solubility model may provide a better agreement with the experimental data. However, such an approach implies nevertheless a solubility limit in the 10^{17} H/cm^3 range, which is inconsistent with previous reports indicating values in the 10^{15} H/cm^3 range.[3] Hence, investigations of other mechanisms responsible for the diffusion behavior shown in Fig. 1 are needed.

Interestingly, it has been shown previously that H in ZnO can be trapped by implantation induced defects[10,11] and impurities,[12,13] including Li.[14,15] Indeed, Li is a major impurity in the studied samples with a concentration of $\sim5\times10^{16}$ cm^{-3}, as determined by SIMS, and one may anticipate that trapping by Li affects the migration of H. Thus, Eqs. (2) and (3) are modified to include trapping and detrapping of the diffusing species as outlined in, e.g., Ref. 16. This results in a trap limited diffusion (TLD) model described by:

$$\frac{\partial[\mathrm{H}]}{\partial t} = D_\mathrm{H}\frac{\partial^2}{\partial x^2}[\mathrm{H_{SS}}] - \frac{\partial[\mathrm{H}a]}{\partial t}, \tag{4}$$

$$\frac{\partial[\mathrm{H}a]}{\partial t} = \kappa[\mathrm{H_{SS}}][a] - \nu[\mathrm{H}a], \tag{5}$$

$$[a] = a_\mathrm{tot} - [\mathrm{H}a], \tag{6}$$

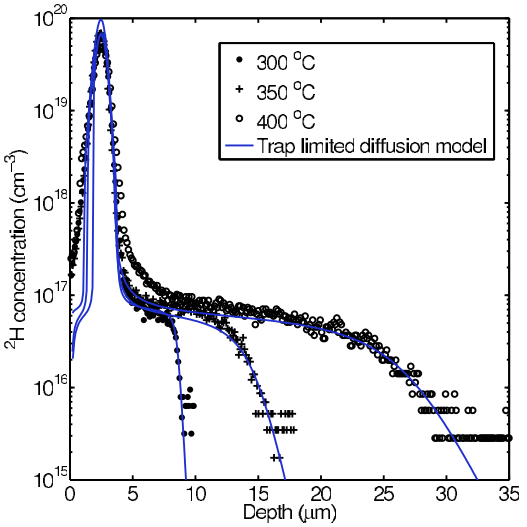

FIG. 3. (Color online) ^{2}H concentration vs depth profiles after 300, 350, and 400 °C heat treatments fitted employing the TLD model.

$$\kappa = 4\pi R D_{\mathrm{H}}, \tag{7}$$

where $[\mathrm{H}a]$ denotes the fraction of trapped ^{2}H atoms, κ is the trapping rate, $[a]$ is the concentration of empty traps, ν is the dissociation rate of Ha, a_{tot} is the total concentration of traps, and R is the reaction radius between ^{2}H and the traps adapted to be on the order of the lattice constant (5 Å). Figure 3 illustrates results from the fitting of the experimental profiles applying Eqs. (4)–(7), solubility values as determined by Thomas and Lander[3] (4×10^{15} cm^{-3} at 400 °C) and treating a_{tot} as a fitting parameter. The best agreement between the experimental and simulation data is found for $a_{\mathrm{tot}}=7\times10^{16}$ cm^{-3}. Keeping the trap concentration constant for all heat treatment steps, the temperature dependency was obtained by varying only the diffusion coefficient D_{H} and the dissociation rate ν. The TLD model describes well the diffusion of ^{2}H into the bulk but is slightly less accurate in the near surface region, close to the implantation peak. This deviation is attributed to trapping by the implantation induced defects,[10] an effect which is not accounted for in the model. As illustrated in Fig. 4, an activation energy of 0.85 ± 0.19 eV and a prefactor of $\sim2.5\times10^{-2}$ cm^2 s^{-1} are extracted for D_{H} from the Arrhenius plot. These data imply that H is rather mobile even at RT ($\sim1.3\times10^{-16}$ cm^2 s^{-1}) and assuming a trap concentration in the range of 1×10^{16} cm^{-3}, H will be trapped after a few hours at 300 K. Further, the E_a value deduced is in agreement with that reported by Thomas and Lander;[3] they used ZnO grown by a vapor phase technique, which is expected to exhibit lower concentration of impurities/traps as compared to ZnO grown by other techniques.[17] Hence, it can be speculated that the discrepancies in the reported diffusivities[4,5] are caused by different defect and impurity concentrations in the samples used and it is crucial to account for trapping when evaluating the diffusion profiles. The dissociation rate of the dominant trapping complex in our samples, possibly Li–H, occurs with an activation energy of 1.5 ± 0.3 eV and a prefactor of 1×10^{12} s^{-1} (Fig. 4). In fact, the value determined for the prefactor is in the range of that anticipated for a dissociation process and provides additional support for the validity of the trapping model.

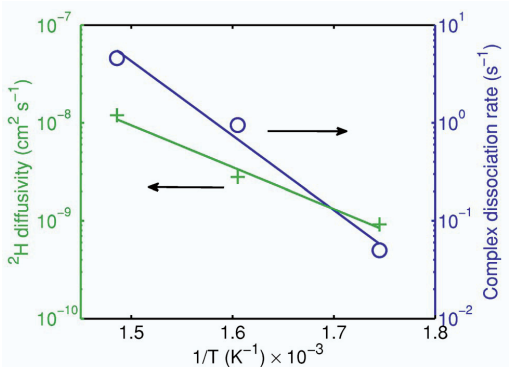

FIG. 4. (Color online) D_{H} (crosses) and ν obtained (circles) from the TLD model vs the reciprocal absolute temperature. E_a for diffusion is estimated to 0.85 ± 0.19 eV with $D_0=2.5\times10^{-2}$ cm^2 s^{-1}, while E_a of dissociation is 1.5 ± 0.3 eV with $\nu_0=1\times10^{12}$ s^{-1}.

The diffusion of H into hydrothermally grown ZnO bulk samples is shown to be accurately described by a TLD mechanism. The concentration of trapping sites is close to that of Li concentration in the samples. We have extracted the activation energy of diffusion for ^{2}H in high resistivity ZnO to be 0.85 ± 0.19 eV with a prefactor of 2.5×10^{-2} cm^2 s^{-1}. Dissociation of the dominant trapping complex, presumably Li–H, is described by an activation energy of 1.5 ± 0.3 eV with an attempt frequency of 1×10^{12} s^{-1}.

The authors would like to acknowledge support from the University of Oslo through the FUNMAT@UiO program.

[1] N. H. Nickel and K. Brendel, Phys. Rev. B **68**, 193303 (2003).
[2] D. M. Hofmann, A. Hofstaetter, F. Leiter, H. Zhou, F. Henecker, B. K. Meyer, S. B. Orlinskii, J. Schmidt, and P. G. Baranov, Phys. Rev. Lett. **88**, 045504 (2002).
[3] D. G. Thomas and J. J. Lander, J. Chem. Phys. **25**, 1136 (1956).
[4] K. Ip, M. E. Overberg, Y. W. Heo, D. P. Norton, S. J. Pearton, C. E. Stutz, B. Luo, F. Ren, D. C. Look, and J. M. Zavada, Appl. Phys. Lett. **82**, 385 (2003).
[5] N. H. Nickel, Phys. Rev. B **73**, 195204 (2006).
[6] $\frac{D_{1\mathrm{H}}}{D_{2\mathrm{H}}}=\left(\frac{M_{2\mathrm{H}}}{M_{1\mathrm{H}}}\right)^{1/2}$.
[7] M. G. Wardle, J. P. Goss, and P. R. Briddon, Phys. Rev. Lett. **96**, 205504 (2006).
[8] S. A. Campbell, *The Science and Engineering of Microelectronic Fabrication* (Oxford University Press, New York, 2001).
[9] E. V. Monakhov, B. G. Svensson, M. K. Linnarsson, A. L. Magna, C. Spinella, C. Bongiorno, V. Privitera, G. Fortunato, and L. Mariucci, Appl. Phys. Lett. **86**, 151902 (2005).
[10] E. V. Monakhov, J. S. Christensen, K. Maknys, B. G. Svensson, and A. Y. Kuznetsov, Appl. Phys. Lett. **87**, 191910 (2005).
[11] K. Ip, M. E. Overberg, Y. W. Heo, D. P. Norton, S. J. Pearton, S. O. Kucheyev, C. Jagadish, J. S. Williams, R. G. Wilson, and J. M. Zavada, Appl. Phys. Lett. **81**, 3996 (2002).
[12] F. Borrnert, E. V. Lavrov, and J. Weber, Phys. Rev. B **75**, 205202 (2007).
[13] X. Li, B. Keyes, S. Asher, S. B. Zhang, S.-H. Wei, T. J. Coutts, S. Limpijumnong, and C. G. V. de Walle, Appl. Phys. Lett. **86**, 122107 (2005).
[14] M. G. Wardle, J. P. Goss, and P. R. Briddon, Phys. Rev. B **71**, 155205 (2005).
[15] G. A. Shi, M. Stavola, and W. B. Fowler, Phys. Rev. B **73**, 081201 (2006).
[16] M. S. Janson, A. Hallén, M. K. Linnarsson, and B. G. Svensson, Phys. Rev. B **64**, 195202 (2001).
[17] D. C. Look, D. C. Reynolds, J. R. Sizelove, R. L. Jones, C. W. Litton, G. Cantwell, and W. C. Harsch, Solid State Commun. **105**, 399 (1998).

Paper III

Li and OH-Li complexes in hydrothermally grown single crystalline ZnO

K. M. Johansen, H. Haug, Ø. Prytz, P. T. Neuvonen, K. E. Knutsen, L. Vines, E. V. Monakhov, A. Yu. Kuznetsov and B. G. Svensson

In press (Published online), *Journal of Electronic Materials*, ISSN 0361-5235

Journal of ELECTRONIC MATERIALS
DOI: 10.1007/s11664-010-1404-0

Li and OH-Li Complexes in Hydrothermally Grown Single-Crystalline ZnO

K.M. JOHANSEN,[1,2] H. HAUG,[1] Ø. PRYTZ,[1] P.T. NEUVONEN,[1] K.E. KNUTSEN,[1] L. VINES,[1] E.V. MONAKHOV,[1] A.YU. KUZNETSOV,[1] and B.G. SVENSSON[1]

1.—Department of Physics/Center for Materials Science and Nanotechnology, University of Oslo, P.O. Box 1048, Blindern, 0316 Oslo, Norway. 2.—e-mail: klausmj@fys.uio.no

Fourier-transform infrared spectroscopy (FTIR) and secondary-ion mass spectrometry (SIMS) have been employed to investigate the relation between the Li concentration and the strength of the 3577 cm^{-1} absorption line in five as-grown hydrothermal ZnO wafers. This line has previously been identified as a local vibrational mode of an OH molecule adjacent to a Li atom on the Zn-site. In this work, we show that the integrated absorption of the 3577 cm^{-1} line does not follow the variation in the total Li concentration between different wafers, providing evidence that the concentration is not the limiting factor for the formation of the 3577 cm^{-1} defect. It is speculated that the presence of inhomogeneously distributed Li along the direction of the *c*-axis, as revealed by SIMS depth profiling in three of the studied wafers, is related to trapping of Li by inversion domain boundaries (IDB). IDBs are expected to have high thermal stability, which may be associated with the high apparent thermal stability reported for the 3577 cm^{-1} line.

Key words: ZnO, hydrothermal, lithium, hydrogen, inversion domain boundaries, 3577, OH-Li complex, secondary-ion mass spectrometry, SIMS, FTIR

Hydrogen and lithium are two important impurities in ZnO, specifically in ZnO grown by the hydrothermal method (HT), where Li is found with concentrations in the range of 1×10^{17} cm^{-3} to 5×10^{17} cm^{-3}. H acts as a donor, either on interstitial sites or on substitutional O-sites,[1,2] and may also form complexes with and passivate acceptors.[3] Li, on the other hand, act as a donor on the interstitial site and as an acceptor on the substitutional Zn-site, which can be passivated by H. Knowledge about and control of these dopants are, therefore, essential if one seeks to realize stable *p*-type ZnO. In HT-ZnO, the dominating OH-related absorption line[4] at 3577 cm^{-1} is due to a stretch mode of a OH-bond in the vicinity of Li on a Zn-site (Li_{Zn}).[3,5] Halliburton et al.[3] found from combined FTIR and electron paramagnetic resonance measurements that 99% of the Li in their samples was contributing to the 3577 cm^{-1} line, i.e., in other words, passivated by H. It is well known that the Li concentration can vary between different as-grown HT-ZnO wafers, and a correlated variation in the integrated absorption coefficient of the 3577 cm^{-1} line may thus be expected. A remarkable feature of the OH-Li complex is the high thermal stability, as it has been reported to be stable at 1200°C during several hours.[4] This is in strong contrast to that found for other OH-related absorption bands in ZnO, which disappear in the range of 150°C to 750°C.[6] However, as pointed out by Lavrov et al.,[7] the temperature stability of the 3577 cm^{-1} band depends on the detailed history of heating and cooling of the sample. This may indicate the involvement of another (in itself highly stable) defect which traps H and Li at low temperatures; when heating the sample H and Li dissociate but are retrapped by the stable defect during cooling down.[7]

(Received August 1, 2010; accepted October 12, 2010)

Published online: 11 November 2010

In this study, results from Fourier-transform infrared spectroscopy (FTIR) and secondary-ion mass spectrometry (SIMS) have been correlated to investigate the 3577 cm^{-1} absorption line in five different hydrothermally grown ZnO wafers. Both the strength of the 3577 cm^{-1} absorption line and the Li concentration are found to vary from sample to sample, but with no clear correlation between the two. It is also found that the Li concentration is highly nonuniform in three of the samples as a function of depth along the direction of the *c*-axis, but with no variation along the lateral directions (normal to the *c*-axis). It is thus considered that the observed inhomogeneity is due to Li decorating defects oriented along the ZnO basal planes normal to the *c*-axis.

Five hydrothermally grown wafers (labeled A, B, C, D, and E) in their as-grown state, purchased from SPC-Goodwill, were used in this study. The Li concentration ([Li]) was measured by SIMS using a Cameca IMS7f microanalyzer. A primary beam of 10-keV O_2^+ ions was rastered over a surface area of 65 μm × 65 μm, an electronic gate of 70% of the raster size was used, and the secondary $^7Li^+$ ions were collected from the central part of the sputtered crater (~30 μm in diameter) for determination of the Li concentration. Crater depths were subsequently measured with a Dektak 8 stylus profilometer, and a constant erosion rate was assumed for depth calibration. The calibration of the Li concentration was performed using an as-implanted sample as reference. The H concentration found in HT-ZnO typically falls below or is close to the SIMS detection limit of ~10^{17} cm^{-3};[8] therefore, detailed information about possible variation in the H concentration cannot be obtained. The infrared absorbance spectra were recorded with a Bruker IFS 113v Fourier-transform spectrometer equipped with a globar light source, a CaF_2 beamsplitter, and a liquid-nitrogen-cooled InSb detector. The samples were mounted in a closed helium CTI-Gryogenics Helix 22 compressor 8200 cryostat, and the temperature was recorded with a LakeShore Cryotronics DRC 82C temperature controller. Measurements were nominally performed at 20 K, with a spectral resolution of 1 cm^{-1}. Transmission electron microscopy (TEM) studies were performed in a JEOL 2000FX microscope operated at an acceleration voltage of 200 kV. Cross-sectional samples were prepared for the TEM studies using standard grinding and ion-milling techniques.

Figure 1 shows absorption spectra in the as-grown state for all five wafers. The integrated absorption coefficient of the 3577 cm^{-1} line (I_{3577}) is found to be 0.55 cm^{-2}, 1.07 cm^{-2}, 2.21 cm^{-2}, 1.80 cm^{-2}, and 1.83 cm^{-2} for wafers A, B, C, D, and E, respectively. This shows that I_{3577} varies between these wafers by a factor of 4. Unfortunately the detailed history of the wafers is not known, so the variation cannot be directly related to growth procedure, position in the boule, etc.

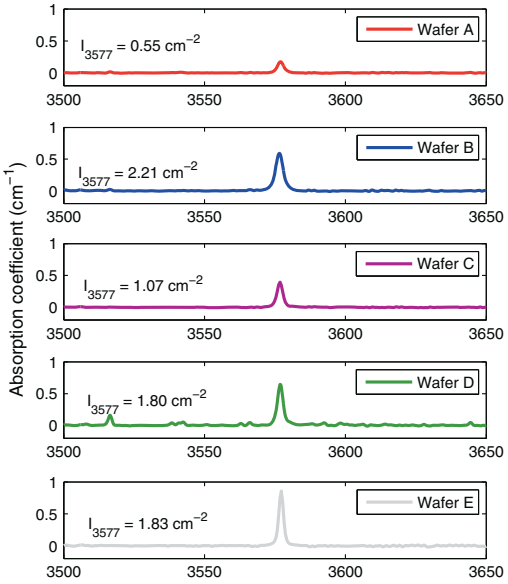

Fig. 1. Infrared absorption spectra measured with light propagating perpendicular to the *c*-axis ($\vec{k} \perp \vec{c}$). The integrated absorption coefficient for the 3577 cm^{-1} absorption line is shown to vary from wafer to wafer.

As mentioned, the 3577 cm^{-1} band has previously been identified as a local vibrational OH-stretch mode adjacent to Li_{Zn}, also referred to as the OH-Li complex.[3] The variation in absorption strength is directly related to the variation in concentration of the complex:

$$\epsilon_{3577} = \frac{I_{3577}}{c_{3577}}, \tag{1}$$

where ϵ_{3577} is the absorption strength of the OH-Li complex and c_{3577} is the concentration of the same complex. Assuming that only one Li atom takes part in the formation of the OH-Li complex, then $c_{3577} \leq$ [Li]. If 99% of the Li present in the material is involved in the OH-Li complex, as argued by Halliburton et al.,[3] one would expect that the variation in I_{3577} should directly reflect [Li]. However, Fig. 2 shows [Li] as a function of depth in the five different wafers, and the average [Li] in A, B, C, D, and E is found to be 2.0 × 10^{17} cm^{-3}, 2.8 × 10^{17} cm^{-3}, 2.5 × 10^{17} cm^{-3}, 3.8 × 10^{17} cm^{-3}, and 2.0 × 10^{17} cm^{-3}, respectively. In other words, there is no clear correlation between the I_{3577} line and the average [Li]. For instance, wafers A and E, have the same [Li] while I_{3577} differs by a factor of more than 3. Hence it is concluded that the [Li] is not the limiting factor in the formation of the OH-Li complex.

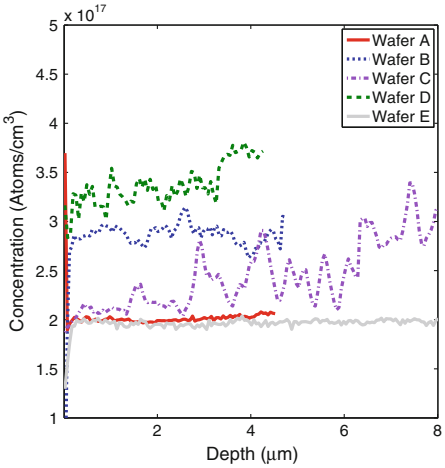

Fig. 2. Li concentration versus depth for five as-grown wafers as measured by SIMS.

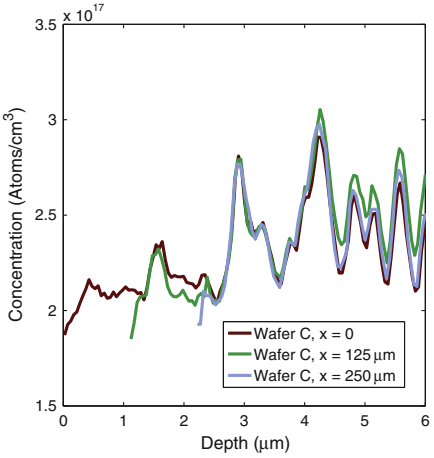

Fig. 3. Li concentration versus depth measured at three different positions (x) of wafer C by SIMS. The depth profiles of the second and third crater is shifted by 1.1 μm and 2.2 μm, respectively, as compared with the first crater due to an offset in the cut angle.

In an attempt to estimate the absorption strength of the OH-Li complex, it is assumed that all of the Li in wafer E contributes to the OH-Li complex. Then a minimum value of 9.3×10^{-18} cm is obtained for ϵ_{3577}. This value is lower than that reported for another OH-related absorption line in ZnO at 3611 cm^{-1}, $\epsilon_{3611} = 2.46 \times 10^{-17}$ cm.[9] This indicates that the true absorption strength might be even higher also for the 3577 cm^{-1} line, with the implication that even in wafer E not all of the Li atoms contribute to the OH-Li complex.

Another interesting feature revealed by Fig. 2 is that in wafers B, C, and D the Li concentration is highly nonuniform as a function of depth along the direction of the c-axis. Interestingly, if different surface positions are investigated on the same wafer, the inhomogeneous features in the Li distribution are almost exactly reproduced except for a shift in depth. An example is shown in Fig. 3, where the Li concentration is depicted as a function of depth for three different crater positions on wafer C. The size of each crater is 65 μm $\times$ 65 μm and the three craters are separated by a distance of 125 μm from center to center. When the recorded Li distributions for the second and third crater in Fig. 3 are displaced towards larger depths by 1.1 μm and 2.2 μm, respectively, the profiles overlap perfectly. The origin of the shift in depth may be due to a small offset in the angle of the polished surface as compared with the c-axis; estimation of this angle (0.5°) shows that it is close to the specified uncertainty of $\pm 0.25°$ as given by SPC-Goodwill. The angle offset may also explain why these features are normally not observed, since a larger area of secondary-ion acceptance would average out the observed features.

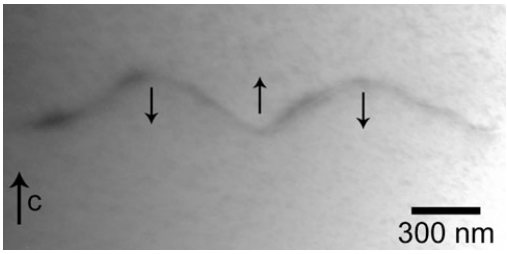

Fig. 4. TEM image of two pyramidal c-axis inversion domains. The orientation of the c-axis is indicated by *arrows*.

The origin of the observed inhomogeneity in the Li distribution has not yet been established, but a plausible explanation may be that Li decorates defect structures which are confined to the basal planes normal to the c-axis. Interestingly, TEM studies reveal the presence of pyramidal inversion domain boundaries (IDB) (Fig. 4), similar to those observed by Köster-Sherger et al.[10] in Fe-doped ZnO samples. In Ref. 10 it was found that the Fe is primarily present in the IDB. It is thus believed that IDBs may also act as traps for both Li and H, facilitating the formation of the OH-Li complex when the wafer is cooled down after growth or high-temperature processing treatments. In this respect, it is also interesting to note that such inversion domains are expected to have high thermal stability and may, indeed, be part of the explanation of the surprisingly high apparent thermal stability of the

3577 cm^{-1} line and the dependency on the detailed history of heat treatment, as reported by Lavrov et al.[7]

In summary, we have shown that there is no direct correlation between the average Li concentration and the integrated absorption coefficient of the 3577 cm^{-1} line, previously identified as a local vibrational mode originating from a OH-Li complex. Thus the formation of this complex is typically not limited by the concentration of Li. In three of the five investigated wafers the Li distribution is highly inhomogeneous along the direction of the *c*-axis, and the features are reproduced in the lateral directions over the surface. By the use of TEM, one of the wafers with inhomogeneous Li distribution is shown to contain *c*-axis inversion domains, which may be the origin of the inhomogeneous Li distribution acting as strong trapping sites for migrating Li and H atoms. This may also explain the high apparent thermal stability of the 3577 cm^{-1} band by trapping of both Li and H at or in the vicinity of the inversion domain boundaries.

ACKNOWLEDGEMENTS

Support from the FUNMAT@UiO Program and the Norwegian Research Council (FRINAT and NANOMAT Programs) is gratefully acknowledged.

OPEN ACCESS

REFERENCES

1. C.G.V. de Walle, *Phys. Rev. Lett*. 85, 1012 (2000).
2. A. Janotti and C.G.V. de Walle, *Nat. Mater*. 6, 44 (2007).
3. L.E. Halliburton, L. Wang, L. Bai, N.Y. Garces, N.C. Giles, M.J. Callahan, and B. Wang, *J. Appl. Phys*. 96, 7168 (2004).
4. E.V. Lavrov, *Physica B: Condensed Matter* 340–342, 195 (2003).
5. G.A. Shi, M. Stavola, and W.B. Fowler, *Phys. Rev. B Condens. Matter Mater. Phys*. 73, 081201 (2006).
6. E.V. Lavrov, J. Weber, F. Börrnert, C.G.V. de Walle, and R. Helbig *Phys. Rev. B* 66, 165205 (2002).
7. E. Lavrov , F. Börrnert, and J. Weber, *Zinc Oxide A Material for Micro- and Optoelectronic Applications* (Netherlands: Springer, 2005), pp. 133–144.
8. L. Vines, E.V. Monakhov, R. Schifano, W. Mtangi, F.D. Auret, and B.G. Svensson, *J. Appl. Phys*. 107, 103707 (2010).
9. E. Lavrov, *Physica B: Condensed Matter* 404, 5075 (2009).
10. O. Köster-Scherger, H. Schmid, N. Vanderschaeghe, F. Wolf, and W. Mader, *J. Am. Ceram. Soc*. 90, 3984 (2007).

Paper IV

Thermal stability of the OH-Li complex in hydrothermally grown single crystal ZnO

K. M. Johansen, H. Haug, E. Lund, E. V. Monakhov and B. G. Svensson

Applied Physics Letters **97**, 211907 (2010)

Thermal stability of the OH–Li complex in hydrothermally grown single crystalline ZnO

K. M. Johansen,[a] H. Haug, E. Lund, E. V. Monakhov, and B. G. Svensson
Centre for Materials Science and Nanotechnology, University of Oslo, 0318 Oslo, Norway

(Received 15 October 2010; accepted 10 November 2010; published online 24 November 2010)

The thermal stability of the prominent 3577 cm^{-1} infrared absorption band in ZnO, assigned to an O–H stretch mode adjacent to a Li atom on Zn site (Li_{Zn}), is studied. Employing slow sample cooling after annealing, the 3577 cm^{-1} peak remains at temperatures $\leq$1250 °C, consistent with previous reports. However, if the samples are cooled rapidly by quenching, the peak disappears after annealing for 1 h at 650 °C. A dissociation energy of less than 2.5 eV is deduced for the OH–Li_{Zn} complex and the apparent high thermal stability after slow cooling is attributed to efficient recapturing of H by Li_{Zn}. Moreover, deuterium (D) is found to replace hydrogen in OH–Li_{Zn} after 1 h at 700 °C in D_2 gas. © *2010 American Institute of Physics*. [doi:10.1063/1.3522886]

Hydrogen (H) and lithium (Li) are two important impurities in ZnO, especially in materials grown by the hydrothermal method (HT), where Li occurs with concentrations in the range of $(1-5)\times10^{17}$ cm^{-3}.[1] Both impurities are electrically active. Doping with H increases the free electron concentration, either by (i) H acting as a donor occupying the interstitial site[2,3] or the substitutional O site[4] or (ii) by forming neutral complexes with residual acceptors (passivation).[5] Li, on the other hand, acts as a donor on the interstitial site and as an acceptor on the substitutional Zn site,[6] where the latter can be passivated by H.[5] A comprehensive review on the role of both H and Li in ZnO can be found in Ref. 7, and further understanding and control of these elements are decisive in order to realize stable p-type ZnO.

In HT-ZnO, the dominating OH-related infrared (IR) absorption line occurs at 3577 cm^{-1} (Ref. 8) and is assigned to a stretch mode of an OH bond adjacent to Li on Zn site (Li_{Zn}).[5,9] A remarkable feature is the high thermal stability reported for this complex, as it has been found to persist after heat treatment at 1200 °C for several hours.[8] Such a high thermal stability is in strong contrast to that typically found for other OH-related absorption peaks in ZnO, which disappear in the temperature range of 150–750 °C.[10,11] However, as pointed out by Lavrov *et al.*,[12] the thermal stability of the 3577 cm^{-1} peak depends on the detailed history of heating and cooling of the sample. It has been speculated that the complex may dissociate at much lower temperatures than 1200 °C and that the high thermal stability is a result of recapturing of H, i.e., reforming the complex, during cooling to room temperature (RT).[12] Such a process may also be facilitated by another (in itself highly stable) defect that traps mobile H (and possibly Li).[13]

Wardle *et al.*[14] studied several different configurations of Li in ZnO, including the Li_{Zn}–H complex. The binding energy was found to be 3.1 eV with respect to the neutral constituents, while the more likely reaction in n-type material, dissociating into the single acceptor state for Li_{Zn}^{-} and the interstitial donor state for H_i^{+}, gives a binding energy of only 1.3 eV. Assuming that the complex disappears according to first order kinetics where dissociation dominates with negligible association, the annealing rate constant is given by

$$\nu(T) = \nu_0 e^{-E_d/kT}, \tag{1}$$

where ν_0 is the attempt frequency, assumed to be on the order of 1×10^{13} s^{-1}, E_d is the dissociation energy, k is the Boltzmann constant, and T is the absolute temperature. The intensity of the corresponding absorption peak, $I(t,T)$, then becomes

$$I(t,T) = I_0 e^{-\nu(T)t}, \tag{2}$$

where I_0 is the initial intensity and t is the heat treatment time. With no recapturing, a value of E_d in excess of ~4.8 eV is required to avoid a "complete" dissociation (remaining fraction <10%) after 1 h at 1200 °C. This value is much higher than that expected from the sum of the binding energy (E_b=1.3 eV) (Ref. 14) and for the diffusion barrier for H(E_a=0.85–0.9 eV).[15,16]

In this work, the integrated absorption coefficient (intensity) of the 3577 cm^{-1} peak has been studied in detail after isochronal heat treatment. The heat treatment was followed by slow cooling (~1.5±0.5 min) or quenching (~1 s) of the samples to RT. In the former case, the previously reported persistency of the 3577 cm^{-1} peak at high temperatures is confirmed,[8] while in the latter case, the peak intensity is below the detection limit already after 1 h at 650 °C. These data imply a dissociation energy of less than 2.5 eV for the OH–Li_{Zn} complex and that retrapping of H plays a crucial role during sample cooling.

Three wafers (A–C) of HT-ZnO with a size of $10\times10\times0.5$ mm^3 obtained from SPC Goodwill were used in this study. The as-grown Li concentration was determined by secondary ion mass spectrometry (SIMS) to be in the range of $(2-4)\times10^{17}$ cm^{-3}. Sample A was heat treated for 30 min at different temperatures in the range of 150–1300 °C, and after each heat treatment, the sample was cooled down to RT within 1.5±0.5 min in air. Three samples of wafer B, each $5\times5\times0.5$ mm^3 in size, were heat treated separately for 1 h and subsequently quenched to RT in de-ionized water. Sample B-1 was treated at 500 and 600 °C, B-2 at 400 and 550 °C, while B-3 was only treated at 650 °C. The heat treatments were performed in a tube furnace using air atmosphere and after every treatment, IR-absorption spectra were recorded with a Bruker IFS 113v Fourier transform spec-

[a]Electronic mail: klausmj@fys.uio.no.

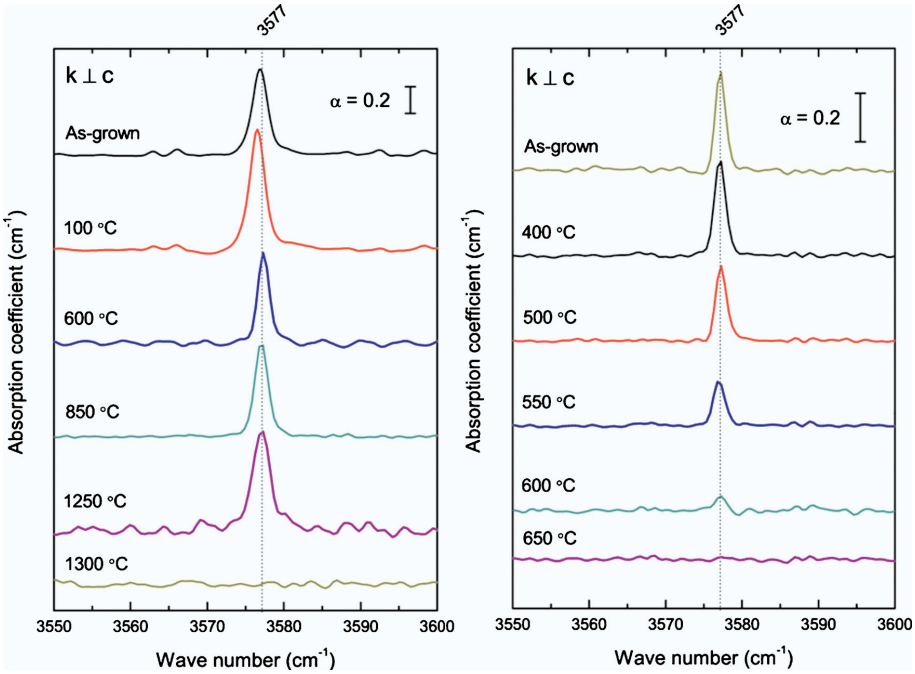

FIG. 1. (Color online) Selected IR-absorption spectra showing the 3577 cm^{-1} peak obtained from (a) wafer A (cooled slowly to RT in air) and (b) wafer B (quenched to RT in de-ionized water). The spectra are offset vertically for clarity. Unpolarized light was used with the wave vector, $\vec{\mathbf{k}}$, directed perpendicular to the c-axis of the sample ($\vec{\mathbf{k}} \perp \vec{\mathbf{c}}$).

trometer at a sample temperature of 20 K and with a spectral resolution of 1 cm^{-1}. No significant change in the Li concentration was observed by SIMS as a result of the heat treatments.

Figure 1 shows selected absorption spectra obtained from wafers A (a) and B (b). In wafer A (slow cooling), the 3577 cm^{-1} peak remains up to 1250 °C but decreases then abruptly below the detection limit after the 1300 °C treatment. In contrast, for wafer B (quenched), the 3577 cm^{-1} peak intensity starts to decrease gradually already at 500 °C and the peak is below the detection limit after 1 h at 650 °C.

Figure 2 shows the normalized intensity (integrated absorption coefficient) of the 3577 cm^{-1} peak as a function of heat treatment temperatures for wafers A and B. For wafer A, it is interesting to note that there are significant variations in the peak intensity already in the temperature range below 300 °C; both growth and loss occur with a net increase by ~20%–30% above 300 °C relative to the peak strength at RT. This indicates that the OH–Li forms at the expense of other, less stable, OH-related defects when H is released.[10,11] The solid line in Fig. 2 is obtained from the first order dissociation model given by Eqs. (1) and (2), with ν_0 and E_d equal to 1×10^{13} s^{-1} and 5.5 eV, respectively. This value of E_d is considerably higher than expected from theoretical predictions. Indeed, if the binding energy of 1.3 eV reported by Wardle *et al.*[14] combined with an activation energy of ~0.8–0.9 eV for diffusion of H in ZnO,[15,16] one obtains $E_d \simeq 2.1$–2.2 eV. Furthermore, a close examination of the experimental data above 1200 °C for wafer A reveals a much more abrupt decrease in the peak intensity than that given by the first order dissociation model.

The results for wafer B (quenching) in Figs. 1 and 2 are in strong contrast to those obtained for wafer A and to the data in Ref. 8. Such a profound influence by the cooling rate implies that retrapping of H is dominant unless rapid quenching is performed. The dashed line in Fig. 2 shows the results from the dissociation model, with ν_0 and E_d equal to 1×10^{13} s^{-1} and 2.5 eV, respectively. The experimental data exhibit a slower decrease than predicted by the calculations, suggesting that recapturing of H upon cooling takes place even during the rapid quenching procedure used. This illus-

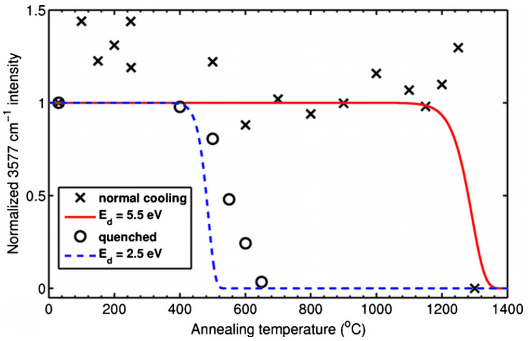

FIG. 2. (Color online) The normalized intensity of the 3577 cm^{-1} peak as a function of heat treatment temperature obtained from wafer A (30 min, followed by slow cooling in air) and wafer B (1 h, followed by rapid quenching in de-ionized water). The solid and the dashed lines show the results from the first order dissociation model where ν_0 is equal to 1×10^{13} s^{-1} and E_d is equal to 5.5 and 2.5 eV, respectively.

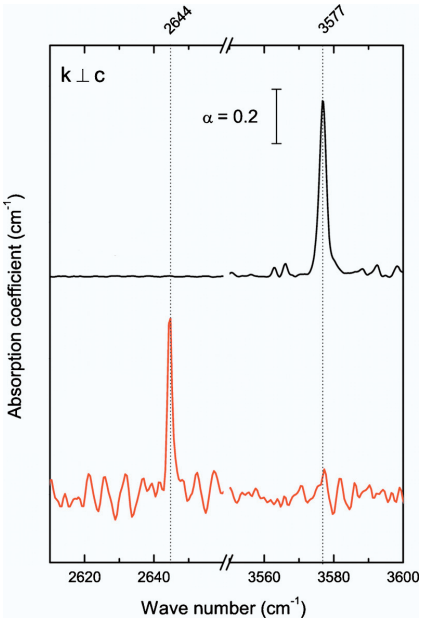

FIG. 3. (Color online) The lower panel shows the absorption spectrum for wafer C after heat treatment at 700 °C for 1 h in an ampoule filled with 0.5 bar wet (D_2O) D_2 gas. The 2644 cm^{-1} absorption peak corresponds to the OD–Li complex. The upper panel shows the spectrum for the as-grown wafer and the 3577 cm^{-1} absorption peak (OH–Li complex) for reference. $\vec{k} \perp \vec{c}$ and unpolarized light was used.

trates how efficient the Li_{Zn} acceptor is as a trap for migrating H in ZnO, and taking retrapping into account, the value of 2.5 eV should be regarded as an upper limit for E_d. In fact, in Ref. 15, the diffusion of hydrogen, using the heavy isotope (deuterium, D) was found to be trap limited in Li-rich samples with a dissociation energy of only 1.5 ± 0.3 eV for the trapped D atoms. This yields an appreciable dissociation rate already at ~200–250 °C, i.e., in the low temperature range where substantial variations in the 3577 cm^{-1} peak intensity occurs for wafer A.

Based on the apparent high stability of the OH–Li complex, there has recently been some controversy in literature about the possibility of exchanging H in the OH–Li complex with D at temperatures around 700 °C.[11,17] According to the results from wafer B, such an exchange may take place. Indeed, Fig. 3 shows the absorption spectra of wafer C, before and after heat treatment at 700 °C in an ampoule filled with 0.5 bar of wet D_2 gas (slow cooling). The exchange is efficient (~90%), possibly indicating a lower total energy (higher stability) for the OD–Li complex relative to the OH–Li complex.

In conclusion, the OH–Li complex starts to dissociate at temperatures below 500 °C and an upper limit for the dissociation energy is found to be 2.5 eV using quenched samples. The apparent high thermal stability of the OH–Li complex (up to 1250 °C) observed in slowly cooled samples is most likely due to efficient retrapping of H by Li_{Zn}, as suggested by Lavrov *et al.*[12] Finally, an efficient exchange of H with D in the OH–Li complex takes place at 700 °C, which may indicate a lower total energy for the OD–Li complex.

Financial support from the FUNMAT@UiO Program, Norwegian Research Council (NANOMAT and FRINAT programs), and NORDFORSK is gratefully acknowledged.

[1]L. Vines, E. V. Monakhov, R. Schifano, W. Mtangi, F. D. Auret, and B. G. Svensson, J. Appl. Phys. **107**, 103707 (2010).
[2]C. G. Van de Walle, Phys. Rev. Lett. **85**, 1012 (2000).
[3]A. R. Hutson, Phys. Rev. **108**, 222 (1957).
[4]A. Janotti and C. G. Van de Walle, Nature Mater. **6**, 44 (2007).
[5]L. E. Halliburton, L. Wang, L. Bai, N. Y. Garces, N. C. Giles, M. J. Callahan, and B. Wang, J. Appl. Phys. **96**, 7168 (2004).
[6]J. J. Lander, J. Phys. Chem. Solids **15**, 324 (1960).
[7]E. V. Monakhov, A. Y. Kuznetsov, and B. G. Svensson, J. Phys. D: Appl. Phys. **42**, 153001 (2009).
[8]E. V. Lavrov, Physica B **340–342**, 195 (2003).
[9]G. A. Shi, M. Stavola, and W. B. Fowler, Phys. Rev. B **73**, 081201 (2006).
[10]E. V. Lavrov, J. Weber, F. Börrnert, C. G. Van de Walle, and R. Helbig, Phys. Rev. B **66**, 165205 (2002).
[11]Y. J. Li, B. Zhang, and W. Lu, J. Appl. Phys. **105**, 093516 (2009).
[12]E. V. Lavrov, F. Börrnert, and J. Weber, Phys. Rev. B **71**, 035205 (2005).
[13]K. M. Johansen, H. Haug, Ø. Prytz, P. T. Neuvonen, K. E. Knutsen, E. V. Monakhov, A. Y. Kuznetsov, and B. G. Svensson, J. Electron. Mater. (in press).
[14]M. G. Wardle, J. P. Goss, and P. R. Briddon, Phys. Rev. B **71**, 155205 (2005).
[15]K. M. Johansen, J. S. Christensen, E. V. Monakhov, A. Y. Kuznetsov, and B. G. Svensson, Appl. Phys. Lett. **93**, 152109 (2008).
[16]D. G. Thomas and J. J. Lander, J. Chem. Phys. **25**, 1136 (1956).
[17]E. V. Lavrov and J. Weber, J. Appl. Phys. **106**, 086104 (2009).

Paper V

Identification of substitutional Li in n-type ZnO and its role as an acceptor

---

K. M. Johansen, A. Zubiaga, I. Makkonen, F. Tuomisto, P. T. Neuvonen, K. E. Knutsen, E. V. Monakhov, A. Yu. Kuznetsov and B. G. Svensson

Submitted to *Physical Review B*

Identification of substitutional Li in n-type ZnO and its role as an acceptor

K. M. Johansen,[1] A. Zubiaga,[2] I. Makkonen,[3] F. Tuomisto,[2] P. T. Neuvonen,[1]
K. E. Knutsen,[1] E. V. Monakhov,[1] A. Yu. Kuznetsov,[1] and B. G. Svensson[1]

[1] *University of Oslo, Centre for Materials Science and Nanotechnology, 0318 Oslo, Norway*
[2] *Department of Applied Physics, Aalto University, P.O. Box 11100, 00076 Aalto, Espoo, Finland*
[3] *Helsinki Institute of Physics and Department of Applied Physics, Aalto University, P.O. Box 14100, 00076 Aalto, Espoo, Finland*

(Dated: March 22, 2011)

Monocrystalline n-type zinc oxide (ZnO) samples prepared by different techniques and containing various amounts of lithium (Li) have been studied by positron annihilation spectroscopy (PAS) and secondary ion mass spectrometry. A distinct PAS signature of negatively charged Li atoms occupying a Zn-site (Li_{Zn}^{-}), so-called substitutional Li, is identified and thus enables a quantitative determination of the content of Li_{Zn}. In hydrothermally grown samples with a total Li concentration of $\sim 2\times10^{17}\,cm^{-3}$, Li_{Zn} is found to prevail strongly with only minor influence by other possible configurations of Li. Also in melt grown samples doped with Li to a total concentration as high as $1.5\times10^{19}\,cm^{-3}$, a considerable fraction of the Li atoms (at least 20%) is shown to reside on the Zn-site, but despite the corresponding absolute acceptor concentration of $\geq$(2-3)$\times10^{18}\,cm^{-3}$ the samples did not exhibit any detectable p-type conductivity. The presence of Li_{Zn} is demonstrated to fully explain the systematic difference in positron lifetime of 10-15 ps between Li-rich and Li-lean ZnO materials as found in the literature.

PACS numbers: 81.05.Dz,71.15.Mb,71.55.Gs,78.70.Bj

I. INTRODUCTION

For a long time, the fundamental challenge of accomplishing stable p-type ZnO has hampered the realization of optoelectronic devices like white light emitting diodes and UV-laser diodes based on ZnO. One of the candidates for p-type doping of ZnO has been Li substituting on the Zn-site (Li_{Zn}) despite results indicating a not very shallow acceptor state in the bandgap.[1–3] However, one ultimate challenge is the amphoteric nature of Li where Li on an interstitial site (Li_i) acts as a donor, leading to self compensation. The fraction between donor and acceptor states is dependent on the electro-chemical potential of the material.[4–6] Further, based on density functional theory Wardle et al.[5] have predicted the existence of a neutral Li_{Zn}-Li_i-complex. Because of the low formation energy of this complex, as compared to the sum of that for isolated Li_{Zn} and Li_i, they suggested that the complex may dominate the behaviour of Li in ZnO. Moreover, Li_{Zn} can also be passivated by H and form the OH-Li_{Zn} complex, which occurs as a neutral defect.[5,7–10]

However, in n-type hydrothermally grown (HT) ZnO samples with unintentional concentrations of Li in the $1\text{-}5\times10^{17}\,cm^{-3}$ range, it is shown experimentally that decreasing the concentration of Li leads to an increase in the conductivity, consistent with Li mainly being in the acceptor configuration, Li_{Zn}^{-}.[11,12] Electron paramagnetic resonance (EPR) measurements of Li-rich ZnO have also revealed that a measurable fraction of the Li atoms reside on the Zn-site.[13] In a few studies, Li has also been observed to contribute to p-type doping in ZnO thin polycrystalline films grown by dc reactive magnetron sputtering.[14,15] Recently, an acceptor state was observed by photoluminescence in Li-doped[16] and H-doped[2] samples in the temperature range between 400 °C - 600 °C and 500 °C-550 °C, respectively, possibly originating from a Li_{Zn}-H-Li_{Zn} complex[2,16]

Positron annihilation spectroscopy (PAS) is an invaluable tool in the search for neutral and negatively charged open volume defects in many semiconductors, including ZnO.[17–19] In 1992, de la Cruz et al.[20] measured the average positron lifetime (τ_{ave}) in flux grown ZnO samples and observed single component lifetimes of 180±3 ps and 169±2 ps in as-grown and thermochemically reduced samples, respectively. The 169 ps lifetime was attributed to the bulk positron lifetime (τ_B), while the defect responsible for the 180 ps lifetime remained un-identified. More recently, Tuomisto et al.[18,21] found the same τ_{ave} of 170 ps in samples prepared by the seeded vapor phase technique (VP-ZnO), supporting the assignment of the 169±2 ps lifetime being the τ_B in ZnO. A bulk positron lifetime of 171±1 ps in VP-ZnO samples (supplied by Eagle-Picher) was also observed by Chen et al.[22]. In as-grown HT-ZnO (SPC-Goodwill), on the other hand, Chen et al. found a single component positron lifetime ranging from 182.2±0.7 ps to 198±1 ps depending on the specific wafer measured[22–24]. They speculated that this variation was related to annihilation of positrons at other sites than those in a perfect crystal, such as impurities, small angle grain boundaries or some other unknown imperfections, homogeneously distributed in the material. In hydrothermally grown material originating from several different suppliers studied by Brauer et al.[25] the τ_{ave} is found to be in the range of 180-182 ps, while in melt grown samples the τ_{ave} is in the range of 165-167 ps. Finally, a similar difference of ∼10 ps between HT-samples (CrysTec) and VP-samples (Eagle-Picher) was also reported by Brunner et al.[17], despite somewhat lower ab-

solute values than those in Refs. 18, 20–25. Further, conducting PAS Doppler broadening experiments Børseth et al.[26] observed a deviation of the annihilation parameter values for N-implanted HT-samples as compared to those for samples grown by the VP-technique. Such a deviation was not observed using ZnO thin films grown by molecular-beam epitaxy[27] or by metalorganic chemical vapor deposition[28].

Brauer et al.[25] have proposed that the discrepancy in the single component positron lifetime of single crystalline ZnO materials grown by different techniques is due to V_{Zn}-H_n complexes; in Ref. 25, samples with H concentration as high as 0.3 at.-%, measured by nuclear reaction analysis, were studied. Such a high H concentration is, as mentioned by the authors themselves, not consistent with the findings of Ohashi et al.[29] and Nickel and Brendel[30]. Furthermore, recent results by Vines et al.[12] reveal H concentrations below $5\times10^{17}\,\mathrm{cm}^{-3}$ in hydrothermally grown ZnO (SPC-Goodwill). H-concentrations in the at.-%-range are also in strong contrast to the H solubility limits estimated by Thomas and Lander[31] and suggest a high concentration of traps for hydrogen, like defects and impurities[29,30,32].

In this work, PAS, secondary ion mass spectrometry (SIMS) and four-point probe measurements have been employed to study n-type bulk ZnO samples prepared by different techniques and with different concentrations of Li. The PAS signature of negatively charged substitutional Li, Li_{Zn} is identified; a clear correlation between the increased single component positron lifetime and the Li_{Zn} concentration is revealed together with distinct signatures deduced from the Doppler broadening spectra. These conclusions are supported by modeling of the PAS parameters using electron structure calculations. Through correlation between the PAS and SIMS data, the fraction of Li in substitutional configuration is quantitatively determined and its importance as an acceptor center in the different samples is discussed.

II. METHODOLOGY

Four n-type HT-ZnO wafers (labeled HT 1-4) supplied by SPC-Goodwill were used in this study. A concentration of $2\times10^{17}\,\mathrm{Li/cm}^3$ was found in the as-grown material (wafer HT-1), as measured by SIMS, using a Cameca IMS7f microanalyzer. Samples HT-2, HT-3 and HT-4 were heat treated in air at 1500 °C for 1 h in order to reduce the Li content to the $10^{15}\,\mathrm{cm}^{-3}$ range and then mechanically polished at the O-face to restore the surface smoothness[11]. The sample HT-2 was subsequently heat treated further at 1100 °C for 1 h to minimize the influence of polishing defects in the near surface region on the slow positron beam measurements[33]. Two melt grown (MG) samples (labeled MG-1 and -2) with a resistivity of 1-2 Ω cm were purchased from Cermet Inc. and contained a Li concentration of $\sim10^{15}\,\mathrm{cm}^{-3}$ in the as-grown state. Li was intentionally introduced into sample MG-2 by annealing at 600 °C for 1 h in a closed quartz ampoule containing a mixture of 10% Li_2O- and 90% ZnO-powder, resulting in highly resistive material (the resistivity exceeded 10 kΩcm as determined by four-point probe measurements).

The positron lifetimes were measured using a conventional fast-fast coincidence spectrometer with a Gaussian time resolution with full width at half maximum of 250 ps (Ref. 34). Two identical sample pieces were sandwiched with a 20 μCi positron source (^{22}Na deposited on a 1.5 μm Al foil). Typically 2×10^6 annihilation events were collected in each positron lifetime spectrum. The lifetime spectra were analyzed as the sum of exponential decay components convoluted with the resolution function of the spectrometer, after subtracting material specific values for the constant background and annihilation in the source material and as positronium (215 ps - 2.0%; 400 ps - 3.4 %, 1500 ps - 0.08%). For the Doppler broadening experiments, the samples were studied with mono-energetic positrons implanted into the O-face at room temperature. The implantation energy of the positrons was varied in the range of 0.5−38 keV, giving a mean positron implantation depth of 0.05−2.4 μm. The Doppler broadening of the annihilation radiation was detected with two Ge detectors with an energy resolution of 1.24 keV at 511 keV. The data were analyzed using the conventional S- and W-parameters, defined as the fractions of counts in the central S, $|E-511\,\mathrm{keV}|\leq 0.8\,\mathrm{keV}$ (corresponding to electron-positron pair momentum of 0.4 a.u.), and the wing W, $2.9\,\mathrm{keV}\leq|E-511\,\mathrm{keV}|\leq 7.4\,\mathrm{keV}$ (1.6 - 4.0 a.u.), parts of the recorded photon spectrum. In addition, coincidence Doppler broadening measurements were conducted at a positron implantation energy of 30 keV (i.e., probing depth of a few microns below the surface), using two Ge detectors in coincidence with a peak-to-background ratio of about 2×10^6.

The so-called ratio curves for positron annihilation at different kinds of defect structures relative to that in a prefect crystal have been calculated. The technical details of the formalism used can be found in Ref.35. To summarize, the positron annihilation parameters are modeled using electronic structure calculations; the valence electron densities are obtained self-consistently via the local-density approximation (LDA), employing the projector augmented-wave (PAW) method[36] and the plane-wave code VASP.[37,38] The positron states and annihilation characteristics are determined using the LDA[39] and the state-dependent scheme[40] for the momentum densities of annihilating electron-positron pairs. For the most part, orthorhombic 96-atom cells are used, but the convergence of the positron state and lifetime have also been confirmed with 768-atom supercells. Defect structures are relaxed taking into account the forces exerted on the ions by the localized positron. The Doppler spectra are computed using the all-electron valence wave functions of the PAW method[41] and atomic orbitals for the core electrons. The spectra are then convoluted with the resolution of the Doppler measurements. The above ap-

proach is well-established and has been proven successful in various PAS studies (see, for instance, Refs. 42–44).

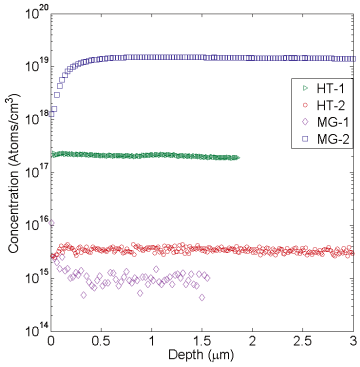

FIG. 1. Li concentration versus depth profiles for samples HT-1, HT-2, MG-1 and MG-2 as measured by SIMS.

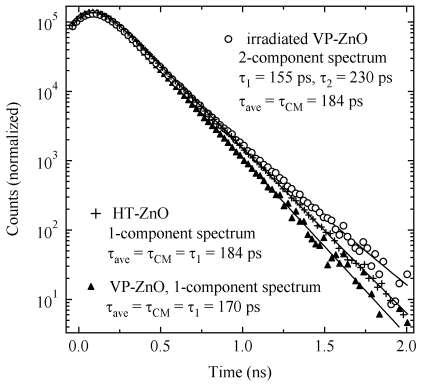

FIG. 2. Positron lifetime spectra measured for an electron irradiated VP-ZnO sample[27], a typical spectrum for HT-ZnO (as well as for Li-enriched MG-ZnO samples) and the bulk lifetime spectrum as measured in the VP-ZnO reference sample.

III. RESULTS AND DISCUSSION

Fig. 1 shows the Li-concentration as a function of depth in the studied samples. The as-grown HT-1 sample and the Li-reduced HT-2 sample contain 2×10^{17} Li/cm^3 and 3×10^{15} Li/cm^3, respectively. It is important to note that the Li concentration is uniform in the samples up to a depth of at least 2-3 μm. The as-grown MG-1 sample and the Li-enriched MG-2 sample contain 1×10^{15} Li/cm^3 and 1.5×10^{19} Li/cm^3, respectively, and except for the near surface region ($\leq 0.2\mu$m) the profiles remain constant.

The average positron lifetime (τ_{ave}) in the sample HT-1 was found to be 187 ps at room temperature (RT), in good agreement with previous studies of HT ZnO in the as grown state, where values in the range of 180 - 190 ps have been reported.[22–24] The τ_{ave} measured for samples HT-3 and HT-4 before and after the removal of Li, reveal a decrease of 6 ps from 184 ps to 178 ps and from 185 ps to 179 ps, respectively. The τ_{ave} in the MG ZnO samples at RT was found to be 170 ps, as in the reference VP sample, and in good agreement with previous observations of the positron lifetime in "defect free" ZnO crystals (bulk lifetime, τ_B)[21]. However, after introducing Li into the sample MG-2, τ_{ave} increased by 10 ps to 180 ps. From this we conclude that the longer τ_{ave} (in the range of 180-190 ps) observed in the HT and Li-indiffused MG samples is related to the presence of Li. This is also consistent with the systematic positron lifetime difference of 10-15 ps between Li-rich (e.g. HT ZnO) and Li-lean ZnO, where a clear vacancy-related signal is not separable in the experimental lifetime spectra.[17–22,24,45] To illustrate the difference in between samples with a low V_{Zn}-concentration and a high Li content fig. 2 shows the positron lifetime spectra for the VP reference sample, HT (or Li-indiffused MG) ZnO, and an electron irradiated VP sample[27] having similar τ_{ave} as the as-grown HT samples. In irradiated samples the longer τ_{ave} (compared to the VP ZnO reference) is due to a longer and clearly resolved lifetime component emerging after 0.7 ns, while in the HT sample the lifetime spectrum seems to consist of only a single component which is slightly longer than that in the VP reference sample. In the electron irradiated sample, the $\tau_2 = 230 \pm 10$ ps component is caused by V_{Zn} while a Li-related defect with less open volume and a significant concentration (at least in the $2\text{-}3\times10^{17}$ cm^{-3} range to produce only a single component) is responsible for the longer τ_{ave} in the HT and Li-indiffused MG samples.

It should be noted that the above-mentioned limit of $(2\text{-}3)\times10^{17}$ cm^{-3} is, in fact, not the limit for saturation trapping (which occurs at $(2\text{-}3)\times10^{18}$ cm^{-3}). The lifetime data recorded in samples HT-3 and HT-4 could not be separated into two components in spite of τ_{ave} being above τ_B by 8-9 ps, which should be enough for reliable separation when only V_{Zn} are trapping positrons. The temperature-dependent data on similar samples in Ref. 45 imply that also shallow traps for positrons (e.g., negatively charged non-open volume defects such as impurities) are present in the samples and are able to trap positrons at room temperature. Even a relatively low concentration of such defects will produce a low-intensity lifetime component equivalent to τ_B in the decay spectra, making the separation of lifetime components in practice impossible. Hence the lower limit given for the Li-related defect concentration is an estimate of minimum concentration for the observation of a major effect in the lifetime

data.

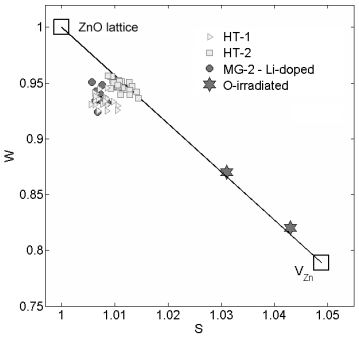

FIG. 3. W-parameter versus S-parameter as measured in the Li-rich (HT-1 and MG-2) and the Li-lean (HT-2) samples. The data points related to surface annihilation are removed for clarity. In addition, values obtained from a ZnO sample irradiated with oxygen ions, containing two different concentrations of V_{Zn}, are shown for comparison.[27]

Doppler broadening experiments were performed on the samples to determine the S- and W- parameters that are specific to different annihilation states. Fig. 3 shows the W-parameter versus the S-parameter for the samples HT-1, HT-2, and MG-2. The parameter values are normalized to those of positrons annihilating in the delocalized state in the ZnO crystal[18] and values for Zn-vacancy saturation trapping are taken from previous experiments on irradiation-induced defects in ZnO.[18,21,27] In Fig. 3, these points are denoted by "ZnO lattice"and "V_{Zn}", respectively, and the line connecting them is referred to as the V_{Zn}-line.

In samples where the V_{Zn} is a dominant open volume positron trap, the S/W parameter values follow the V_{Zn}-line, with the experimental points gathered on a position determined by the actual V_{Zn}-concentration[18]; this holds for sample HT-2, where the V_{Zn} concentration can be estimated as $5\pm1\times10^{16}$ cm^{-3} (corresponding to S=1.012 and W = 0.947),which is one order of magnitude higher than the total Li-concentration in the sample, see Fig. 1. Such a V_{Zn}-concentration is consistent with the average positron lifetime of 178-179 ps found after Li-removal (HT-3 and HT-4), assuming that the longer lifetime, as compared to τ_B, is due to V_{Zn}. However, in all the measured samples containing significant amounts of Li (e.g. HT-1 and MG-2), the S/W parameter values fall below the V_{Zn}-line indicating the presence of a positron trap different from the V_{Zn}, in agreement with the lifetime results. It should be noted that in absolute numbers the Doppler broadening results vary slightly between different HT wafers (not shown), probably due to differences in the concentration of V_{Zn} and Li_{Zn}, but all of them exhibit the same trend, where the data points fall below the V_{Zn}-line. This trend is also present for the data in Ref. 46.

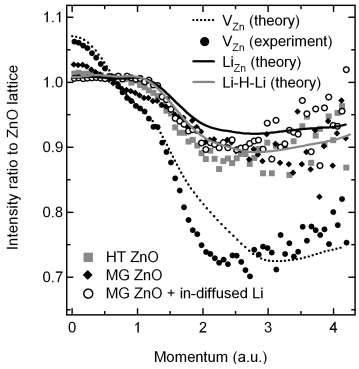

FIG. 4. Coincidence Doppler Broadening measurements for as-grown HT-ZnO (HT-1), as-grown MG-ZnO and Li-doped MG-ZnO as compared to the theoretical values obtained for V_{Zn}, Li_{Zn} and the Li_{Zn}-H-Li_{Zn}-complex. The experimental data obtained for a ZnO sample irradiated with oxygen ions with high concentration of V_{Zn} is shown for comparison.[27]

In order to shed more light on the identity of the defects dominating the trapping of positrons in Li-rich samples, coincidence Doppler broadening measurements were undertaken. The so-called ratio curves, i.e., the Doppler broadening spectra measured for the HT- and in-diffused MG-samples divided by the spectrum measured for the VP reference sample, are shown in Fig. 4 together with the corresponding ratio curves obtained theoretically for the V_{Zn}, the substitutional Li_{Zn} and the Li_{Zn}-H-Li_{Zn}-complex proposed in Ref.2. Also the OH-Li_{Zn} and $Li_{Zn}-Li_i$ complexes have been calculated, using the ground state configurations predicted by Wardle et al.[5], but they are omitted in Fig. 4; the $Li_{Zn}-Li_i$ pair is not found to be active as positron trap while the curve for OH-Li_{Zn} is indistinguishable from the one for Li_{Zn}. The latter result is perhaps somewhat surprising since an extra H is expected to increase the high-momentum intensity, but this is compensated by a decrease caused by outward relaxation of Li.[5]

For comparison, Fig. 4 includes also data obtained for an oxygen ion-irradiated sample with a high concentration of V_{Zn}'s (Ref. 27) illustrating that the features of the experimental and theoretical ratio curves (such as the shoulder at 1-1.2 a.u.) agree very well. From this, it is evident that the experimental ratio curves obtained in the Li-rich materials cannot be explained by assuming non-saturated trapping by V_{Zn}. On the other hand, the theoretical curves for the Li_{Zn}, Li_{Zn}-H-Li_{Zn} and OH-Li_{Zn} complexes all show an excellent agreement with the data obtained from the Li-indiffused MG sample. This holds also for the lifetime measurements, where the calculated lifetime of the positron trapped at the Li_{Zn} defect is 6-8 ps longer than the bulk one depending on whether we

consider the center or off-center geometries predicted by Lany and Zunger[47]. For the Li-H-Li defect it is 8 ps, for OH-Li_{Zn} 7 ps, and for V_{Zn} 81 ps longer.

It should be mentioned that our calculations predicted a bulk ZnO lifetime of 137 ps, which is considerably shorter than the experimental value of 170 ps. Such an underestimation is typical[35] for our specific choice of LDA parametrization[39] for electron-positron correlation effects, and it occurs especially for materials containing electronic states derived from atomic d orbitals. We stress that we have chosen the approximations we use so that the Doppler ratio spectra, rather than the positron lifetimes, would be reproduced in accordance with experiments as well as possible (please see the benchmarks done for other materials in Ref. 35). However, even though the absolute values of the positron lifetimes do not match, lifetime differences between the defect lifetimes and the bulk lifetime give a valid comparison between experiments and theory.

As will be discussed below, the concentration of the dominant positron trap in the Li-indiffused MG sample is at least (2-3)$\times 10^{18}\,cm^{-3}$, which exceeds the hydrogen content of $\leq 6\times 10^{17}\,cm^{-3}$ in the sample, as determined by SIMS and limited by the sensitivity of the measurements, by a factor of 5 (or more). Thus, it can be concluded that the main positron trap is Li_{Zn}, with only a minor contribution (if any) from Li_{Zn}-H-Li_{Zn} and OH-Li_{Zn}. The low H concentration also excludes the V_{Zn}-H_n-complexes suggested by Brauer et al.[25]

The differences between the V_{Zn} and Li_{Zn} ratio spectra in Fig. 4 are largely explained by the smaller open volume seen by the positron in the latter case. The Li repels the positron towards neighboring ion cores thereby increasing the high-momentum intensity relative to the V_{Zn} spectrum. The direct contribution of the Li orbitals to the Li_{Zn} spectrum can be quantified by considering the system as a superposition of free atoms and decomposing the total annihilation rate to contributions due to different atomic orbitals. The Li contribution turns out to be only 5% of the total annihilation rate. Furthermore, the direct Li contribution to the Doppler spectrum is rather featureless. In conclusion, our calculations indicate that we do not observe any clear "Li fingerprint", which would provide the possibility to unambiguously identify Li-related defects in a more general case. However, the flat region with the ratio slightly above 1.0 extending from 0 to 1.3 a.u. is unique for Li_{Zn}. It has been found previously[43] in the GaN-system that addition of hydrogen to vacancy defects flattens out the ratio curves slightly, but preserves the qualitative features (such as the shoulder observed between 1-1.2 a.u.).

The data in Fig. 4 obtained for HT ZnO also match closely to Li_{Zn} but a small contribution from V_{Zn} (without Li) can be revealed (namely the slightly higher intensity at low momenta, and a hint of a shoulder-like feature at around 1 a.u.). According to Sann et al.[2] the Li_{Zn}-H-Li_{Zn}-complex does not appear in as-grown HT-material and it has also been found previously that the concentration of OH-Li_{Zn} is low compared to the total concentration of Li in as grown HT ZnO.[10] Hence, Li_{Zn} occurs as the dominant trap also in HT ZnO, but with detectable contribution from V_{Zn}. In the as-received MG sample, the high-momentum (above 1.5 a.u.) region displays similar intensity as that in the HT sample while in the low-momentum region (less than 0.5 a.u.) the MG sample exhibits clearly higher intensity, consistent with non-saturation trapping by V_{Zn}. Thus, these data give clear evidence of the presence of V_{Zn} in the near surface region of the as-received MG sample, even if the lifetime experiments employing fast positrons show a V_{Zn} concentration below the detection limit in the bulk of the sample. This is not surprising, as surface treatments are known to affect the ZnO crystal on the scale of several microns below the surface.[33]

When positrons are trapped by one type of defect, saturation trapping is observed in lifetime experiments when the trapping rate at a given defect is $\kappa_d = \tau_B^{-1}$ $(\tau_{ave} - \tau_B)/(\tau_d - \tau_{ave}) \gtrsim 20\ \tau_B^{-1}$, where τ_d is the defect positron lifetime. Using the typical value for the trapping coefficient for negatively charged defects $\mu_d = 3\times 10^{15}\,s^{-1}$ (Ref. 18), a defect concentration of about (2-3)$\times 10^{18}\,cm^{-3}$ is required for saturation trapping. However, if several kinds of defects (with comparable concentration) compete in positron trapping, a lower concentration (of roughly one order of magnitude) is sufficient for producing a lifetime spectrum where the components of the different defects cannot be resolved. In this case, it is primarily the lifetime of the dominant defect species that defines the lifetime spectrum. The latter situation is encountered for the HT-1 sample (as-grown) where, in addition to Li_{Zn}, a detectable concentration of V_{Zn} is present as well. In order to produce data resembling saturation trapping, as observed in Fig. 2, essentially all of the Li atoms in sample HT-1 ($2\times 10^{17}\,cm^{-3}$) must reside on the Zn-site, in accordance with previously reported results for electrical measurements of similar samples.[11,12] The V_{Zn} concentration in sample HT-1 is difficult to determine with a high degree of accuracy, but an approximate value of $5\times 10^{16}\,cm^{-3}$ can be deduced also taking into account the results in Fig. 4. Interestingly, from the Doppler broadening data (Fig. 3) a similar value of the V_{Zn} concentration is obtained for sample HT-2 (post-growth annealed and Li-lean). In this sample V_{Zn} is the prevailing positron trap, and these data may suggest that the content of V_{Zn} already exists after growth and remains during the high temperature post-growth treatment. However, we would like to point out that the isolated V_{Zn} has previously been found to anneal out already at 300 °C.[21] Thus the V_{Zn} observed in the as-grown and thermally treated ZnO crystals may not be in its isolated form, but rather be stabilized by other intrinsic defects or impurities (including hydrogen). However, since they retain their V_{Zn}-like defect characteristics from the PAS point of view even when complexed with substitutional impurities, they are labelled V_{Zn} for simplicity. In principle, also Li_{Zn} could be regarded as a V_{Zn} perturbed

by a Li-atom inside the open volume, but the clearly different Doppler broadening signal (e.g., no shoulder at 1-1.2 a.u.) justifies the use of Li_{Zn}.

For the Li-indiffused MG-2 sample containing 1.5×10^{19} Li/cm^3 there is no detectable contribution from V_{Zn} (Figs. 3 and 4) and Li_{Zn} leads to saturation trapping on its own, i.e., the difference in the positron lifetime of 10 ps relative to the VP reference sample occurs without the presence of the clearly longer lifetime component of V_{Zn} illustrated for the electron-irradiated sample in Fig. 2. Thus, at least (2-3)$\times10^{18}$ cm^{-3} of the Li-atoms must exist as Li_{Zn}, but no p-type conductivity was detected. If an acceptor state located 0.26 eV above the valence band edge (E_v)[3] for Li_{Zn} together with ordinary thermal ionization is assumed this would yield a hole concentration of $\geq10^{16}$ cm^{-3} at room temperature. However, the sample is highly resistive (>10 kΩcm) indicating that self-compensation, presumably caused by Li_i, prevails at high Li-concentrations. Alternatively, formation of electrically inactive $Li_{Zn}-Li_i$ pairs may be pronounced in highly doped materials, as suggested by Wardle et al.[5], but this does not account for the non-detectable hole concentration in the in-diffused MG-2 sample unless the acceptor state of Li_{Zn} is substantially deeper than 0.26 eV above E_v or a balancing donor concentration exists.

Finally, it should be noted that the positron data do not provide evidence on the exact position of Li on the substitutional Zn-site. We performed ab initio calculations for both the negatively charged on-center and the neutral off-center configurations predicted by Lany et al.[47], and, interestingly[48], found negligible differences in predicted positron localization, lifetime and Doppler broadening signals. A convergence test was performed using a larger 768-atom supercell, which are unfortunately currently too large to allow accurate calculations of Doppler spectra, we observe no significant difference in the localized positron density between the 96 and 768-atom supercells and find that the calculated positron lifetimes agree within 2 ps. Using the 768-atom cell we estimate the positron binding energies to the Li-related defects examined to be on the order of 0.2-0.3 eV. Similar calculations made for semiconductor point defects in general under-bind the positron[49], so we regard this estimate as a lower bound for the binding energy and do not expect positron detrapping from defects to play a role in measurements. For V_{Zn}, a much deeper positron trap, we estimate the positron binding energy to be on the order of 2 eV.

IV. CONCLUSION

In conclusion, the positron annihilation signature of negatively charged substitutional Li, Li_{Zn}, has been identified. It has an open volume smaller than that of the V_{Zn}. Essentially all Li atoms present in n-type HT ZnO resides on the Zn-site and the resulting open volume is thus responsible for the increase in the single component positron lifetime observed in as-grown HT ZnO as compared to samples produced by other growth techniques yielding Li-lean material. This also explains the discrepancy in the reported values for the bulk positron lifetime in ZnO. A large concentration of Li^-_{Zn} ($\geq10^{18}$ cm^{-3}) is observed after in-diffusion of Li at 600 °C, but no p-type conductivity is detected indicating that self-compensation prevails in highly doped samples with a total Li concentration in excess of 10^{19} cm^{-3}.

ACKNOWLEDGMENTS

Financial support from the FUNMAT@UiO-program and the Norwegian Research Council (NANOMAT and FRINAT programs), NORDFORSK and the Academy of Finland is gratefully acknowledged.

[1] R. T. Cox, D. Block, A. Hervé, R. Picard, C. Santier, and R. Helbig, Solid State Communications **25**, 77 (1978).
[2] J. Sann, A. Hofstaetter, D. Pfisterer, J. Stehr, and B. K. Meyer, physica status solidi (c) **3**, 952 (2006).
[3] O. Lopatiuk, L. Chernyak, A. Osinsky, and J. Q. Xie, Applied Physics Letters **87**, 214110 (2005).
[4] J. J. Lander, Journal of Physics and Chemistry of Solids **15**, 324 (1960).
[5] M. G. Wardle, J. P. Goss, and P. R. Briddon, Physical Review B **71**, 155205 (2005).
[6] A. Carvalho, A. Alkauskas, A. Pasquarello, A. Tagantsev, and N. Setter, Physica B: Condensed Matter **404**, 4797 (2009).
[7] L. E. Halliburton, L. Wang, L. Bai, N. Y. Garces, N. C. Giles, M. J. Callahan, and B. Wang, Journal of Applied Physics **96**, 7168 (2004).
[8] E. V. Lavrov, Physica B: Condensed Matter **340-342**, 195 (2003).
[9] G. A. Shi, M. Stavola, and W. B. Fowler, Physical Review B (Condensed Matter and Materials Physics) **73**, 081201 (2006).
[10] K. M. Johansen, H. Haug, ø. Prytz, P. T. Neuvonen, K. E. Knutsen, L. Vines, E. V. Monakhov, A. Y. Kuznetsov, and B. G. Svensson, Journal of Electronic Materials **40:4**, 429 (2011).
[11] B. G. Svensson, T. M. Børseth, K. M. Johansen, T. Maqsood, R. Schifano, U. Grossner, J. S. Christensen, L. Vines, P. Klason, Q. X. Zhao, et al., in *Mater. Res. Soc. Symp. Proc.*, vol. 1035, pp. L04–01 (2008).
[12] L. Vines, E. V. Monakhov, R. Schifano, W. Mtangi, F. D. Auret, and B. G. Svensson, Journal of Applied Physics **107**, 103707 (2010).
[13] P. H. Kasai, Physical Review **130**, 989 (1963).
[14] Y. J. Zeng, Z. Z. Ye, W. Z. Xu, D. Y. Li, J. G. Lu, L. P. Zhu, and B. H. Zhao, Applied Physics Letters **88**, 062107 (2006).

[15] Y. J. Zeng, Z. Z. Ye, J. G. Lu, W. Z. Xu, L. P. Zhu, B. H. Zhao, and S. Limpijumnong, Applied Physics Letters **89**, 042106 (2006).

[16] B. Meyer, J. Sann, and A. Zeuner, Superlattices and Microstructures **38**, 344 (2005), e-MRS 2005 Symposium G: ZnO and Related Materials - Part 1.

[17] S. Brunner, W. Puff, A. G. Balogh, and P. Mascher, Materials Science Forum **363-365**, 141 (2001).

[18] F. Tuomisto, V. Ranki, K. Saarinen, and D. C. Look, Physical Review Letters **91**, 205502 (2003).

[19] Z. Q. Chen, M. Maekawa, and A. Kawasuso, Chinese Physics Letters **23**, 675 (2006).

[20] R. M. de la Cruz, R. Pareja, R. González, L. A. Boatner, and Y. Chen, Physical Review B **45**, 6581 (1992).

[21] F. Tuomisto, K. Saarinen, D. C. Look, and G. C. Farlow, Physical Review B **72**, 085206 (2005).

[22] Z. Q. Chen, S. Yamamoto, M. Maekawa, A. Kawasuso, X. L. Yuan, and T. Sekiguchi, Journal of Applied Physics **94**, 4807 (2003).

[23] Z. Q. Chen, A. Kawasuso, Y. Xu, H. Naramoto, X. L. Yuan, T. Sekiguchi, R. Suzuki, and T. Ohdaira, Physical Review B **71**, 115213 (2005).

[24] Z. Q. Chen, K. Betsuyaku, and A. Kawasuso, Physical Review B **77**, 113204 (2008).

[25] G. Brauer, W. Anwand, D. Grambole, J. Grenzer, W. Skorupa, J. Čížek, J. Kuriplach, I. Procházka, C. Ling, C. So, et al., Physical Review B **79**, 115212 (2009).

[26] T. M. Børseth, F. Tuomisto, J. S. Christensen, E. V. Monakhov, B. G. Svensson, and A. Y. Kuznetsov, Physical Review B **77**, 045204 (2008).

[27] A. Zubiaga, F. Tuomisto, V. A. Coleman, H. H. Tan, C. Jagadish, K. Koike, S. Sasa, M. Inoue, and M. Yano, Physical Review B **78**, 035125 (2008).

[28] A. Zubiaga, F. Tuomisto, F. Plazaola, K. Saarinen, J. A. Garcia, J. F. Rommeluere, J. Zuniga-Perez, and V. Munoz-Sanjose, Applied Physics Letters **86**, 042103 (2005).

[29] N. Ohashi, T. Ishigaki, N. Okada, H. Taguchi, I. Sakaguchi, S. Hishita, T. Sekiguchi, and H. Haneda, Journal of Applied Physics **93**, 6386 (2003).

[30] N. H. Nickel and K. Brendel, Physical Review B **68**, 193303 (2003).

[31] D. G. Thomas and J. J. Lander, The Journal of Chemical Physics **25**, 1136 (1956).

[32] K. M. Johansen, J. S. Christensen, E. V. Monakhov, A. Y. Kuznetsov, and B. G. Svensson, Applied Physics Letters **93**, 152109 (2008).

[33] F. A. Selim, M. H. Weber, D. Solodovnikov, and K. G. Lynn, Physical Review Letters **99**, 085502 (2007).

[34] K. Saarinen, P. Hautojärvi, and C. Corbel, in *Identification of Defects in Semiconductors*, edited by M. Stavola (Elsevier, 1998), vol. Volume 51, Part 1, pp. 209–285.

[35] I. Makkonen, M. Hakala, and M. J. Puska, Physical Review B **73**, 035103 (2006).

[36] P. E. Blöchl, Phys. Rev. B **50**, 17953 (1994).

[37] G. Kresse and J. Furthmüller, Phys. Rev. B **54**, 11169 (1996).

[38] G. Kresse and D. Joubert, Phys. Rev. B **59**, 1758 (1999).

[39] E. Boroński and R. M. Nieminen, Phys. Rev. B **34**, 3820 (1986).

[40] M. Alatalo, B. Barbiellini, M. Hakala, H. Kauppinen, T. Korhonen, M. J. Puska, K. Saarinen, P. Hautojärvi, and R. M. Nieminen, Phys. Rev. B **54**, 2397 (1996).

[41] I. Makkonen, M. Hakala, and M. Puska, Journal of Physics and Chemistry of Solids **66**, 1128 (2005).

[42] M. Rummukainen, I. Makkonen, V. Ranki, M. J. Puska, K. Saarinen, and H.-J. L. Gossmann, Phys. Rev. Lett. **94**, 165501 (2005).

[43] S. Hautakangas, I. Makkonen, V. Ranki, M. J. Puska, K. Saarinen, X. Xu, and D. C. Look, Phys. Rev. B **73**, 193301 (2006).

[44] I. Makkonen, A. Snicker, M. J. Puska, J.-M. Mäki, and F. Tuomisto, Phys. Rev. B **82**, 041307 (2010).

[45] F. Tuomisto and D. C. Look, in *Proc. SPIE*, edited by F. H. Teherani and C. W. Litton (2007), vol. 6474, p. 647413.

[46] T. M. Børseth, F. Tuomisto, J. S. Christensen, W. Skorupa, E. V. Monakhov, B. G. Svensson, and A. Yu. Kuznetsov, Physical Review B **74**, 161202 (2006).

[47] S. Lany and A. Zunger, Physical Review B **80**, 085202 (2009).

[48] It is generally thought that positron localization in a deep state requires at least a monovacancy-sized open volume. Our result suggest that the observed trapping could be possible also in other cases where the Z of the substitutional atom is much smaller than that of the host atom.

[49] I. Makkonen and M. J. Puska, Phys. Rev. B **76**, 054119 (2007).

Paper VI

H passivation of Li on Zn-site in ZnO

K. M. Johansen, A. Zubiaga, F. Tuomisto, E. V. Monakhov, A. Yu. Kuznetsov and B. G. Svensson

Manuscript in preparation

H passivation of Li on Zn-site in ZnO

K. M. Johansen,[1] A. Zubiaga,[2] F. Tuomisto,[2] E. V. Monakhov,[1] A. Yu. Kuznetsov,[1] and B. G. Svensson[1]

[1] *University of Oslo, Centre for Materials Science and Nanotechnology, 0318 Oslo, Norway*
[2] *Department of Applied Physics, Aalto University, P.O. Box 11100, 00076 Aalto, Espoo, Finland*

(Dated: March 24, 2011)

Hydrothermally grown n-type zinc oxide (HT-ZnO) samples have been intentionally doped with hydrogen (H) via in-diffusion and the interaction of H with lithium (Li), a main residual impurity in HT-ZnO, and zinc vacancies (V_{Zn}), a main intrinsic defect, is studied using positron annihilation spectroscopy (PAS) and secondary ion mass spectrometry. Li on Zn-site (Li_{Zn}) is found to be the dominant trap for migrating H-atoms while the trapping efficiency of V_{Zn} is considerably smaller. After hydrogenation, where the Li_{Zn} acceptor is passivated via formation of neutral Li_{Zn}-H pairs, V_{Zn} occurs as the prime PAS signature and with a concentration similar to that observed in non-hydrogenated Li-lean samples. Despite a low efficiency as H-trap, the apparent concentration of V_{Zn} in Li-lean samples decreases after hydrogenation, as detected by PAS, and evidence for formation of the neutral $V_{Zn}H_2$ complex is presented.

Hydrogen (H) and lithium (Li) are two common impurities in hydrothermally grown (HT) zinc oxide (ZnO) with concentrations typically in the $10^{17}\,\mathrm{cm}^{-3}$-range[1] and both elements are electrically active. H can act as a shallow donor[2–4] or indirectly contribute to n-type activity by passivating compensating acceptors[5]. Li on the other hand behaves as an amphoteric impurity being a donor on interstitial site (Li_i) and acceptor on Zn-site (Li_{Zn})[5]. The relative abundance of Li_i and Li_{Zn} depends on the Fermi-level position and the detailed ZnO-stoichiometry[6,7]. H is a relatively fast diffuser exhibiting an activation energy in the range of 0.8-0.9 eV[8,9]. Less is known about Li-diffusion. However, an early study by Lander[10] suggests an activation energy of 1 eV for migration of Li_i.

In as-grown HT-ZnO the dominant infrared absorption peak, observed at $3577\,\mathrm{cm}^{-1}$, is found to involve both H and Li, based upon isotope shift for both elements[11,12]. Halliburton et al.[5] proposed that this local vibrational mode originates from a OH-Li_{Zn} complex and they concluded, based on quantification of the absorption line and the strength of electron paramagnetic resonance (EPR) signal of the Li_{Zn}, that 99% of the Li in their as-grown sample was in the form of such OH-Li complexes. The high apparent thermal stability ($\sim$1250 °C) of this absorption peak illustrates how efficiently H is trapped by Li_{Zn}, where rapid quenching of the samples to room temperature is needed to avoid re-trapping of H upon cooling after high temperature heat treatment[13].

However, electrical measurements of similar type of samples[1,14] showed that the major contribution of Li in as-grown n-type HT-ZnO is in the acceptor state (Li_{Zn}^-) and not in the neutral OH-Li_{Zn} center. By combining secondary ion mass spectrometry with infrared absorption spectroscopy, it has also been found that the absorption strength of the 3577 cm^{-1} line did not scale with the total Li-concentration[15]. These results do therefore not support the conclusion that the majority (99%) of Li_{Zn} would be passivated by H in as-grown material via formation of the OH-Li_{Zn} complex[5]. This is also in line with the conclusions of Johansen et al.[16], where the positron annihilation signature of Li_{Zn} has been identified.

In this work, H is deliberately introduced by shallow ion implantation and subsequent annealing (in-diffusion), and its interaction with Li_{Zn}^- and V_{Zn}^- is studied by positron annihilation spectroscopy (PAS) and secondary ion mass spectrometry (SIMS). Both Li-rich and Li-lean HT ZnO samples have been employed. In the former case, H is found to predominantly passivate the Li_{Zn}^--acceptor leaving V_{Zn} as the main positron trap, while in the latter case an apparent reduction in the concentration of V_{Zn} occurs. V_{Zn} is anticipated to be in a double negative charge state in n-type material[17] and the results from the Li-lean samples suggest the formation of a neutral $V_{Zn}H_2$ complex.

Two n-type HT ZnO wafers (labeled A and B) with a size of $10 \times 10 \times 0.5\,\mathrm{mm}^3$ were used in this study and supplied by SPC-Goodwill. A concentration of $2{\times}10^{17}$ $\mathrm{Li/cm}^3$ was found in wafer A, as measured by SIMS employing a Cameca IMS7f microanalyzer (details about the SIMS-analysis can be found in Ref. 16). Wafer B was post-growth annealed in air at 1500 °C (1 h) in order to reduce the Li content followed by mechanical polishing of the O-face to restore the surface smoothness[14]. After polishing, wafer B was further annealed in air at 1100 °C (1 h) to minimize the polishing damage in the near surface region and its influence on positron annihilation spectroscopy Doppler broadening measurements[18]. The concentration of Li in wafer B measured by SIMS after this treatment was below $3{\times}10^{15}\,\mathrm{cm}^{-3}$, see Fig. 1. The resistivity of wafer A and wafer B (after the post-growth treatment) was found by four point probe to be $2\,\mathrm{k\Omega\,cm}$ and $0.6\,\Omega\,\mathrm{cm}$, respectively. One quarter of wafer A and of wafer B (A-2 and B-2) were then implanted on the O-face at room temperature (RT) with 35 keV H- ions to a dose of $1{\times}10^{16}\,\mathrm{cm}^{-2}$, while two pieces (A-1 and B-1) was kept as is. The projected range (Rp) was 265 nm, as estimated by SRIM[19]. A-2 and B-2 were subsequently heat treated at 350 °C (30 min) for diffusion of H into the bulk of the samples[9].

Monoenergetic positrons with energies in the 0.5−38 keV range, giving mean penetration depths

of 0.05−2.4 μm, were implanted into the O-face of the samples at RT in order to conduct depth-resolved PAS Doppler broadening experiments. The Doppler broadening of the annihilation radiation was detected using two Ge detectors with an energy resolution of 1.24 keV at 511 keV. The data were analyzed applying the conventional S- and W-parameters, defined as the fractions of counts in the central S, $|E - 511\,\text{keV}| \leq 0.8\,\text{keV}$ (corresponding to electron momenta of <0.4 a.u.), and the wing W, $2.9\,\text{keV} \leq |E - 511\,\text{keV}| \leq 7.4\,\text{keV}$ (1.6 - 4.0 a.u.), parts of the recorded photon spectrum. Also positron lifetime measurements were undertaken, where a conventional fast-fast coincidence spectrometer with a Gaussian time resolution with full width at half maximum of 250 ps was used[20]. During these measurements, the sample and one piece of a reference (high purity) vapor phase (VP) grown ZnO specimen were sandwiched with a 20 μCi positron source (^{22}Na deposited on 1.5 μm Al foil). Typically, 2×10^6 annihilation events were collected in each lifetime spectrum, which was analyzed as the sum of exponential decay components convoluted with the Gaussian resolution function of the spectrometer. In the data analysis, material specific values for the constant background (including the VP-specimen) and annihilation in the source material were accounted for.

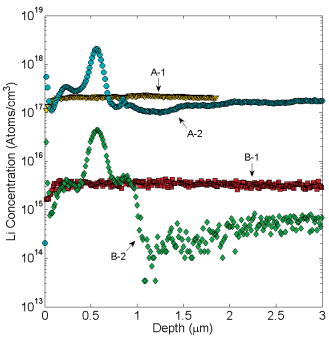

FIG. 1. Li-concentration versus depth for samples A-1, A-2, B-1 and B-2 as measured by SIMS. The as-grown HT sample A and the post-treated HT sample B contain 2×10^{17} Li/cm^3 and 3×10^{15} Li/cm^3, respectively. After implantation and diffusion Li has been re-arranged in the peak region but still reach about 1-2$\times10^{17}$ cm^{-3} for A-2 and 6×10^{14} cm^{-3} for B-2 at depths exceeding $\sim$1 μm and $\sim$2 μm, respectively.

Figure 1 shows the Li-concentration as a function of depth for samples A-1, A-2, B-1 and B-2. A-1 and B-1 have a uniform Li concentration of 2×10^{17} cm^{-3} and 3×10^{15} cm^{-3}, respectively. However, in A-2 and B-2, Li has redistributed and accumulated in the implantation peak region on the expense of the concentration in the bulk. This process is very similar to that reported by Børseth et al.[21] where Li was found to be trapped by implantation-induced vacancy clusters. It should also be noted that despite the accumulation in the implanted region, the Li concentration in sample A-2 remains close to 2×10^{17} cm^{-3} for depths $> 1\,\mu$m while in B-2 it is in the 10^{14} cm^{-3} range for depths up to $\sim$3-4 μm.

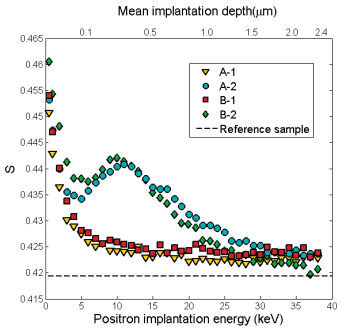

FIG. 2. The measured S-parameter plotted versus the positron implantation energy (0.5−38 keV) for the A-1, A-2, B-1 and B-2 samples. Positrons implanted with an energy $\leq$ 5 keV may reach the surface by diffusion and annihilate there, leading to the increased S-parameter values observed for low energies. The observed peak in S-parameter value at $\sim$ 10 keV for sample A-2 and B-2 is caused by the end-of-range defects induced by the H-implantation.

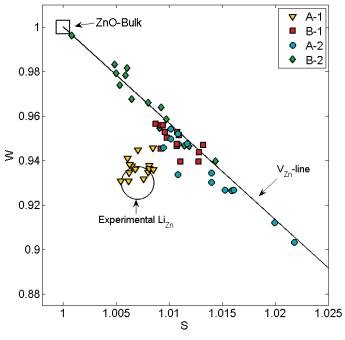

FIG. 3. The normalized W-parameter versus S-parameter obtained for positron implantation energies ranging from 25-38 keV for the Li-rich (A) and the Li-lean (B) HT-samples before and after hydrogenation. The black circle represents previously obtained experimental values of the W- and S-parameter for Li_{Zn} in Li-rich ZnO[16,21].

Doppler broadening experiments were conducted for

Sample	$[V_{Zn}]$, cm^{-3}	Sample	$[V_{Zn}]$, cm^{-3}
A-1	(5×10^{16})	B-1	5×10^{16}
A-2	5×10^{16}	B-2	(1×10^{16})
A-3	5×10^{16}	B-3	(1×10^{16})

TABLE I. Estimated apparent V_{Zn}-concentration ($[V_{Zn}]$) for sample A-2, A-3, B-1, B-2 and B-3 in bulk (beyond the implanted peak). The value given for A-1 is in parenthesis since this value can not be estimated directly and is only assumed. The values for B-2 and B-3 are effectively estimated values, not taking into account the presence of $V_{Zn}H_2$ complexes.

all the samples and Fig. 2 shows the S-parameter as a function of positron implantation energy with the corresponding mean positron penetration depth depicted on the upper x-axis. The peak at ∼10 keV for sample A-2 and B-2 is related to the damage induced by the H implantation of H (Rp ∼ 300 nm). Our main focus is the region probed by > 25 keV positrons (depths > 1 μm) and Fig. 3 displays the W- versus the S-parameter as measured for energies 25-38 keV. The parameter values are normalized to those of the de-localized bulk annihilation in the VP-reference specimen, marked as "ZnO-lattice". The values for V_{Zn} saturation trapping are established from previous studies employing electron and oxygen irradiated samples[22–24], and taking into account the detector resolution used in the present experiment, giving $S/S_{ref} = 1.049(3)$ and $W/W_{ref} = 0.79(1)$.

The line connecting the "ZnO-lattice"value with the value for V_{Zn} saturation trapping is referred to as the V_{Zn}-line. In samples where the V_{Zn} is the dominant positron trap, the S- and W-parameter values will follow the V_{Zn}-line and the position along the line is determined by the V_{Zn}-concentration[22]. The black circle in Fig. 3 represents experimental S- and W-parameter values previously found for Li_{Zn} in Li-rich ZnO[16,21]. The difference found between sample A-1 and B-1 is similar to that reported previously for Li-rich and Li-lean samples[16] and is related to the removal of Li_{Zn}, leaving V_{Zn} as the dominant positron trap.

Interestingly, even though Fig. 1 reveals a Li-concentration close to 2×10^{17} cm^{-3} for sample A-2, the W- and S-parameter values in Fig. 3 follow the V_{Zn}-line. This indicates that after hydrogenation Li_{Zn} is not the dominant positron trap, but rather V_{Zn}.

To gain additional insight into the passivation process, positron lifetime measurements were conducted with a probe depth up to ∼100 μm using samples A-1, B-1, A-3 and B-3. Samples A-3 and B-3 were both hydrogenated by heating in a sealed quartz-ampoule filled with 0.5 bar of wet ^{2}H-gas for 1 h at 700 °C, expected to give a uniform concentration of ^{2}H in the 10^{17} cm^{-3} range throughout the samples.[9] For sample A-1, an average lifetime (τ_{ave}) of 187 ps is recorded, consistent with that typically found for as-grown (Li-rich) HT ZnO[16]. However, for sample A-3 (Li-rich, hydrogenated) the τ_{ave} is reduced to 176-177 ps, similar to that for sample B-1 (Li-lean, not hydrogenated), while for sample B-3 τ_{ave} is even further reduced to 171 ps, close to the bulk value of ∼170 ps (τ_B) for ZnO[23]. These results are fully consistent with those obtained by the Doppler broadening experiments and support a scenario where H primarily interacts with (passivates) the Li_{Zn} acceptor in Li-rich samples and has only a minor effect on the background concentration of V_{Zn} (∼5×10^{16} cm^{-3}). On the other hand, in Li-lean samples V_{Zn} prevails as a major trap for H and the apparent V_{Zn}-concentration deduced by PAS is reduced by a factor of ≥5 to ≤1×10^{16} cm^{-3}. An overview of the estimated values for the bulk V_{Zn}-concentration in samples A-2, A-3, B-1, B-2 and B-3 is given in Table I.

In principle, one could argue that the disappearance of Li_{Zn} as the main positron trap in Li-rich samples after hydrogenation (sample A-2) is not due to passivation, but caused by a change of configuration to Li_i. However, local-density-functional calculations of formation energies performed by Wardle et al.[6] show that the abundance of Li_{Zn} exceeds that of Li_i by many orders of magnitude in n-type samples prepared under normal conditions. Hence, the formation of Li_i is ruled out as a likely explanation and in addition, the results in Ref. 6 demonstrate that OH-Li_{Zn} is a highly preferred defect in the presence of hydrogen. It should be mentioned that it was found theoretically that OH-Li_{Zn} show a similar positron annihilation signature as Li_{Zn} (Ref. 16). However, in the neutral charge state the trapping coefficient may be significantly reduced compared to the negative charge state due to the relatively small open volume of the defect.

The close resemblance between the concentrations of V_{Zn} in samples B-1 and A-2 indicates that the high temperature anneals at 1500 °C and 1100 °C and the hydrogenation process of A-2 exhibits only a minor (if any) influence on the V_{Zn}-concentration. Thus we make the assumption that the V_{Zn} in sample A-1 equals the concentration found in A-2 and B-1 (See Table I). This is, as already mentioned in Ref. 16, in contrast to previous results where irradiation induced V_{Zn} is found to anneal out already at 300 °C[23], therefore we do not rule out the possibility that these V_{Zn} are not isolated, but rather stabilized by other intrinsic defects or impurities. Such a stabilization has already been reported for the Ga-vacancy in the GaN-system[25].

The strong dominance of Li_{Zn} relative to V_{Zn} as a trap for migrating H atoms in wafer A can be partly attributed to its higher concentration (∼2×10^{17} cm^{-3} versus ∼5×10^{16} cm^{-3}), but not entirely; assuming diffusion-limited reactions and equal capture radii of H by Li_{Zn} and V_{Zn} only a difference by a factor of ∼4 in trapping rate is expected while experimentally a factor of ≥20 is obtained. On the other hand, if the relative content of Li is sufficiently reduced V_{Zn} becomes the dominant H-trap despite its limited efficiency. This is evidenced by the results for sample B-2 where the Li-content is in the

low or mid $10^{14}\,\mathrm{cm}^{-3}$ range for depths less than $\sim$3 μm (Fig. 1) while the V_{Zn}-content (before hydrogenation) is at least two orders of magnitude higher (sample B-1). A likely reason for the modest H-trapping efficiency of V_{Zn} (versus Li_{Zn}) is that the neutral $V_{Zn}H_2$ complex forms[26]. The formation of $V_{Zn}H_2$ requires consecutive trapping of two H-atoms and hence, a low rate of decrease of the apparent V_{Zn}-concentration occurs. Further, the formation of the V_{Zn}-H_2 complex fully explains the apparent low V_{Zn} concentration in samples B-2 and B-3. The effect of adding two H atoms into the Ga vacancy in GaN (with very similar positron characteristics as the Zn vacancy in ZnO) results in a reduction of τ_V-τ_B by 45 ps (from 70 ps)[25]. A similar lifetime reduction is likely for the V_{Zn}-H_2 complex, and is enough to explain the decrease of the average lifetime as seen for B-3 as compared to B-1 without a change in the vacancy concentration. Similarly the addition of 2 H atoms into the vacancy draws the S and W parameters of the vacancy defect much closer to the ZnO lattice values, explaining the apparent low V_{Zn} concentration obtained for B-2. Hence it can be concluded that the hydrogenation does not reduce the Zn vacancy concentration, but reduces the open volume in the Zn vacancies by hydrogen filling.

In summary, in as-grown HT ZnO samples the Li_{Zn} acceptor is found to be efficiently passivated by hydrogen, introduced via diffusion from the O-face, and its characteristic PAS signal disappears while forming the neutral OH-Li_{Zn} complex. For V_{Zn}, the opposite holds and it emerges as the dominant positron trap after the hydrogenation with a concentration similar to that detected in post-growth-annealed Li-lean HT samples. However, in the latter samples, where the Li-content is about two orders of magnitude lower than the V_{Zn}-content and Li does not truly compete for H-trapping, hydrogenation gives rise to a decrease of the PAS signal of V_{Zn}. This decrease is presumably due to formation of the neutral $V_{Zn}H_2$ complex and the apparent V_{Zn} concentration, as detected by PAS, approaches the bulk value of high purity VP samples ($\leq 1\times10^{16}\,\mathrm{cm}^{-3}$).

Financial support from the FUNMAT@UiO-program and the Norwegian Research Council (NANOMAT and FRINAT programs), NORDFORSK and the Academy of Finland is gratefully acknowledged.

[1] L. Vines, E. V. Monakhov, R. Schifano, W. Mtangi, F. D. Auret, and B. G. Svensson, Journal of Applied Physics **107**, 103707 (2010).

[2] C. G. V. de Walle, Physical Review Letters **85**, 1012 (2000).

[3] S. F. J. Cox, E. A. Davis, S. P. Cottrell, P. J. C. King, J. S. Lord, J. M. Gil, H. V. Alberto, R. C. Vilo, J. P. Duarte, N. A. de Campos, et al., Physical Review Letters **86**, 2601 (2001).

[4] A. Janotti and C. G. V. de Walle, Nat Mater **6**, 44 (2007).

[5] L. E. Halliburton, L. Wang, L. Bai, N. Y. Garces, N. C. Giles, M. J. Callahan, and B. Wang, Journal of Applied Physics **96**, 7168 (2004).

[6] M. G. Wardle, J. P. Goss, and P. R. Briddon, Physical Review B **71**, 155205 (2005).

[7] A. Carvalho, A. Alkauskas, A. Pasquarello, A. Tagantsev, and N. Setter, Physica B: Condensed Matter **404**, 4797 (2009).

[8] D. G. Thomas and J. J. Lander, The Journal of Chemical Physics **25**, 1136 (1956).

[9] K. M. Johansen, J. S. Christensen, E. V. Monakhov, A. Y. Kuznetsov, and B. G. Svensson, Applied Physics Letters **93**, 152109 (2008).

[10] J. J. Lander, Journal of Physics and Chemistry of Solids **15**, 324 (1960).

[11] E. V. Lavrov, Physica B: Condensed Matter **340-342**, 195 (2003).

[12] G. A. Shi, M. Stavola, and W. B. Fowler, Physical Review B (Condensed Matter and Materials Physics) **73**, 081201 (2006).

[13] K. M. Johansen, H. Haug, E. Lund, E. V. Monakhov, and B. G. Svensson, Applied Physics Letters **97**, 211907 (2010).

[14] B. G. Svensson, T. M. Børseth, K. M. Johansen, T. Maqsood, R. Schifano, U. Grossner, J. S. Christensen, L. Vines, P. Klason, Q. X. Zhao, et al., in *Mater. Res. Soc. Symp. Proc.* (2008), vol. 1035, pp. L04–01.

[15] K. M. Johansen, H. Haug, ø. Prytz, P. T. Neuvonen, K. E. Knutsen, L. Vines, E. V. Monakhov, A. Y. Kuznetsov, and B. G. Svensson, Journal of Electronic Materials **40:4**, 429 (2011), ISSN 0361-5235.

[16] K. M. Johansen, A. Zubiaga, I. Makkonen, F. Tuomisto, P. T. Neuvonen, K. E. Knutsen, E. V. Monakhov, A. Y. Kuznetsov, and B. G. Svensson, pRB, REF will be updated later.

[17] A. Janotti and C. G. V. de Walle, Journal of Crystal Growth **287**, 58 (2006).

[18] F. A. Selim, M. H. Weber, D. Solodovnikov, and K. G. Lynn, Physical Review Letters **99**, 085502 (2007).

[19] J. Ziegler, *SRIM–The Stopping and Range of Ions in Matter, version SRIM-2006, computer code.*

[20] K. Saarinen, P. Hautojärvi, and C. Corbel, in *Identification of Defects in Semiconductors*, edited by M. Stavola (Elsevier, 1998), vol. Volume 51, Part 1, pp. 209–285.

[21] T. Børseth, F. Tuomisto, J. Christensen, W. Skorupa, E. Monakhov, B. Svensson, and A. Kuznetsov, Physical Review B **74**, 161202 (2006).

[22] F. Tuomisto, V. Ranki, K. Saarinen, and D. Look, Physical Review Letters **91**, 205502 (2003).

[23] F. Tuomisto, K. Saarinen, D. C. Look, and G. C. Farlow, Physical Review B **72**, 085206 (2005).

[24] A. Zubiaga, F. Tuomisto, K. Koike, S. Sasa, M. Inoue, and M. Yano, Physical Review B **78**, 035125 (2008).

[25] S. Hautakangas, I. Makkonen, V. Ranki, M. J. Puska, K. Saarinen, X. Xu, and D. C. Look, Phys. Rev. B **73**, 193301 (2006).

[26] E. V. Lavrov, J. Weber, F. Börrnert, C. G. V. de Walle, and R. Helbig, Physical Review B **66**, 165205 (2002).